**Title**
Contribution of Multisensory Stimuli to the Representation of Space in the Hippocampus and Medial Entorhinal Cortex



**Author**
Kees, Ashley Linda

**Publication Date**
2015

Peer reviewed|Thesis/dissertation

UNIVERSITY OF CALIFORNIA

Los Angeles

# Contribution of Multisensory Stimuli to the Representation of Space in the Hippocampus and Medial Entorhinal Cortex

A dissertation submitted in partial satisfaction

of the requirements for the degree

Doctor of Philosophy in Neuroscience

by

Ashley Linda Kees

2015

ABSTRACT OF THE DISSERTATION

# Contribution of Multisensory Stimuli to the Representation of Space in the Hippocampus and Medial Entorhinal Cortex

by

Ashley Linda Kees

Doctor of Philosophy in Neuroscience

University of California, Los Angeles, 2015

Professor Mayank R. Mehta, Chair

How the brain integrates information over multiple sensory modalities to encode highly complex stimuli is a central question of neuroscience. The mammalian brain structures that encode space provide a tractable system in which to explore this question, as there are several well-defined cell types that have spatially selective firing. Place cells in the hippocampus fire when an animal is in a particular location in the environment. Grid cells, found in the upstream medial entorhinal cortex (MEC), have multiple firing fields located on the vertices of a triangular grid. Also found in the MEC are border cells that fire along the boundaries of an environment, and head direction (HD) cells that fire when the animal's head is facing a particular direction. Using virtual reailty for rats, we explored the contribtion of multiple sensory modalities to the spatial selectivity of these cell types.

The hippocampal cognitive map is thought to be driven by distal visual cues and self-motion cues. In VR place cells showed robust spatial selectivity, however a much smaller proportion were track active, compared to the RW. This indicates that distal visual and non-vestibular self-motion cues are indeed sufficient to provide selectivity, but vestibular and other sensory cues present in RW are necessary to fully activate the place cell population. Additionally, bidirectional cells preferentially encoded distance along the track in VR, but encoded absolute position in RW. Taken together these results suggest the differential contributions of sensory cues in shaping the hippocampal population code.

Similarly, we also measured the activity of grid cells and head direction cells in open field environments in VR and RW. Here, we found that grid cells lost their spatial selectivity and periodicity, demonstrating that the cues available in the VR were insufficient. Most HD cells, likewise, did not retain their directional tuning in a body-fixed VR, suggesting that visual cues might maintain only a partial ability to update the firing directions of HD cells in the absence of reliable angular vestibular cues. However, a small portion of HD cells found to maintain their selectivity in the VR warrant further investigation.

These results provide insight to the contributions of individual sensory modalities to the firing of spatially selective cell types, as well as the mental representation of space.

The dissertation of Ashley Linda Kees is approved.

Mark Frye

Michael Fanselow

Dean Buonomano

Mayank R. Mehta, Committee Chair

University of California, Los Angeles

2015

to Mom and Dad,

who gave me this opportunity

to Taylor,

who always believed in me

to Pascal,

without whom none of this would have been possible

# Table of Contents

# List of Figures and Tables

## CHAPTER 2. METHODS AND MATERIALS DEVELOPED FOR THIS DISSERTATION

Virtual Reality Apparatus



VR Pretraining Protocol



MEC Implantation Surgeries



Spherical Environments in Virtual Reality

# Acknowledgments

**Chapter 2, sections 2 and 3** include excerpts and figures from:

Jesse D. Cushman*, Daniel B. Aharoni*, Bernard Willers, Pascal Ravassard, Ashley Kees, Cliff Vuong, Briana Popeney, Katsushi Arisaka, Mayank R. Mehta. (2013). Multisensory control of multimodal behavior: Do the legs know what the tongue is doing? *PLoS ONE*, *8*(11).

This work was supported by grants to MRM from the National Science Foundation (NSF) Career #0969034, NIH/CRCNS #1-R01-MH- 092925-01, Whitehall foundation and the W. M. Keck foundation. These findings were published in an abstract form at the annual Society for Neuroscience meeting, Abstract # 812.01 and 812.10 (2012). Conceived and designed the experiments: JDC, DBA, MRM. Performed the experiments: JDC, PR, AK, CV, BP. Analyzed the data: DBA, JDC. Wrote the manuscript: JDC, DBA. Built the hardware for these experiments: DBA, BW. Wrote the software for these experiments: DBA, BW. Principal investigators: KA, MRM. We would like to thank Jason Moore, Zhiping Chen and David Ho for their expert technical assistance. Special thanks to Laura Porter for her work on the VR air cushion.

**Chapter 2, section 5**: Special thanks to Laura Porter for helping conduct experiments and performing preliminary analyses. Also thanks to Bernard Willers for designing the spherical virtual environment.

**Chapter 3** is a version of:

Pascal Ravassard*, Ashley Kees*, Bernard Willers*, David Ho, Daniel Aharoni, Jesse Cushman, Zahra M. Aghajan, Mayank R. Mehta. (2013). Multisensory control of hippocampal spatiotemporal selectivity. *Science*, *340*, 1342–6.

This work was supported by the NSF Career award to MRM and grants awarded to MRM from: NIH 5R01MH092925-02 and the W. M. Keck foundation. These findings were presented as two abstracts and posters at the Society for Neuroscience Meeting entitled: P. Ravassard, B. Willers, A. L. Kees, D. Ho, D. Aharoni, M. R. Mehta, 'Directional tuning of place cells in rats performing a virtual landmark navigation task', Soc. Neurosci. Abs. # 812.05 (2012). A. Kees, B. Willers, P.M. Ravassard, D. Ho, D. Aharoni, M. R. Mehta, 'Hippocampal rate and temporal codes in a virtual visual navigation task', Soc. Neurosci. Abs. # 812.07 (2012). PR, AK, DH, JC performed data collection; BW & DA developed the virtual reality system; BW & ZA performed analysis; PR, AK, BW, ZA wrote the manuscript; PR, AK, BW, DH, DA, JC designed the experiment; Principal Investigator: MRM.

**Chapter 4** includes work that has not been submitted for publication.

Contributed to this work: Ashley Kees, Zahra M. Aghajan, Paavana Varanasi, Sophia Shandhu, Bernard Willers, Pascal Ravassard, Mayank R. Mehta.

This work was supported by grants to AK from the NIH: NS058280-04S1 and 1F31MH102969. AK, PV, SS performed data collection; ZA, BW, PV performed analysis; AK, ZA wrote the chapter; AK designed the experiment; PR provided technical assistance (also in Chapter 2, section 4); Principal Investigator: MRM.

For their support, both scientifically and emotionally, I would like to thank Pascal Ravassard, Lavanya Acharya, and Zahra Aghajan.

For their mentorship, I would like to especially acknowledge Dr. Mark Frye and Dr. Felix Schweizer.

And thank you to my committee, Dr. Mayank Mehta, Dr. Dean Buonomano, Dr. Michael Faneslow, and Dr. Mark Frye.

# Vita

## EDUCATION

| | |
|---|---|
| 2009 – present | University of California, Los Angeles<br>Candidate for Doctor of Philosophy in Neuroscience |
| 2005 - 2009 | University of California, Los Angeles<br>Bachelor of Science, Psychobiology, summa cum laude |

## AWARDS & HONORS

| | |
|---|---|
| 2013 | NRSA Predoctoral Fellow<br>NIH Ruth L. Kirschstein National Research Service Award |
| 2012 | Insitutional Training Grant Fellow<br>UCLA Nerual Microcircuits Training Program |
| 2009 | Phi Beta Kappa honor society |

## RESEARCH EXPERIENCE

| | |
|---|---|
| 2010 - present | Graduate Student, University of California, Los Angeles<br>PI: Mayank Mehta, PhD<br>Place and grid cells in virtual environments |
| 2010 | Research Rotation, University of California, Los Angeles<br>PI: Felix Schweizer, PhD<br>The ubiquitin proteasome system in synaptic transmission |
| 2009 | Research Rotation, University of California, Los Angeles<br>PI: Mark Frye, PhD<br>Virtual reality and visual processing in drosophila |
| 2007 - 2009 | Undergraduate Research, University of California, Los Angeles<br>PIs: Elizabeth Bjork, PhD, and Robert Bjork, PhD<br>Retrieval induced forgetting in educational materials |

## TEACHING EXPERIENCE

| | |
|---|---|
| 2014 | Teaching Assistant, Department of Physiological Science<br>University of California, Los Angeles<br>Comparative Animal Physiology |
| 2007 - 2009 | Academic Tutor, Covel Tutoring<br>University of California, Los Angeles<br>Cells, Tissues and Organs; Music Appreciation; Matrices and Probability |

## PUBLICATIONS

Pascal Ravassard*, **Ashley Kees***, Bernard Willers*, David Ho, Daniel Aharoni, Jesse Cushman, Zahra M. Aghajan, Mayank R. Mehta. (2013). Multisensory control of hippocampal spatiotemporal selectivity. *Science*, *340*, 1342–6.

Jesse D. Cushman*, Daniel B. Aharoni*, Bernard Willers, Pascal Ravassard, **Ashley Kees**, Cliff Vuong, Briana Popeney, Katsushi Arisaka, Mayank R. Mehta. (2013). Multisensory control of multimodal behavior: Do the legs know what the tongue is doing? *PLoS ONE*, *8*(11).

## INVITED TALKS

**Ashley Kees**, Pascal Ravassard, Bernard Willers, Mayank R. Mehta (2012). Place cells in real and virtual environments. Neuroscience Interdisciplinary Program Retreat, University of California, Los Angeles.

## POSTER PRESENTATIONS

**A. Kees**, B. Willers, P. Ravassard, D. Ho, D. Aharoni, M. R. Mehta. Hippocampal rate and temporal codes in a virtual visual landmark navigation task. Poster presented at: Neuroscience 2012. 42nd Annual Conference of the Society for Neuroscience; 2012 Oct13-17; New Orleans, LA.

## UNIVERSITY SERVICE

2011 - 2014 Co-organizer, Neuroscience Awesome Research Forum

# Chapter 1

# A Review of Spatially Selective Cell Types

## 1.1 Introduction

Neural representations form the basis of all perceptions. Particular cells fire in response to certain incoming stimuli, and the firing pattern of entire populations forms the neural code. Some cells code for low-level aspects of a stimulus, such as its presence or absence in small receptive fields. Other cells further in processing code for higher-level aspects, and fire in response to particular features or combinations thereof. A classic example of the conversion, or integration, of a neural representation across levels of processing can be found in the visual system. In the retina, photoreceptors fire in response to the presence of certain wavelengths of light in their visual receptive fields. At the next stage of processing, after only a few synapses, neurons in the primary visual cortex no longer respond to spots of light, but to bars of light at particular orientations. There are biologically accurate computational models explaining how the input from cells responding to spots of light can be converted into a signal encoding bars of varying orientations. In this case, the inputs, outputs, and computations performed by this small part of the visual system are well determined.

This bottom-up approach of determining how the sensory inputs determine cell firing has been a common and successful one in the study of the brain. It does not represent the whole story, however, as many neural processes have been found to be much more complicated than

the simple example described above. For example, even within the visual system, there are higher orders of processing such as object recognition whose mechanisms have yet to be understood. In addition, in many sensory systems, the visual system included, it is becoming clear that many representations are highly influenced by feedback loops from extra-sensory brain areas. These top-down processes interact with and modify the representation created by incoming sensory stimuli. Nevertheless, even at high levels of processing, determining the sensory inputs is a useful first step to understanding the system. It is important to remember, however, that other modulatory processes may be playing a role as well.

Several cell types have been discovered that code for stimuli at a very high level of processing. In these cases, the inputs as well as the computations the brain completes to create such a neural representation are not as clear as the example above. The discovery of place cells by O'Keefe and Dostrovsky in 1971 provided a tractable system through which neural representations of highly processed information could be dissected in a bottom-up approach. Place cells, found historically in the mammalian hippocampus, fire when the animal is in a particular location in the environment. These cells thus have place fields, or specific regions of space to which the cells are responsive. Different place cells are responsive to different regions of the environment, such that a full representation of the space can be formed by a small population of these cells. Drawing on the idea of a cognitive map, first suggested by Tolman (1948), O'Keefe and Nadel suggested that hippocampal place cells are the neural basis of spatial cognition (O'Keefe and Nadel, 1978). Importantly, this system maps absolute space in an allocentric framework; that is, the reference frame of the representation is in relation to the external environment. This is in contrast to egocentric maps, found in other brain areas, in which spatial relationships are represented in relation to the animal. Cognitive maps of absolute space are hypothesized to underlie animals' abilities to navigate and form novel paths (Tolman et al., 1946; Tolman, 1948).

How does the brain integrate information across sensory modalities and levels of processing to represent something so complex as an allocentric cognitive map? A neural representation of space must be based on incoming sensory information from the environment, but the cells do not respond directly to any one stimulus or sensory modality. Thus, place cells most likely respond to combinations of highly processed cues. Theoretically, location in the environment could be defined by many different combinations of stimuli: by the local cues present, by the triangulation of distal cues, by a calculation of the animal's own movements. What sensory information, then, do place cells use to determine the animal's location in the environment, thus creating a neural representation of space?

## 1.2 Influences of Sensory Cues on Spatially Selective Cells

### 1.2.1 An overview of typical place cell experiments

The discovery of place cells allowed for the study of a cognitive process to be carried out in the rodent, allowing for a more mechanistic approach than can be achieved in humans. Although place cells and other spatial cells have been reported in rats (O'Keefe and Dostrovsky, 1971), mice (McHugh et al., 1996; Rotenburg et al., 1996), primates (Rolls, 1999; Hori et al., 2003), humans (Ekstrom et al., 2003), and bats (Ulanovsky and Moss, 2007; Yartsev and Ulanovsky, 2013), most of the research continues to be done in rats. In the standard experimental paradigm, a rat is allowed to forage for food rewards in an environment while electrical recordings are made of individual cells in the hippocampus. The recording environment usually consists of an open box either square or circular in shape, with an area on the order of 1 square meter. Rats are naturally curious animals and will obtain adequate coverage of this area in 10-20 minutes. Extracellular voltage recordings are made from chronically implanted electrodes positioned in the pyramidal layer of the hippocampus. In the rat, the size, position, and orientation of the dorsal CA1 make it particularly convenient for

electropysiological recordings. Voltage recordings are analyzed off-line to extract spikes and determine which spikes likely came from the same cell. Typical sessions can include simultaneous activity from tens of active place cells. Video of the rat's position is time-synced with cell firing to determine the spatial activity of the cell.

Many experiments also include a baseline session, where recordings are taken when the rat is not required to perform a task. Ideally, the rat sleeps during such sessions. During sleep, more hippocampal cells will become active than during the task (Thompson and Best, 1989). This is because in any given environment only a portion of the cells will be active; the rest are silent. Of the active hippocampal pyramidal complex-spike cells, however, nearly all will have spatial selectivity (O'Keefe, 1979).

### 1.2.2 An overview of spatially informative sensory cues

There are three broad classes of spatially informative sensory cues: distal cues, self-motion cues, and local cues.

Distal cues are those that are either on or outside the boundaries of the environment; the rat can only approach them from one side, so they can act as strong polarizing cues. While distal cues can be of many modalities, in most experiments they are usually visual, often consisting of one large white cue either on the black walls of the environment, or on a black curtain external to the environment. From different locations in the environment, the views of these distal visual cues will be different in relative size and angle. Triangulation of location using distal visual cues can provide the basis of a spatial representation.

Local cues are those that are within the environment; the animal can approach them from any angle, and they provide an inherently allocentric mapping of space. These tend to be visual, olfactory, or tactile. It is difficult to make an experimental environment completely uniform; inevitably there are small irregularities that the rat can detect. In addition, the rat himself leaves behind scent marks as he explores the environment, presumably as an explicit

navigational aid. Since these cues are difficult to control, they are likely present in most experiments. Spatial information can be easily extracted by local cues. If there is a sufficient amount of varying local cues, every location in an environment could be marked by a unique combination. If place cells were tuned to these associations, they could have firing fields based purely on local cues.

Self-motion cues are those that result from the locomotion of the animal. These include the proprioceptive detection of ambulatory movements, the vestibular sense of both linear and angular acceleration, and optic flow. It is through these cues that animals might be able to perform path integration. Path integration is the ability to take a direct path back to a starting point, even if the outbound journey was not direct. The same calculations underlying path integration could be extended to integrate these egocentric cues into an allocentric representation of current position at all times. Even though all three self-motion cues occur together in a correlated fashion, they provide redundant information about position and it could be possible that one modality is more important than the others for the brain's path integration system.

While all of these types of cues provide spatial information, it is unclear exactly which ones are used in the formation and stability of place fields. Anatomical pathways are consistent with all possibilities. The hippocampus's main input, through the temporoammonic and perforant paths, comes from the entorhinal cortex (Witter et al., 1988; Witter et al., 1989; van Strien et al., 2009), an association cortex that gets no input from thalamus. The entorhinal cortex receives input from many primary sensory cortices as well as other association cortices. It is thought that the entorhinal cortex is a main point of integration before information is sent to the hippocampus. Therefore, although the paths may be indirect, most sensory information reaches the hippocampus and can thus potentially be used to determine spatial selectivity. The purpose of this thesis is to explore the relative influence of different sensory cues on spatial selectivity in cells in the hippocampus and entorhinal cortex.

### 1.2.3 Influences of sensory cues on place cell firing

Since their discovery, a lot of work has been put into trying to determine how place cells encode space and form a cognitive map. The neural representation of space is based on sensory experience, but what particular aspects of that experience are most important? Is triangulation from distal landmarks sufficient for the spatial selectivity of place cells? Do combinations of local cues play a role? Or is path integration based on self-motion inputs the most important contributor to the cognitive map? In all these possibilities, is there a set of cues that are always sufficient, or does this change based on the sensory landscape and task demands on the animal?

Many years of experimental research have resulted in the hypothesis that a combination of self-motion and distal visual cues contributes most heavily to determining the location of place cell firing. When a rat is allowed to explore an environment with a single cue card, place cells will form firing fields. After the rat is removed and subsequently replaced after any length of time, the same cells will have the same firing field locations, meaning the map is stable. If the experimenter moves the location of the cue card, the place fields will also rotate, maintaining the same firing locations relative to the cue card (Muller and Kubie, 1987; Muller et al., 1987). This shows a strong ability of distal visual cues to drive firing locations. Place cells are not performing a simple stimulus response to individual cues, though, because they continue to fire in the same location even if some cues are removed (O'Keefe and Speakman, 1987). Place cells do not depend on visual cues, either, because their firing fields remain intact when the lights are turned off (Quirk et al., 1990). This was initially interpreted to mean that self-motion cues are sufficient for spatial selectivity in place cells. An alternative explanation is that local cues, such as sent marks, are used in the absence of visual information to maintain the representation of space. Consistent with this hypothesis, it was found that when the local olfactory cues are disrupted by cleaning the apparatus, the place cell representation rotates by a random amount, showing that self-motion cues are insufficient for maintaining the orientation

of the place cell map (Save et al., 2000). However, they may play a role in maintaining the relative locations of place fields, independent of their orientation with respect to external cues.

Several experiments demonstrate the importance of self-motion cues in spatial selectivity. When rats are restrained and passively moved about an environment, place cell firing rates drop dramatically (Foster et al., 1989). The authors interpreted this to mean that the ability or intention to move is an important prerequisite in activating place cells, perhaps because of the necessity for a functional path integration system. Alternatively, when the vestibular input is blocked, place cells also lose their spatial selectivity. Presumably, the vestibular sense is a necessary input to the brain's path-integration system, and place cell selectivity depends on this system (Stackman et al., 2002). It is worth mentioning, however, that these results may partially be due to nonspecific effects of the vestibular lesions, such as loss of balance leading to differences in behavior. Thus, corroborating evidence from non-lesion studies will be important.

More graded effects are seen with more mild manipulations of self-motion cues. Removing proprioceptive cues by putting the rat in a cart reduces the spatial information content of place fields. The key difference between this and the Foster study is perhaps that the rat was free to move within the cart and also was responsible for driving it, which reintroduced voluntary locomotion. Spatial information content is further reduced when both proprioceptive and vestibular self-motion cues are removed by moving the scene passively past the animal (Terrazas et al., 2005). Even in studies where self-motion cues are left intact, there is evidence that these cues play a role in determining the locations of at least some firing fields. In one study, rats were trained to run back and forth on a linear track where the location of one of the reward zones changed on every trial, thus making the track different lengths. In these conditions, the place cells that fired close to the moveable reward zone changed their firing positions every trial to maintain a stable relative distance to this reward zone (Gothard et al., 1996; Redish et al., 2000). This means, on laps when the rat was running away from the

moveable reward zone, its firing position was mostly determined by self-motion cues, since the reward zone was outside their field of vision and all other external sensory cues were uncorrelated with the firing location. The authors concluded that firing fields in the beginning of a run are influenced more by self-motion cues, while those further along are influenced more by external cues.

The aforementioned experiments manipulate one type of cue and are important for determining which are involved in place cell selectivity. Studies that put different cues in conflict with one another attempt to dissect the relative influence of different cues in determining firing locations. For example, if a cue card is rotated while the rat is in the environment, this introduces a conflict between that visual cue and all the other external and internal cues. Interestingly enough, when the relative change is a small rotation (45 degrees), the place fields follow the visual cues. But when the change is large (180 degrees), the place fields remain stable (Rotenberg and Muller, 1997). The authors concluded from the small rotation that visual information dominates in the control of firing field locations, because place fields shift even in the face of conflicting self-motion and other static external cues. They conclude further that self-motion is only used when there is a great conflict in the visual cues. This relationship between self-motion and visual cues need not be static, however. Indeed, it has been observed that when cue shifting experiments are repeated, the manipulated cues have a smaller and smaller effect on place cells over time, showing an experience-dependent change in the relative influence of different cues (Knierim et al., 1995; Jeffery, 1998). Taken together, these experiments suggest there is a dynamic relationship between self-motion and visual cues for the control of place cell firing locations that depends on the experimental conditions.

Place cells have been known to interact with other environmental parameters as well. When the walls of a well-known environment are moved, the place cells will stretch in the corresponding directions, maintaining the same position and dimensions relative to the environment walls (O'Keefe and Burgess, 1996). Place cells also remap when the context is

changed, either by changing the ambient odor or colors of an environment (Anderson and Jeffery, 2003), or by changing the task demands (Markus et al., 1995). Similar environments have similar place cell representations, but when the rat is allowed to walk freely between two similar environments, the place cell representations start to orthogonalize (Skaggs and McNaughton, 1998). This differentiation by the place cells is diminished with four similar environments, as all four compartments are represented the same by the place cells (Spiers et al., 2013).

Clearly, place cell firing is influenced by many sensory modalities. The exact hierarchy of their influence remains to be seen, but there is evidence that even when some cues are absent, the hippocampus can use the remaining available cues to maintain at least some spatial selectivity. Accordingly, one of the aims of this thesis is to determine which sensory cues are necessary and sufficient for the spatial selectivity of place cells.

### 1.2.4 Theta and phase precession

Local field potential (LFP) is the difference in the potential in the extracellular medium, compared to an external reference, usually the skull or a distant brain area. The voltage recorded from chronically implanted extracellular wire electrodes includes both the LFP and the superimposed spikes of nearby cells. While it is not completely known, the LFP is usually thought of as the aggregate activity of many nearby neurons and reflects the ionic exchanges through their membranes (for a recent review, see Buzsaki et al., 2012). The resulting signal is similar to EEG, and indeed there are many characteristic signals that appear on both the EEG and LFP. Brain activity recorded either with EEG or LFP has long been described to include a variety of oscillations of different frequencies, which occur in relation to different brain states. One such signal is theta, a prominent oscillation in the 6-12 Hz range. Theta occurs in the hippocampus during a variety of behaviors, including when the rat runs, and also during rapid eye movement (REM) sleep. Both the power and frequency of theta increase with the running

speed of the rat (McFarland et al., 1975). Manipulations involving self-motion cues, especially the vestibular sense, usually result in alterations in theta (Terrazas et al., 2005; Russell et al., 2006).

Theta is an important LFP characteristic to consider when studying the neural representation of space. Not only is it sensitive to self-motion cues, but place cells fire with a specific relation to theta. Place cells tend to fire in bursts, and these bursts are separated by about one theta cycle. So, when a rat runs through a place field, the place cell will fire a few bursts grouped within theta cycles. On each successive theta cycle, the spikes from that cell will occur at earlier and earlier phases of theta, a phenomenon called phase precession (O'Keefe and Recce, 1993). Several models have been suggested to explain how place cells do this (Mehta et al., 2002; Kamondi et al., 1998; Lengyel et al., 2003; also see Harvey et al., 2009), but it is currently unknown what purpose it serves. One theory is that it gives a finer representation of space within the place field (Jensen and Lisman, 2000), or that it assists with memory formation (Skaggs et al., 1996; Mehta et al., 2002; Dragoi and Buzsaki 2006).

### 1.2.5 Influences of sensory cues on grid cell firing

Hippocampal place cells are not the only spatially selective cells in the brain. The medial entorhinal cortex, which is reciprocally connected to the hippocampus (Witter et al., 1989), contains other spatially selective cell types, including grid cells (Fyhn et al., 2004; Hafting et al., 2005), border cells (Solstad et al., 2008), and head direction cells (Sargolini et al., 2006). Grid cells, like place cells, fire only when the rat is in specific locations of the environment. They also display phase precession (Hafting et al., 2008) and rotate with salient visual cues (Hafting et al., 2005). Unlike place cells, however, grid cells have multiple firing fields which are located at the vertices of a triangular lattice. Different grid cells have different spacings between their fields, but all are active in any given environment, and all have firing fields tessellating the entire environment (Hafting et al., 2005). It has been proposed that grid cells provide a spatial metric

onto which the cognitive map can be formed (Fuhs and Touretzky, 2006; McNaughton et al., 2006; Moser et al., 2008).

Grid cells fire in triangular lattices of different spacings, ranging from tens of centimeters to several meters (Brun et al., 2008b). It is now known that there are several modules of grid cells that act somewhat independently of one another. Within each module, grid cells' firing fields will have the same spacing, orientation, and ellipticity, but will be offset in their 2-dimensional phase, meaning that the grid cells in one module will collectively map the entire space. Anatomically, these modules partially overlap, so that two cells adjacent in the brain may belong to separate modules (Stensola et al., 2012). Overall, though, cells belonging to a module with small spacing tend to be in the dorsal part of the MEC, while those with larger spacing tend to be more ventral (Brun et al., 2008b). This dorso-ventral increase in grid scale matches the increase in place field size along the same axis in the hippocampus (Kjelstrup et al., 2008), which also matches their anatomical connections (Witter et al., 1989). Modularity, however, has not been found in the hippocampus, nor has any anatomical or functional clustering, as has been seen in the MEC (Ray et al., 2014; Tang et al., 2014).

It is currently unknown what mechanism allows grid cells to fire in an organized grid pattern. Two major classes of models have been proposed: cell attractor models and dual oscillator models. Dual oscillator models (Burgess et al., 2007; Hasselmo et al., 2007; Blair et al., 2007) claim that peaks in the subthreshold membrane potential of grid cells are created by the summed waveform of two oscillators, each around the frequency of theta. Summing two sine waves results in a waveform that has regularly spaced beats; these beats result in the firing fields of the grid cell. To have firing fields that are stable in space and not time, the beat waveform has to be continually updated by current speed and heading direction information, meaning that at least one of the oscillators needs to change frequency with running speed. Continuous attractor models (Samsonovich and McNaughton, 1997; McNaughton et al., 2006; Fuhs and Touretzky, 2006; Burak and Fiete, 2009), on the other hand, claim that grid cells with

the same spacing but displaced firing fields are connected to each other through recurrent inhibitory connections (Couey et al., 2013). Thus, in the network, there are a high number of stable states; the attractor states of the network. The state of the network, and thus which grid cells are firing, is translocated by information about current speed and heading direction. It should be noted that the two types of models are not mutually exclusive. In both, however, self-motion information is crucial for the spatial selectivity and periodicity of grid cell firing fields.

At least theoretically, self-motion cues are sufficient to produce spatial selectivity and periodicity in grid cells. Empirically, grid fields can persist in the absence of visual cues (Hafting et al., 2005), and grid cells can maintain the same activation and grid pattern in every environment, regardless of the other cues present. These observations are consistent with the hypothesis that grid cells can rely solely on self-motion cues. But there is some evidence showing that grid cells are responsive to other sensory cues.

First, the grid pattern rotates in conjunction with distal visual cues, similar to place cells, meaning that their orientation is updated by visual landmarks (Hafting et al., 2005).

Second, the grid pattern is highly influenced by the boundaries around and within an environment. When an environment is broken into smaller, connected subenvironments by internal boundaries, the grid pattern will only be continuous within each subenvironment and will not maintain a grid over the whole environment. This occurs even when the rat can see the whole environment and when he has had previous experience in the environment without the internal boundaries (Derdikman et al., 2009). This means that self-motion information is insufficient to maintain the grid pattern across subenvironments. Seemingly, the grid network is reset at the entrance to every subenvironment, and is thus influenced by the presence of boundaries. Regardless of the purpose of this resetting, it is clear that environmental boundaries exert control over grid cells, and self-motion cues are not the sole determinant.

Furthermore, there is evidence that grid fields can become associated with particular boundaries in the environment. In a familiar environment, grid cells will maintain their

characteristic spacing. However, if the environment is shortened or lengthened, the spacing will change accordingly in the same dimension (Barry et al., 2007). This happens in a module-dependent manner, with some modules matching the change in the environment and others maintaining their characteristic spacing (Stensola et al., 2012). This phenomenon is not consistent with the hypothesis that self-motion cues are the sole determinant of grid cell selectivity and periodicity; if this were the case, changing the environment dimensions would not affect the spacing of any grid cells. Clearly, grid cells receive sensory input from environmental boundaries, and this input is capable of modifying the locations of firing fields.

Also, like place cells, the task demands can change grid cell firing. When rats perform an alternating task on a T-shaped maze, both the place and grid cells have different firing patterns on the center arm depending on whether it is a left- or right-turn trial (Wood et al., 2000; Frank et al., 2000). It is also known that novelty affects grid cells, presumably because the network is engaged in memory encoding rather than retrieval. Specifically, most grid cells increase their spacing when the environment is novel. This spacing relaxes back to the characteristic spacing of the cell over a period of days (Barry et al., 2012).

Taken together, these findings suggest that although self-motion might be a strong contributor to the spatial selectivity and periodicity of grid cells, they are not the only factor. Boundaries play a strong role, and top-down factors such as task demands and novelty influence their firing as well. It remains to be seen precisely how all these cues interact to influence spatial selectivity and periodicity in grid cells.

### 1.2.6 Influences of sensory cues on border cell firing

Border cells comprise another subset of excitatory cells in the MEC (Solstad et al., 2008). A similar cell type, the boundary vector cell, is found in the subiculum (Lever et al., 2009). Both cell types have firing fields along the borders of environments, and behave similarly under a variety of circumstances. Interestingly, they fire whether the boundary is a wall or the

edge of a raised platform. Because of the physical differences between these two types of boundaries, it is difficult to say which modality of the stimulus is causing border cells to fire. It could be the tactile experience of sharp edges or discontinuities in the visual scene. One might think instead that border cells respond not to some sensory quality of borders, but to some behavioral implication of borders; an inability to traverse, for example. But, boundary vector cells will fire along short walls and small gaps in the surface of the environment, even if these are small enough for the rat to traverse (Lever et al., 2009). It remains unknown then, what is the key information that defines an environmental boundary.

Relatively little data has been reported about border and boundary vector cells. Is it known, however, that these cells fire alongside their preferred boundary even if the boundary is moved or the environment is stretched or compressed. If there are two parallel boundaries in an environment, border and boundary vector cells fire along both. Like other spatially selective cells, these cells also update their preferred boundary to stay in register with a rotated visual cue card, and persist in the dark (Solstad et al., 2008; Lever et al., 2009).

One of the original goals of this thesis was to find the sensory aspects of boundaries that control the firing of border cells. Unfortunately, perhaps due to their low occurrence in the MEC (Solstad et al., 2008), I was unable to record any border cells during the course of the experiment.

### 1.2.7 Influences of sensory cues on head direction cell firing

Head direction (HD) cells fire when the animal's head is facing a particular direction in the allocentric reference frame. These cells do not respond to body direction, egocentric turning directions, or rotations in planes other than those parallel to the rat's plane of motion (Taube et al., 1990a).

Head direction cells are found in many connected brain areas, including the lateral mammillary nucleus (LMN) of the hypothalamus (Stackman and Taube, 1998), the anterior

dorsal nucleus (ADN) of the thalamus (Taube, 1995), the postsubiculum (Taube et al., 1990a and b), the retrosplenial cortex (Chen et al., 1994; Cho and Sharp, 2001), and medial entorhinal cortex (Sargolini et al., 2006). The lateral mammillary nuclei receive input from vestibular brain areas (Groenewegen and van Dijk, 1984; Hayakawa and Zyo, 1984), where cells are tuned to angular head velocity (Bassett and Taube, 2001; Sharp et al., 2001). The LMN and ADN appear to be the origin of the head direction signal; lesions in these areas destroy the head direction signal in all other brain areas (Goodridge and Taube, 1997; Sharp and Koester, 2008). It has been suggested that a ring attractor network creates head direction tuning. According to the model, excitatory connections exist between HD cells with similar tuning angles, and inhibitory between HD cells with different tuning angles. Similar to the continuous attractor network of grid cells, the activity bump of the network is translocated according to vestibular information about angular acceleration (Redish et al., 1996; Zhang, 1996).

Theoretically, angular vestibular cues are sufficient to create a directionally tuned signal. However, we know that distal visual cues play a role as well. Just like place cells, HD cells rotate in conjunction with distal visual cues, either when the rotation is done with the rat outside (Taube et al., 1990b) or inside the apparatus (Goodridge and Taube, 1995). Visual control over place cell rotation seems to act independently from the HD signal, however; place cells will still rotate with visual cues even when the tuning of HD cells is destroyed due to a lesion in ADN. This visual input seems to enter the HD system through the postsubiculum; a lesion in this area not only destroys HD tuning in downstream regions, it also destroys the ability of place cells (Calton et al., 2003) and all other remaining HD cells (Goodridge and Taube, 1997) to update their firing location based on a cue card. Each time the lesioned rat is put into the environment, place cells will adopt a random orientation unrelated to the position of the visual cue. The postsubiculum receives a large input from visual areas and thus is uniquely positioned to integrate visual and head direction information. The postsubiculum also seems to be the brain

area that relays visual information to place cells, somewhat independently of head direction information.

Most of the available data on HD cells is consistent with the hypothesis that angular tuning is controlled primarily by self-motion information with a strong ability of distal visual cues to update orientation. Less is known about the dynamic interaction between these two cues for control of HD preferred firing directions.

### 1.2.8 Interactions between hippocampus and MEC

It is currently unclear whether grid cell information is important for place cell formation or vice versa. The hippocampus and MEC are connected recurrently. MEC layers II and III provide input to the DG/CA3 and CA1 of hippocampus, respectively (Steward and Scoville, 1976). CA1 projects back to MEC layers V and VI (Room and Groenewegen, 1986; Witter et al., 1989). While grid cells are most prominent in layer II, they are present in layers III, V, and VI as well (Sargolini et al., 2006). If feedback loops between the layers of MEC are considered as well, it becomes difficult to make a prediction about where the spatial signal is generated. At the very least, it is known that grid cells, along with other spatial cell types in the MEC, make functional connections with hippocampal place cells (Zhang et al., 2013). Furthermore, it is known that changes in place cells and grid cells happen coherently. First, place and grid cells (and other spatial cell types) rotate coherently when a visual stimulus is rotated (Hargreaves et al., 2007). Further, global remapping in place cells is accompanied by a realignment of the phase of grid cells, while rate remapping is accompanied by no realignment in grid cells (Fyhn et al., 2007), supporting a hypothesis that the spatial selectivity in one brain area is a direct consequence of spatial information in the other.

The spatial firing properties of cells in preweanling rats provide some clue as to where the spatial signal is generated. The spatial firing properties of head direction (Wills et al., 2010; Langston et al., 2010; Bjerknes et al., 2015; Tan et al., 2015) and border cells (Bjerknes et al,

2014) in p16 rats are very similar to those in adults. Place cells are also present at this age, but have lower information content. This improves over days. Grid-like firing properties appear in MEC cells around p22-30 (Wills et al., 2010; Langston et al., 2010). This is consistent with the hypothesis that grid cells require place cell information in order to fire in a spatially selective and periodic fashion.

Lesion studies seem to also support the hypothesis that spatial tuning in place cells can arise independently from grid cell firing, and perhaps grid cells depend on input from the hippocampus. Inactivating the medial septum reduces grid-like firing properties in MEC cells, but spatial tuning in place cells remains intact (Koenig et al., 2011; Brandon et al., 2011). Similarly, selective lesions of layer III of the MEC lowers the information content in hippocampal place cells, but does not destroy their spatial selectivity (Brun et al., 2008a). Lesions of CA3 input to CA1 also do not destroy spatial selectivity in CA1 place cells, suggesting that MEC layer III input is sufficient (Nakashiba et al., 2008). In a recent study, the $GABA_A$ agonist muscimol was injected into the dorsal hippocampus, inhibiting the firing of principal cells in that region. Grid cell firing rates decreased dramatically, and the grid pattern was destroyed. There was no grid pattern even on short time scales, and there was no consistent pattern of firing between grid cells. HD cells remained intact, however, showing that the effect was not the result of a global shut down of the whole brain region. The authors did not conclude from these data that the spatial information from place cells is important for the grid pattern. Instead, they argued that it was merely the excitatory input from the hippocampus that was necessary. They claimed that since grid cells are connected to each other via mainly inhibitory connections, they require an external excitatory input to drive the network (Bonnevie et al., 2013). A manipulation that removes the spatial information content of place cells but not their firing rates would be necessary to determine whether this hypothesis is correct.

In short, it is clear that cell activity between the hippocampus and MEC tend to be correlated, and thus a functional relation exists, but it is unclear which brain area is responsible for the origin of spatial selectivity.

## 1.3 Virtual Reality

### 1.3.1 Introduction

Virtual reality is an emerging tool for studying behavior and cell activity. Use of virtual reality in neuroscience research serves two main advantages over real world environments. First, the animal can be held stationary, which allows for cell recording techniques that require head-fixation, such as 2-photon calcium and voltage-sensitive dye imaging. Virtual reality makes it possible to use these powerful techniques to study spatial activity in neurons. Second, virtual reality allows for precise control of the sensory cues available to the animal. Cues can be taken away or put into conflict with one another in a way that is difficult or even impossible in the real world. In a related vein, virtual reality can allow for the study of environments that have practical limitations in the real world, such as very large environments, or environments that would be otherwise impossible in the real world. This will allow for unprecedented studies about navigation and the hippocampal formation's ability to map environments traditionally unable to be studied in the lab environment. In this thesis, virtual reality was used to control the amount and type of spatial information available so inferences could be made about its specific contribution to cell firing.

### 1.3.2 Use of VR to study spatial cognition in humans and nonhuman primates

Because of technical limitations in performing electrophysiological recordings in human patients, the only studies of spatial cognition in humans have been done with the simplest of virtual reality apparatuses: first-person views of environments on small flat screens. Patients

control the avatar's position with keystrokes and joysticks, rather than walking. Nevertheless, small portions of cells in hippocampal regions display place and grid cell like activity in these conditions (Ekstrom et al., 2003; Jacobs et al., 2013). It is currently unclear whether the small numbers are due to the relative lack of spatially informative cues in the virtual environment, or if it reflects a true difference in proportions of spatially selective cells between humans and rodents.

Also in nonhuman primates, studies are just now beginning in which monkeys are allowed to explore a virtual environment while recordings are made in hippocampal areas. Interestingly, though, cells in the monkey hippocampus have spatial view selectivity, meaning that cells respond when the animal looks at a particular location in space (Rolls et al., 1989; Rolls, 1999). In a related vein, when monkeys visually explore flat images, cells in the entorhinal cortex have grid properties in the visual field (Killian et al., 2012). Similar studies have not yet been done in rodents, but it might be reasonable to expect that due to the ethological differences in the two species, rodent hippocampal cells might not display this property.

It is significant that spatially selective cells have been found in humans and nonhuman primates, but clearly more work needs to be done to reconcile the results from primate and rodent literature. Virtual reality may help make these studies possible.

### 1.3.3 Use of VR to study spatial cognition in rodents

For the past ten years, one basic style of virtual reality apparatus has dominated neuroscience research in rodents. Very recently, several new styles of virtual reality have been introduced, but it is currently unclear how widespread their use will become, and are thus outside the scope of this introduction. The style that has been most used so far consists of a spherical treadmill on top of which the rat or mouse is held (Hölscher et al., 2005). The rodent's walking movements turn the treadmill, the rotation of which is detected by two orthogonally

positioned optical sensors. The image of the virtual environment is displayed on a screen either in front of or surrounding the rodent, and is updated by his movements. The screen is either several monitors or a curved projection screen; these vary in their geometry and the extent to which they fill the rodent's visual field.

An important variation in this basic design is the way in which the rodent is held on top of the spherical treadmill. Most VR apparatuses for mice employ head-fixation. In this version, a metal bar that is permanently affixed to the mouse's skull allows for reversible attachment to the apparatus. This holds the mouse in the apparatus, and also keeps the head completely fixed (Harvey et al., 2009; Dombeck et al., 2010; Youngstrom and Strowbridge, 2012; Chen et al., 2013; Domnisoru et al., 2013; Schmidt-Hieber and Häusser; 2013). This allows for the aforementioned recording techniques that require the head to be still, but also creates a particular sensory experience for the mouse. Specifically, this prevents any linear or angular acceleration of the head, which is usually detected by the vestibular organs in the inner ear. In contrast, most VR apparatuses for rats do not employ head-fixation. Instead, the rats are held in the apparatus with a harness around the rat's chest (Hölscher et al., 2005; Ravassard et al., 2013; Aronov and Tank, 2014). The rat VR apparatus in this thesis work uses body fixation in which the rat is held always facing the same way (Ravassard et al., 2013; Cushman et al., 2013; Aghajan et al., 2014). In contrast, in other rat VR apparatuses, a commutator allows the rats to turn a full 360 degrees on top of the spherical treadmill (Hölscher et al., 2005; Aronov and Tank, 2014). In the body-fixed version, the rat can turn his head and body within the range allowed by the harness, but must turn the spherical treadmill underneath him in order to turn around in the virtual environment. In the body-rotating version, the rat turns himself on top of the spherical treadmill to make a turn. In the former version, the rat receives angular acceleration cues that are largely decorrelated with his movements in the virtual environment; in the latter, the correlation between visual and vestibular cues is maintained. Furthermore, in the latter, the

virtual environment always maintains its orientation relative to any uncontrolled cues in the surrounding room.

Before and during this thesis work, several labs were exploring spatial cognition in virtual environments. First, it was established that rodents could complete spatial tasks in virtual environments (Hölscher et al., 2005; Youngstrom and Strowbridge, 2012). This work was later expanded in our lab to show that rats could navigate virtual environments to locate unmarked locations based on spatial memory of distal visual cues (Cushman et al., 2013). This work was important because it showed behaviorally that rats are capable of learning a representation of the virtual environment sufficient to allow them to navigate. Concurrent with these behavioral studies, other studies showed that place and grid cells in head-fixed mice remained spatially selective on linear tracks (Harvey et al., 2009; Dombeck et al., 2010; Chen et al., 2012; Domnisoru et al., 2013; Schmidt-Hieber and Häusser, 2013). These studies focused on the subthreshold dynamics of place and grid cells, and didn't focus on spatial coding in virtual environments, per say. The first experiments in this thesis tackled that question by comparing the activity of place cells in real and virtual environments. As explained in Chapter 3, we found that while place cells remained spatially selective in virtual linear tracks, their activation, information content, and coding strategies differed, suggesting that place cells do not code virtual environments exactly the same as real world environments, perhaps due to the differences in available sensory cues (Ravassard et al., 2013). To date, no similar comparison has been done with grid cells in this particular VR apparatus.

Since place and grid cells were spatially selective on virtual linear tracks in both head-fixed mice and body-fixed rats, it seemed safe to assume they would be spatially selective in virtual open fields as well. This is exactly what was found in a body-rotating version of the VR (Aronov and Tank, 2014). Interestingly, our lab, which uses a body-fixed version of virtual reality, found that place cells lost their spatial selectivity in such environments (Aghajan et al., 2014). Chapter 4 will explore my preliminary data suggesting that grid and head direction cells

similarly lose their selectivity. The next step for the field will be to determine exactly which differences between the two VR apparatuses caused either the presence or absence of spatial selectivity. This will be very useful in determining the key sensory modalities governing place and grid cell firing.

## 1.4 Goals of the Dissertation

In sum, it is not yet clear which sensory cues are crucial in the firing of spatially selective cell types. Virtual reality provides a unique opportunity to precisely control which sensory cues are spatially informative, and thus allows us to make inferences about each sensory modality's contribution to spatial firing. In addition, a detailed characterization of firing properties in the VR compared to RW will provide a basis for interpretation of future studies using VR.

In Chapter 2, I provide a description of the methods and materials I was involved in optimizing for this thesis work. I helped with some hardware elements of the VR apparatus, and also took part in creating a protocol to train the rats to complete tasks in virtual reality. Also in this chapter, I describe my attempts to learn and optimize how to chronically implant tetrodes to record grid cells, HD cells, and border cells in the MEC and surrounding areas. Last, I include some behavioral data from rats running on a small spherical environment in virtual reality. To my knowledge, this is the first report of rat behavior in a virtual environment of such geometry.

Chapter 3 is an expanded version of previously published work. Here, we compared the properties in both the rate and temporal code of hippocampal place cells in similar linear tracks in RW and VR. We found that place cells retain their spatial selectivity in VR, but fewer place cells are activated, and those that are have wider place fields. In addition, cells that have place fields in both running directions code for absolute position in RW, but distance in VR. We concluded that the self-motion and distal visual cues available in the VR are sufficient for some spatial selectivity in place cells, but local cues are necessary for activation of place cells, fine

tuning of place fields, and coding of position rather than distance. For the temporal code, we found that despite an overall reduction in theta frequency and a loss of speed dependence of theta, phase precession in place cells remained intact. This puts constraints on models of phase precession.

Chapter 4 includes unpublished preliminary data collected from the MEC. In this project, we compared the activity of grid and HD cells in similar open fields in RW and VR. Unlike the previously described results in place cells, we found that spatial selectivity of grid cells was completely destroyed in VR. From this, we concluded that the self-motion and distal visual cues that were spatially informative in VR were insufficient to produce spatial selectivity. For HD cells, we found that while most cells lose their directional tuning in the VR, some maintain it, raising questions about what determines the relative influence of distal visual and angular acceleration cues on HD tuning. In addition, some evidence was found supporting the hypothesis that in VR, the preferred firing directions of HD cells constantly shift relative to the VR frame of reference, opening up new possibilities for decoding the activity of HD and grid cells in VR.

Overall, the results presented in this thesis allow us to make conclusions about the smallest set of sensory cues required to elicit spatially selective firing in place, grid, and head direction cells. Furthermore, the differences between firing in RW and VR constrain the questions that can be answered using this technique.

## 1.5 References

Hasselmo, M. E., Giocomo, L. M., & Zilli, E. A. (2007). An oscillatory interference model of grid cell firing. *Hippocampus*, *17*, 1252–71.

Aghajan, Z. M., Acharya, L., Moore, J. J., Cushman, J. D., Vuong, C., & Mehta, M. R. (2014). Impaired spatial selectivity and intact phase precession in two-dimensional virtual reality. *Nature Publishing Group*, *18*(1), 121–128. Nature Publishing Group.

Anderson, M. I., & Jeffery, K. J. (2003). Heterogeneous modulation of place cell firing by changes in context. *The Journal of neuroscience : the official journal of the Society for Neuroscience*, *23*(26), 8827–8835.

Aronov, D., & Tank, D. W. (2014). Engagement of Neural Circuits Underlying 2D Spatial Navigation in a Rodent Virtual Reality System. *Neuron*, *84*(2), 442–456. Elsevier Inc.

Barry, C., Ginzberg, L. L., O'Keefe, J., & Burgess, N. (2012). Grid cell firing patterns signal environmental novelty by expansion. *Proceedings of the National Academy of Sciences*, *109*(43), 17687–17692.

Barry, C., Hayman, R., Burgess, N., & Jeffery, K. J. (2007). Experience-dependent rescaling of entorhinal grids. *Nature neuroscience*, *10*(6), 682–4.

Bassett, J. P., & Taube, J. S. (2001). Neural correlates for angular head velocity in the rat dorsal tegmental nucleus. *The Journal of neuroscience : the official journal of the Society for Neuroscience*, *21*(15), 5740–5751.

Bjerknes, T. L., Langston, R. F., Kruge, I. U., Moser, E. I., & Moser, M. (2015). Coherence among Head Direction Cells before Eye Opening in Rat Pups. *Current Biology*, *25*(1), 103–108. Elsevier Ltd.

Bjerknes, T. L., Moser, E. I., & Moser, M. B. (2014). Representation of geometric borders in the developing rat. *Neuron*, *82*(1), 71–78. Elsevier Inc.

Blair, H. T., Welday, A. C., & Zhang, K. (2007). Scale-invariant memory representations emerge from moiré interference between grid fields that produce theta oscillations: a computational model. *The Journal of neuroscience : the official journal of the Society for Neuroscience*, *27*(12), 3211–3229.

Bonnevie, T., Dunn, B., Fyhn, M., Hafting, T., Derdikman, D., Kubie, J. L., Roudi, Y., et al. (2013). Grid cells require excitatory drive from the hippocampus. *Nature neuroscience*, *16*(3), 309–17.

Brandon, M. P., Bogaard, A. R., Libby, C. P., Connerney, M. A., Gupta, K., & Hasselmo, M. E. (2011). Reduction of Theta Rhythm Dissociates Grid Cell Spatial Periodicity from Directional Tuning. *Science*, *332*, 595–599.

Brun, V. H., Leutgeb, S., Wu, H. Q., Schwarcz, R., Witter, M. P., Moser, E. I., & Moser, M. B. (2008a). Impaired Spatial Representation in CA1 after Lesion of Direct Input from Entorhinal Cortex. *Neuron*, *57*, 290–302.

Brun, V. H., Solstad, T., Kjelstrup, K. B., Fyhn, M., Witter, M. P., Moser, E. I., & Moser, M. B. (2008b). Progressive increase in grid scale from dorsal to ventral medial entorhinal cortex. *Hippocampus*, *18*, 1200–1212.

Burak, Y., & Fiete, I. R. (2009). Accurate path integration in continuous attractor network models of grid cells. *PLoS Computational Biology*, *5*(2), 1–16.

Burgess, N., Barry, C., & O'Keefe, J. (2007). An oscillatory interference model of grid cell firing. *Hippocampus*, *17*, 801–812.

Buzsáki, G., Anastassiou, C. A., & Koch, C. (2012). The origin of extracellular fields and currents — EEG, ECoG, LFP and spikes. *Nature Reviews Neuroscience*, *13*(6), 407–420. Nature Publishing Group.

Calton, J. L., Stackman, R. W., Goodridge, J. P., Archey, W. B., Dudchenko, P. A., & Taube, J. S. (2003). Hippocampal place cell instability after lesions of the head direction cell network. *The Journal of neuroscience : the official journal of the Society for Neuroscience*, *23*(30), 9719–9731.

Chen, G., King, J. A., Burgess, N., & O'Keefe, J. (2013). How vision and movement combine in the hippocampal place code. *Proceedings of the National Academy of Sciences of the United States of America*, *110*(1), 378–83.

Chen, L. L., Lin, L. H., Green, E. J., Barnes, C. A., & McNaughton, B. L. (1994). Head-direction cells in the rat posterior cortex. I. Anatomical distribution and behavioral modulation. *Experimental brain research.*, *101*, 8–23.

Cho, J., & Sharp, P. E. (2001). Head direction, place, and movement correlates for cells in the rat retrosplenial cortex. *Behavioral neuroscience*, *115*(1), 3–25.

Couey, J. J., Witoelar, A., Zhang, S.-J., Zheng, K., Ye, J., Dunn, B., Czajkowski, R., Moser, M.-B., Moser, E. I., Roudi, Y., Witter, M. P. (2013). Recurrent inhibitory circuitry as a mechanism for grid formation. *Nature neuroscience*, *16*(3), 318–24. Nature Publishing Group.

Cushman, J. D., Aharoni, D. B., Willers, B., Ravassard, P., Kees, A., Vuong, C., Popeney, B., Arisaka, K., Mehta, M. R. (2013). Multisensory control of multimodal behavior: Do the legs know what the tongue is doing? *PLoS ONE*, *8*(11).

Derdikman, D., Whitlock, J. R., Tsao, A., Fyhn, M., Hafting, T., Moser, M.-B., & Moser, E. I. (2009). Fragmentation of grid cell maps in a multicompartment environment. *Nature neuroscience*, *12*(10), 1325–32. Nature Publishing Group.

Dombeck, D. A., Harvey, C. D., Tian, L., Looger, L. L., & Tank, D. W. (2010). Functional imaging of hippocampal place cells at cellular resolution during virtual navigation. *Nature neuroscience*, *13*(11), 1433–40.

Domnisoru, C., Kinkhabwala, A. A., & Tank, D. W. (2013). Membrane potential dynamics of grid cells. *Nature*, 1–26.

Dragoi, G., & Buzsáki, G. (2006). Temporal Encoding of Place Sequences by Hippocampal Cell Assemblies. *Neuron*, *50*, 145–157.

Ekstrom, A. D., Kahana, M. J., Caplan, J. B., Fields, T. A., Isham, E. A., Newman, E. L., & Fried, I. (2003). Cellular networks underlying human spatial navigation. *Nature*, *425*(September), 184–188.

Foster, T. C., Castro, C. A., & McNaughton, B. L. (1989). Spatial selectivity of rat hippocampal neurons: dependence on preparedness for movement. *Science (New York, N.Y.)*, *244*, 1580–1582.

Frank, L. M., Brown, E. N., & Wilson, M. (2000). Trajectory encoding in the hippocampus and entorhinal cortex. *Neuron*, *27*, 169–178.

Fuhs, M. C., & Touretzky, D. S. (2006). A spin glass model of path integration in rat medial entorhinal cortex. *The Journal of neuroscience : the official journal of the Society for Neuroscience*, *26*(16), 4266–4276.

Fyhn, M., Hafting, T., Treves, A., Moser, M.-B., & Moser, E. I. (2007). Hippocampal remapping and grid realignment in entorhinal cortex. *Nature*, *446*(7132), 190–4.

Fyhn, M., Molden, S., Witter, M. P., Moser, E. I., & Moser, M.-B. (2004). Spatial representation in the entorhinal cortex. *Science (New York, N.Y.)*, *305*(August), 1258–1264.

Goodridge, J. P., & Taube, J. S. (1995). Preferential use of the landmark navigational system by head direction cells in rats. *Behavioral neuroscience*, *109*(1), 49–61.

Goodridge, J. P., & Taube, J. S. (1997). Interaction between the postsubiculum and anterior thalamus in the generation of head direction cell activity. *The Journal of neuroscience : the official journal of the Society for Neuroscience*, *17*(23), 9315–9330.

Gothard, K. M., Skaggs, W. E., & McNaughton, B. L. (1996). Dynamics of Mismatch Correction in the Hippocampal Ensemble Code for Space: Interaction between Path Integration and Environmental Cues. *J. Neurosci.*, *16*(24), 8027–8040.

Groenewegen, H. J., & Van Dijk, C. A. (1984). Efferent connections of the dorsal tegmental region in the rat, studied by means of anterograde transport of the lectin Phaseolus vulgaris-leucoagglutinin (PHA-L). *Brain Research*, *304*(1984), 367–371.

Hafting, T., Fyhn, M., Bonnevie, T., Moser, M.-B., & Moser, E. I. (2008). Hippocampus-independent phase precession in entorhinal grid cells. *Nature*, *453*(7489), 1248–1252.

Hafting, T., Fyhn, M., Molden, S., Moser, M.-B., & Moser, E. I. (2005). Microstructure of a spatial map in the entorhinal cortex. *Nature*, *436*(August), 801–806.

Hargreaves, E. L., Yoganarasimha, D., & Knierim, J. J. (2007). Cohestiveness of spatial and directional representations recorded from neural ensembles in the anterior thalamus, parasubiculus, medial entorhinal cortex, and hippocampus. *Hippocampus*, *17*, 826–841.

Harvey, C. D., Collman, F., Dombeck, D. A., & Tank, D. W. (2009). Intracellular dynamics of hippocampal place cells during virtual navigation. *Nature*, *461*(7266), 941–6. Nature Publishing Group.

Hasselmo, M. E., Giocomo, L. M., & Zilli, E. A. (2007). An oscillatory interference model of grid cell firing. *Hippocampus*, *17*, 1252–71.

Hayakawa, T., & Zyo, K. (1984). Comparative anatomical study of the tegmentomammillary projections in some mammals: A horseradish peroxidase study. *Brain Research*, *300*, 335–349.

Hölscher, C., Schnee, A., Dahmen, H., Setia, L., & Mallot, H. A. (2005). Rats are able to navigate in virtual environments. *The Journal of experimental biology*, *208*, 561–9.

Hori, E., Tabuchi, E., Matsumura, N., Tamura, R., Eifuku, S., Endo, S., Nishijo, H., Ono, T. (2003). Representation of place by monkey hippocampal neurons in real and virtual translocation. *Hippocampus*, *13*(February 2002), 190–196.

Jacobs, J., Weidemann, C. T., Miller, J. F., Solway, A., Burke, J. F., Wei, X.-X., Suthana, N., Sperling, M. R., Sharan, A. D., Fried, I., Kahana, M. J. (2013). Direct recordings of grid-like neuronal activity in human spatial navigation. *Nature neuroscience*, *16*(9), 1188–90.

Jeffery, K. J. (1998). Learning of landmark stability and instability by hippocampal place cells. *Neuropharmacology*, *37*(4-5), 677–87.

Jensen, O., & Lisman, J. E. (2000). Position reconstruction from an ensemble of hippocampal place cells: contribution of theta phase coding. *Journal of neurophysiology*, *83*, 2602–2609.

Kamondi, A., Ascady, L., Wang, X.-J., & Buzsaki, G. (1998). Theta Oscillations in Soma and Dendrites of Hippocampal Pyramidal Cells In Vivo: Activity-Dependent Phase-Precession of Action Potentials. *Hippocampus*, *8*, 244–261.

Killian, N. J., Jutras, M. J., & Buffalo, E. A. (2012). A map of visual space in the primate entorhinal cortex. *Nature*, *491*(7426), 761–4. Nature Publishing Group.

Kjelstrup, K. B., Solstad, T., Brun, V. H., Hafting, T., Leutgeb, S., Witter, M. P., Moser, E. I., Moser, M.-B. (2008). Finite Scale of Spatial Representation in the Hippocampus. *Science*, *321*, 140–143.

Knierim, J. J., Kudrimoti, H. S., & McNaughton, B. L. (1995). Place cells, head direction cells, and the learning of landmark stability. *The Journal of neuroscience : the official journal of the Society for Neuroscience*, *15*, 1648–1659.

Koenig, J., Linder, A. N., Leutgeb, J. K., & Leutgeb, S. (2011). The Spatial Periodicity of Grid Cells. *Science*, *332*, 592–595.

Langston, R. F., Ainge, J. A., Couey, J. J., Canto, C. B., Bjerknes, T. L., Witter, M. P., Moser, E. I., Moser, M.-B. (2010). Development of the spatial representation system in the rat. *Science (New York, N.Y.)*, *328*(2010), 1576–1580.

Lengyel, M., Szatmáry, Z., & Érdi, P. (2003). Dynamically detuned oscillations account for the coupled rate and temporal code of place cell firing. *Hippocampus*, *13*, 700–714.

Lever, C., Burton, S., Jeewajee, A., O'Keefe, J., & Burgess, N. (2009). Boundary vector cells in the subiculum of the hippocampal formation. *The Journal of neuroscience : the official journal of the Society for Neuroscience*, *29*(31), 9771–9777.

Markus, E. J., Qin, Y. L., Leonard, B., Skaggs, W. E., McNaughton, B. L., & Barnes, C. A. (1995). Interactions between location and task affect the spatial and directional firing of hippocampal neurons. *The Journal of neuroscience : the official journal of the Society for Neuroscience*, *15*(11), 7079–7094.

McFarland, W. L., Teitelbaum, H., & Hedges, E. K. (1975). Relationship between hippocampal theta activity and running speed in the rat. *Journal of comparative and physiological psychology*, *88*(1), 324–328.

McHugh, T. J., Blum, K. I., Tsien, J. Z., Tonegawa, S., & Wilson, M. A. (1996). Impaired hippocampal representation of space in CA1-specific NMDAR1 knockout mice. *Cell*, *87*, 1339–1349.

McNaughton, B. L., Battaglia, F. P., Jensen, O., Moser, E. I., & Moser, M.-B. (2006). Path integration and the neural basis of the "cognitive map". *Nature reviews. Neuroscience*, *7*(August), 663–678.

Mehta, M. R., Lee, A. K., & Wilson, M. A. (2002). Role of experience and oscillations in transforming a rate code into a temporal code. *Nature*, *417*, 741–746.

Moser, E. I., Kropff, E., & Moser, M.-B. (2008). Place cells, grid cells, and the brain's spatial representation system. *Annual review of neuroscience*, *31*, 69–89.

Muller, R. U., & Kubie, J. L. (1987). The Effects of Changes in the Environment Hippocampal Cells on the Spatial Firing of. *Journal of Neuroscience*, *7*(July), 1951–1968.

Muller, R. U., Kubie, J. L., & Ranck, J. B. (1987). Spatial firing patterns of hippocampal complex-spike cells in a fixed environment. *The Journal of neuroscience : the official journal of the Society for Neuroscience*, *7*(July), 1935–1950.

Nakashiba, T., Young, J. Z., McHugh, T. J., Buhl, D. L., & Tonegawa, S. (2008). Transgenic inhibition of synaptic transmission reveals role of CA3 output in hippocampal learning. *Science (New York, N.Y.)*, *319*(2008), 1260–1264.

O'Keefe, J. (1979). A review of the hippocampal place cells. *Progress in Neurobiology*, *13*, 419–439.

O'Keefe, J., & Burgess, N. (1996). Geometric determinants of the place fields of hippocampal neurons. *Nature*.

O'Keefe, J., & Dostrovsky, J. (1971). The hippocampus as a spatial map. Preliminary evidence from unit activity in the freely-moving rat. *Brain research*, *34*, 171–175.

O'Keefe, J., Nadel, L. (1978). *The Hippocampus as a Cognitive Map*. Oxford: Oxford University Press

O'Keefe, J., & Recce, M. L. (1993). Phase relationship between hippocampal place units and the EEG theta rhythm. *Hippocampus*, *3*(3), 317–330.

O'Keefe, J., & Speakman, A. (1987). Single unit activity in the rat hippocampus during a spatial memory task. *Experimental Brain Research*, *68*, 1–27.

Quirk, G. J., Muller, R. U., & Kubie, J. L. (1990). The Firing of Hippocampal Place Cells in the Dark Depends on the Rat's Recent Experience. *Journal of Neurophysiology*, *10*(June 1990), 2008–2017.

Ravassard, P., Kees, A., Willers, B., Ho, D., Aharoni, D., Cushman, J., Aghajan, Z. M., Mehta, M. R. (2013). Multisensory control of hippocampal spatiotemporal selectivity. *Science (New York, N.Y.)*, *340*, 1342–6.

Ray, S., Naumann, R., Burgalossi, A., Tang, Q., Schmidt, H., & Brecht, M. (2014). Grid-layout and theta-modulation of layer 2 pyramidal neurons in medial entorhinal cortex. *Science (New York, N.Y.)*, *343*(6173), 891–6.

Redish, A. D., Rosenzweig, E. S., Bohanick, J. D., McNaughton, B. L., & Barnes, C. A. (2000). Dynamics of Hippocampal Ensemble Activity Realignment: Time versus Space. *J. Neurosci.*, *20*(24), 9298–9309.

Redish, A., Elga, A., & Touretzky, D. (1996). A coupled attractor model of the rodent head direction system. *Network: Computation in Neural Systems*, *7*(4), 671–685.

Rolls, E. T. (1999). Spatial view cells and the representation of place in the primate hippocampus. *Hippocampus*, *9*, 467–480.

Rolls, E. T., Miyashita, Y., Cahusac, P. M. B., Kesner, R. P., Niki, H., Feigenbaum, J. D., & Bach, L. (1989). Hippocampal Neurons in the Monkey Place in Which a Stimulus Is Shown Activity Related. *J Neurosci*, *9*(June), 1835–1845.

Room, P., & Groenewegen, H. J. (1986). Connections of the Parahippocampal Cortex. I. Cortical Afferents. *The Journal of comparative neurology*, *251*, 415–450.

Rotenberg, A., & Muller, R. U. (1997). Variable place-cell coupling to a continuously viewed stimulus: evidence that the hippocampus acts as a perceptual system. *Philosophical transactions of the Royal Society of London. Series B, Biological sciences*, *352*, 1505–1513.

Rotenberg, A., Mayford, M., Hawkins, R. D., Kandel, E. R., & Muller, R. U. (1996). Mice expressing activated CaMKII lack low frequency LTP and do not form stable place cells in the CA1 region of the hippocampus. *Cell*, *87*(1971), 1351–1361.

Russell, N. A., Horii, A., Smith, P. F., Darlington, C. L., & Bilkey, D. K. (2006). Lesions of the vestibular system disrupt hippocampal theta rhythm in the rat. *Journal of neurophysiology*, *96*, 4–14.

Samsonovich, A., & McNaughton, B. L. (1997). Path integration and cognitive mapping in a continuous attractor neural network model. *The Journal of neuroscience : the official journal of the Society for Neuroscience*, *17*(15), 5900–20.

Sargolini, F., Fyhn, M., Hafting, T., McNaughton, B. L., Witter, M. P., Moser, M.-B., & Moser, E. I. (2006). Conjunctive representation of position, direction, and velocity in entorhinal cortex. *Science*, *312*, 758–62.

Save, E., Nerad, L., & Poucet, B. (2000). Contribution of multiple sensory information to place field stability in hippocampal place cells. *Hippocampus*, *10*(1), 64–76.

Schmidt-Hieber, C., & Häusser, M. (2013). Cellular mechanisms of spatial navigation in the medial entorhinal cortex. *Nature neuroscience*, *16*(3), 325–31. Nature Publishing Group.

Sharp, P. E., & Koester, K. (2008). Lesions of the mammillary body region severely disrupt the cortical head direction, but not place cell signal. *Hippocampus*, *18*, 766–784.

Sharp, P. E., Tinkelman, A., & Cho, J. (2001). Angular velocity and head direction signals recorded from the dorsal tegmental nucleus of gudden in the rat: implications for path integration in the head direction cell circuit. *Behavioral neuroscience*, *115*(3), 571–588.

Skaggs, W. E., & McNaughton, B. L. (1998). Spatial firing properties of hippocampal CA1 populations in an environment containing two visually identical regions. *The Journal of neuroscience : the official journal of the Society for Neuroscience*, *18*(20), 8455–66.

Skaggs, W. E., McNaughton, B. L., Wilson, M. A., & Barnes, C. A. (1996). Theta phase precession in hippocampal neuronal populations and the compression of temporal sequences. *Hippocampus*.

Solstad, T., Solstad, T., Boccara, C. N., Boccara, C. N., Kropff, E., Kropff, E., Moser, M.-B., Moser, E. I. (2008). Representation of geometric borders in the entorhinal cortex. *Science*, *322*(December), 1865–1868.

Spiers, H. J., Hayman, R. M. A., Jovalekic, A., Marozzi, E., & Jeffery, K. J. (2013). Place Field Repetition and Purely Local Remapping in a Multicompartment Environment. *Cerebral cortex (New York, N.Y. : 1991)*, 1–16.

Stackman, R. W., Clark, A. S., & Taube, J. S. (2002). Hippocampal spatial representations require vestibular input. *Hippocampus*, *12*(3), 291–303.

Stackman, R. W., & Taube, J. S. (1998). Firing properties of rat lateral mammillary single units: head direction, head pitch, and angular head velocity. *The Journal of neuroscience : the official journal of the Society for Neuroscience*, *18*(21), 9020–9037.

Stensola, H., Stensola, T., Solstad, T., Frøland, K., Moser, M.-B., & Moser, E. I. (2012). The entorhinal grid map is discretized. *Nature*, *492*(7427), 72–8. Nature Publishing Group.

Steward, O., & Scoville, S. A. (1976). Cells of origin of entorhinal cortical afferents to the hippocampus and fascia dentata of the rat. *The Journal of comparative neurology*, *169*(3), 347–370.

van Strien, N. M., Cappaert, N. L. M., & Witter, M. P. (2009). The anatomy of memory: an interactive overview of the parahippocampal-hippocampal network. *Nature reviews. Neuroscience*, *10*, 272–282.

Tan, H. M., Bassett, J. P., O'Keefe, J., Cacucci, F., & Wills, T. J. (2015). The Development of the Head Direction System before Eye Opening in the Rat. *Current Biology*, *25*(4), 479–483.

Tang, Q., Burgalossi, A., Ebbesen, C. L., Ray, S., Naumann, R., Schmidt, H., Spicher, D., Brecht, M. (2014). Pyramidal and Stellate Cell Specificity of Grid and Border Representations in Layer 2 of Medial Entorhinal Cortex. *Neuron*, *84*(6), 1191–1197.

Taube, J. S. (1995). Head direction cells recorded in the anterior thalamic nuclei of freely moving rats. *The Journal of neuroscience : the official journal of the Society for Neuroscience*, *15*(January), 70–86.

Taube, J. S., Muller, R. U., & Ranck, J. B. (1990a). Head-direction cells recorded from the postsubiculum in freely moving rats. I. Description and quantitative analysis. *The Journal of neuroscience : the official journal of the Society for Neuroscience*, *10*(February), 420–435.

Taube, J. S., Muller, R. U., & Ranck, J. B. (1990b). Head-direction cells recorded from the postsubiculum in freely moving rats. II. Effects of environmental manipulations. *The Journal of neuroscience : the official journal of the Society for Neuroscience*, *10*(February), 436–447.

Terrazas, A., Krause, M., Lipa, P., Gothard, K. M., Barnes, C. A., & McNaughton, B. L. (2005). Self-motion and the hippocampal spatial metric. *The Journal of neuroscience : the official journal of the Society for Neuroscience*, *25*(35), 8085–96.

Thompson, L. T., & Best, P. J. (1989). Place cells and silent cells in the hippocampus of freely-behaving rats. *The Journal of neuroscience : the official journal of the Society for Neuroscience*, *9*(July), 2382–2390.

Tolman, E. C. (1948). Cognitive maps in rats and men. *Psychological review*, *55*(4), 189–208.

Tolman, E. C., Ritchie, B. F., & Kalish, D. (1946). Studies in spatial learning: Orientation and the short-cut. *Journal of experimental psychology*, *36*, 13–24.

Ulanovsky, N., & Moss, C. F. (2007). Hippocampal cellular and network activity in freely moving echolocating bats. *Nature neuroscience*, *10*(2), 224–233.

Wills, T. J., Cacucci, F., Burgess, N., & O'Keefe, J. (2010). Development of the hippocampal cognitive map in preweanling rats. *Science (New York, N.Y.)*, *328*, 1573–1576.

Witter, M. P., Griffioen, A. W., Jorritsma-Byham, B., & Krijnen, J. L. (1988). Entorhinal projections to the hippocampal CA1 region in the rat: an underestimated pathway. *Neuroscience letters*, *85*(2), 193–198.

Witter, M. P., Groenewegen, H. J., Lopes da Silva, F. H., & Lohman, A. H. M. (1989). Functional organization of the extrinsic and intrinsic circuitry of the parahippocampal region. *Progress in Neurobiology*, *33*, 161–253.

Wood, E. R., Dudchenko, P. A., Robitsek, R. J., & Eichenbaum, H. (2000). Hippocampal neurons encode information about different types of memory episodes occurring in the same location. *Neuron*, *27*, 623–633.

Yartsev, M. M., & Ulanovsky, N. (2013). Representation of Three-Dimensional Space in the Hippocampus of Flying Bats. *Science*, *340*(April), 367–372.

Youngstrom, I. A., & Strowbridge, B. W. (2012). Visual landmarks facilitate rodent spatial navigation in virtual reality environments. *Learning & Memory*, *19*, 84–90.

Zhang, K. (1996). Representation of spatial orientation by the intrinsic dynamics of the head-direction cell ensemble: a theory. *The Journal of neuroscience : the official journal of the Society for Neuroscience*, *16*(6), 2112–2126.

Zhang, S.-J., Ye, J., Miao, C., Tsao, A., Cerniauskas, I., Ledergerber, D., Moser, M.-B., Moser, E. I. (2013). Optogenetic dissection of entorhinal-hippocampal functional connectivity. *Science (New York, N.Y.)*, *340*(6128).

# Chapter 2

# Methods and Materials Developed for this Dissertation

## 2.1 Introduction

This chapter details the methodological developments that I was involved in making during the course of my thesis. In order to explore the effects of multimodal stimuli on the mental representation of space, we needed a virtual reality apparatus suitable for rats and a training protocol to optimize behavioral performance. For the second experiment in this thesis work, it was necessary to implant electrodes in the medial entorhinal cortex of rats, a procedure that had not yet been performed in my thesis lab. Finally, one of the original aims of this thesis was to analyze the firing properties of grid cells in environments without borders, so the appropriate VR tracks and training protocol had to be designed to achieve this goal. Included is a preliminary analysis of rat behavior in this virtual environment.

## 2.2 Virtual Reality Apparatus

### 2.2.1 Introduction

The VR hardware was developed by Daniel Aharoni and the software by Bernard Willers. The VR system contains a Styrofoam sphere that floats freely on an air cushion (Fig 2.1A and B). A hinged harness holds the rat on the Styrofoam ball (Fig 2.1C). The ball rotation is measured by two sensors (ADNS-9500, Avago) and used by custom software to change the

surrounding visual scene. When the rat turns the Styrofoam ball underneath him, either by walking forward or turning, there is a corresponding one-to-one change in the visual scene. A micro projector (MPro160, 3M) projects visual stimuli on a convex mirror, which reflects the stimuli onto a cylindrical screen (Hollywood Lamp & Shade, Hollywood, CA). Our VR system allows presentation of an undistorted visual scene of any dimensions in all directions around the rat (Fig 2.1D and E). A stainless steel tube mounted in front of the rat dispenses liquid rewards. VR data, including the animal's virtual speed, position and heading, are recorded by the software at a sampling rate of 60Hz.

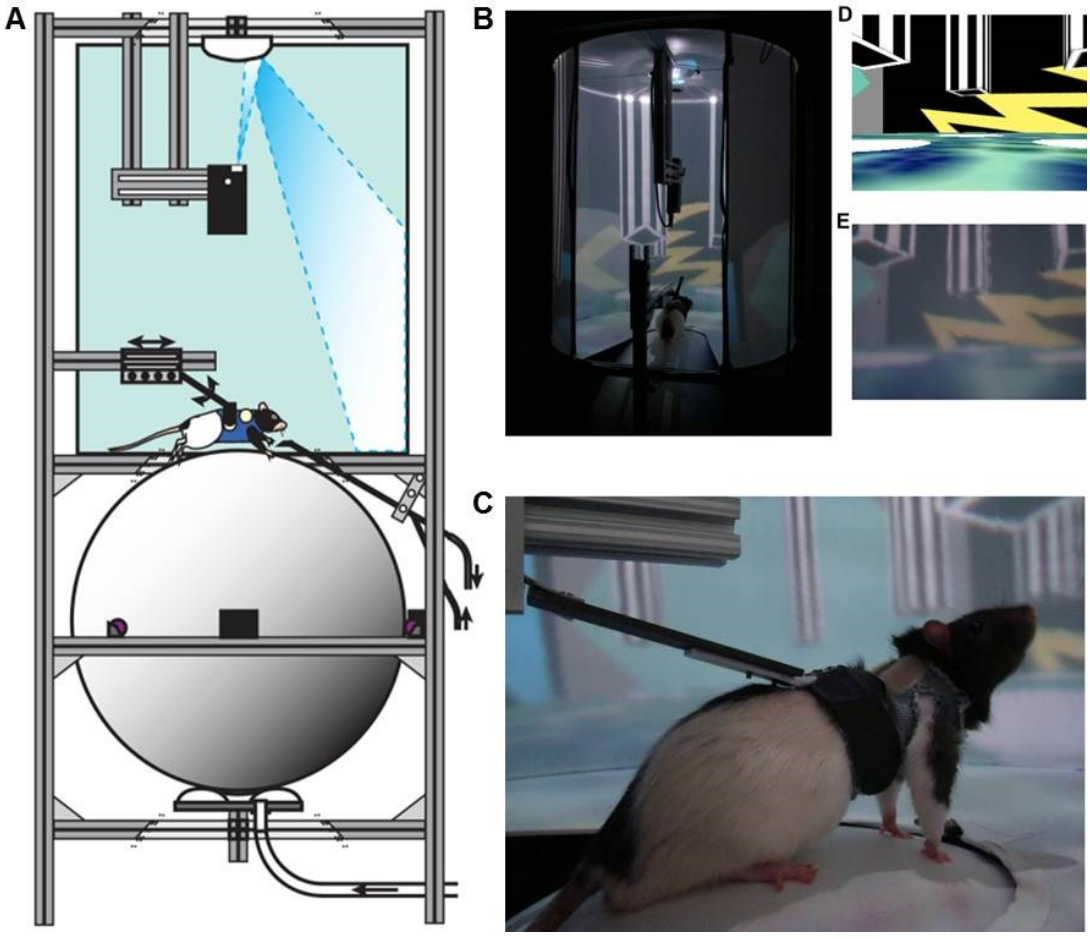


**Fig 2.1:** Virtual reality apparatus. **A)** Cross-section schematic of VR system showing the overall frame, mirror, micro-projector, reward tube, holding mechanisms for the rat, spherical treadmill and air cushion. **B)** Picture of VR system from behind while the rat is performing the virtual random foraging task. **C)** A rat in VR system. Note the hinge and harness that allows a natural posture for the rat. **D)** A view of the virtual random foraging environment generated by the software. **E)** Picture taken inside the VR from the point of view of the rat from the same point as in **(D)**.

The aspects of the VR apparatus on which I was most involved were the air cushion and the rat harness, described in more detail below.

### 2.2.2 VR air cushion

A large part of what makes this VR apparatus unique is the way the Styrofoam ball is suspended. Most other VR systems for rodents use a semispherical acrylic bowl with an input of air on the bottom (Holscher et al., 2005; Harvey et al., 2009; Youngstrom and Strowbridge 2012; Schmidt-Hieber and Hausser, 2013). The air flows up and around the ball, preventing it from resting in the bowl, and allowing it to rotate freely in any direction. The disadvantage of this design is that a lot of air is necessary to keep the ball afloat, and with a ball large enough to support a rat, this amount of air creates a lot of acoustical noise. Since one of the purposes of using VR is to enable the precise presentation of sensory cues, including auditory cues, minimizing background noise was a key goal in the VR design. In the first iteration of the VR, the Styrofoam ball floated on top of a small pool of water at the bottom of a semispherical bowl. This was acoustically quiet, but since rats dislike being wet, it was not an ideal solution.

Daniel Aharoni and Zhiping Chen had the original idea to use a small air cushion, rather than the air bowl used by other labs (Fig 2.2A). The design consists of a sheet of thin plastic (originally a trash bag) bolted to the middle of a 9” diameter circular piece of thick plastic, and wrapped around the sides with some slack remaining. When inflated, this creates a semi-toroid shape. There is one large hole in the thick plastic where the air enters, and 4-6 1/4” holes around the center of the thin plastic though which the air escapes (Fig 2.2B). The ball rests on top of the toroidal cushion, and the air makes a thin space between the ball and the plastic. This uses much smaller air flow rates of 1.5-3.5 liters per minute, and acoustical noise levels were measured at 44 dB.

The disadvantage of this design was the thin plastic that comprised the air cushion stretched and tore easily, after which it was useless and had to be replaced. Making a new air

cushion took about 1-2 hours and had to be done as often as once a week. An undergraduate research assistant under my supervision, Laura Porter, did the research and tests to find a more suitable material. Ultimately, she determined the best material is 1.3oz silicone-coated ripstop nylon (Rockywoods), the same family of fabrics used to make camping gear and parachutes (Fig 2.2C-D). The material is airtight, lightweight, nonelastic, and difficult to tear. Any tears that do occur are often small and sometimes do not affect the efficiency of the air cushion. Thus, air cushions using this fabric last several months, which is a large improvement both for efficiency and for stability of experimental recordings. As an added advantage, these air cushions tend to be even quieter and have less friction than the ones made out of plastic, making the ball easier to rotate.

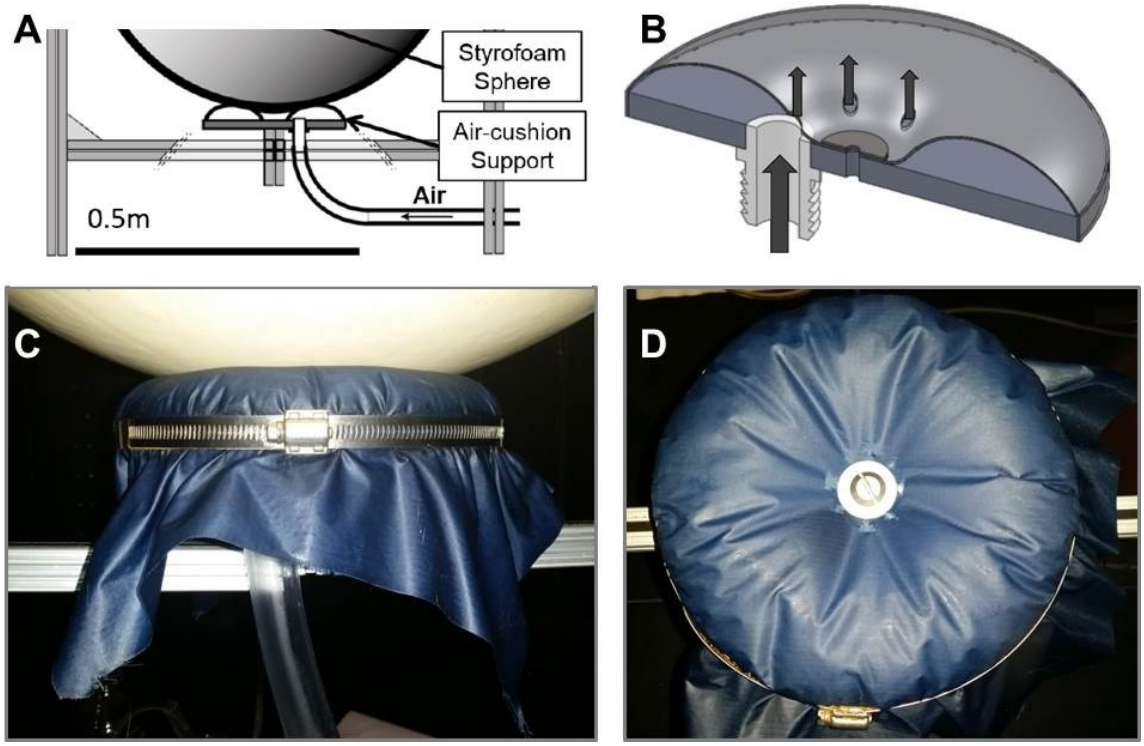


**Fig 2.2:** Air cushion for the spherical treadmill. **A)** Schematic of the air cushion supporting the spherical treadmill (Styrofoam sphere) in the VR apparatus. **B)** Detailed schematic of the air cushion. Arrows indicate airflow. **C)** Side view photograph of the air cushion supporting the spherical treadmill. Blue fabric is the ripstop nylon incorporated by Laura Porter. **D)** Top view photograph of the air cushion, with spherical treadmill removed.

### 2.2.3 VR harness

A key aspect of the VR apparatus is the harness that holds the rat on top of the freely-floating Styrofoam ball. Our harness design was based off of those previously used for VR (Holscher et al., 2005; Schnee, 2008). After several iterations, the final version is made of elastic denim and Velcro (Fig 2.3A and B).

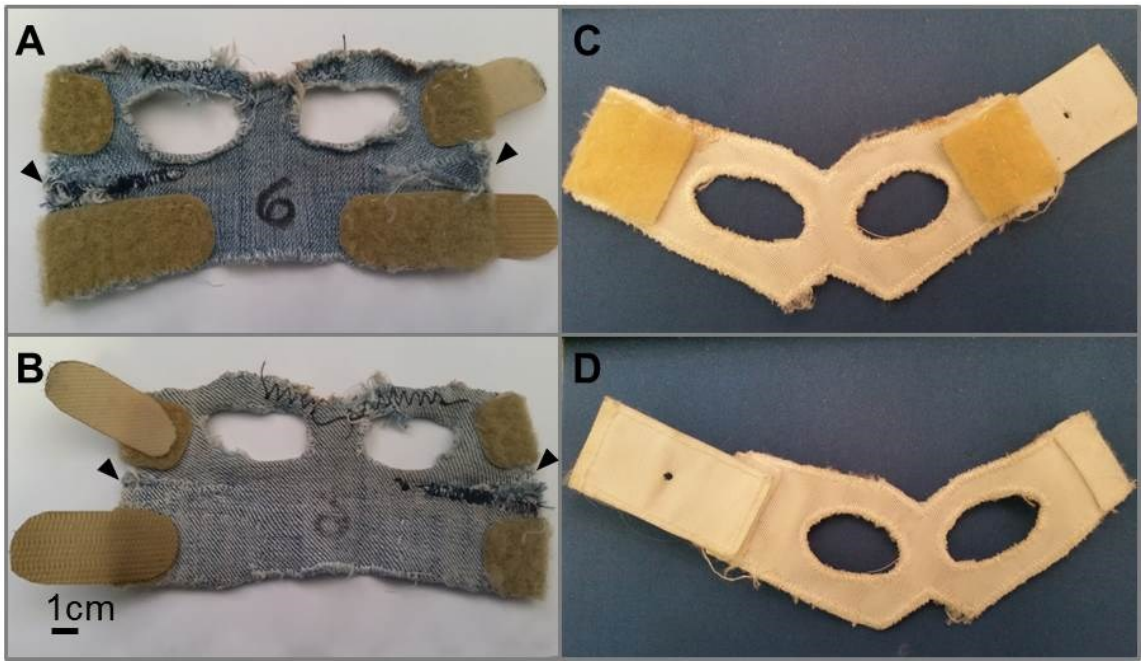


**Fig 2.3:** Rat harness for VR apparatus. **A and B)** Elastic denim harness with Velcro attachments. Outside **(A)** and inside **(B)** views are shown. Arrowheads mark the darts incorporated into the design to provide a better fit. **C and D)** As in A and B, for medium white rat harness from Braintree Scientific.

Elastic denim provides the best combination of support and comfort. An ideal composition is roughly 96-97% cotton and 3-4% spandex. Some elasticity in the fabric is necessary so that the rats are comfortable, and the harness can be made tight enough to prevent escape, but not tight enough to cause discomfort. It is worthwhile to note that some denims are only elastic in one dimension. It is important to orient the harness such that the plane of the elasticity is around the circumference of the rat's trunk, rather than along his length.The slight stiffness of denim is beneficial because it provides support when the rat tries to turn the Styrofoam ball underneath him. Thinner, less stiff fabrics make it difficult for rats to

maintain their balance on the ball. Elastic denim wears out quickly, however, with the average harness having to be replaced after several months of every day use.

Velcro proved to be the best way to attach the harness. It is easier to fasten than a tie or snap, and has the added benefit of being adjustable on a continuous range of sizes, allowing each harness to fit snugly on a range of body sizes. High quality Velcro is strong enough to hold when the rat tries to escape the harness, but will detach under stronger forces, such as in emergency circumstances. This helps reduce the risk of harm to the rat and the implant.

The current design consists of a roughly trapezoid-shaped piece of fabric with two arm holes. The rat's arms fit through the holes, and the Velcro is used to fasten the harness over the rat's back (Fig 2.4). The anterior part of the harness, including the arm holes, has the same dimensions as the size medium rat harnesses available from Braintree Scientific (Fig 2.3C and D). Our harness is made to extend further down the rat's body, about 6.5cm of total length, to allow enough space for the Velcro that will ultimately attach to the VR apparatus. The dimensions of the harness are important. Because of the roughly conical shape of a rat's body, it is important for the anterior part of the harness to be smaller than the posterior part. This is difficult to obtain in a continuous piece of fabric; a common issue in the current harness design is that it is difficult to make the harness tight enough around his chest without making it too tight around his torso. Therefore, it might be beneficial in the future to make the front and back attachments more independent (by making a small cut in the fabric between the anterior and posterior pieces of Velcro, for example) so that each can be tightened the appropriate amount. The size of the armholes is also crucial. These should be made as small as possible while still allowing the rat's arms to fit. The long axis of the oval-shaped armhole should be no more than 3cm, and armholes as small as 2.5cm will still fit the rat's arm. If the arm holes are bigger than 3cm, the rat can push his front paw through the front part of the armhole, and once he achieves this, it is very easy for him to escape from the harness.

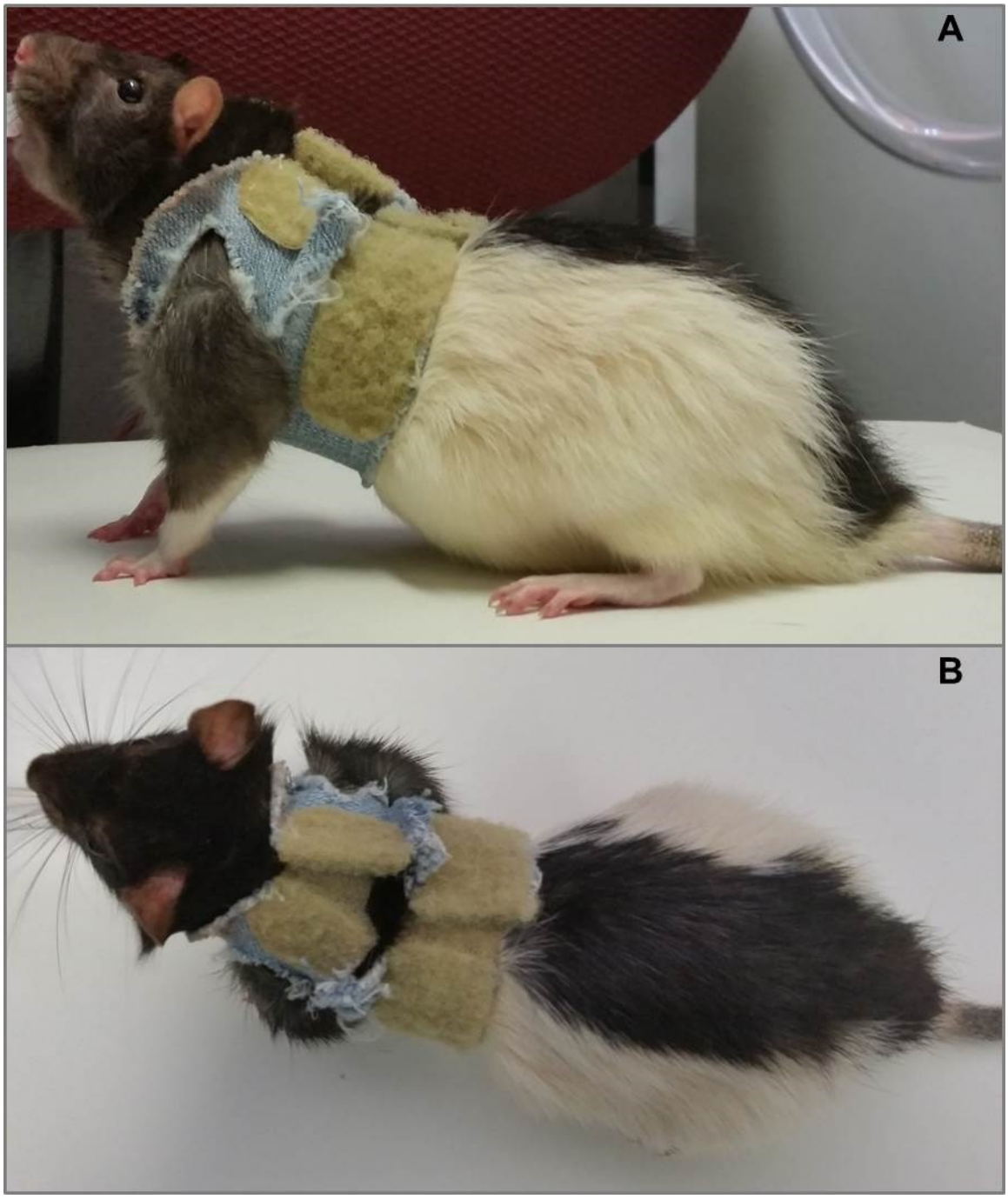


**Fig 2.4:** Picture of a rat in the harness, shown from the side **(A)** and from the top **(B)**.

One of the earlier iterations of the harness had two straps that extended from the rat's belly, between his legs, and reattached to the harness on the rat's back. This ensured that that rat could not push the harness up and over his head, allowing him to back out of it. However,

these straps seemed uncomfortable for the rats, and they never seemed to run confidently and naturally on the VR. These straps were necessary with the thinner, non-stretchy fabrics like suede, but became obsolete in the harnesses made out of elastic denim. The elasticity allowed for a tighter fit, and the thick, stiff fabric made it more difficult for the rats to bend their bodies in positions that would allow them to escape the harness. It should be noted, however, that under certain circumstances, the harnesses made of elastic denim are extremely easy for the rats to remove. For example, if the rat is held by the harness on top of the Styrofoam ball and the ball becomes stuck, the rat can easily push himself backwards out the back of the harness. It is for this reason this particular harness design may be unsuitable for linear treadmills, as the rat could orient himself orthogonally to the treadmill and gain traction to push himself out of the harness.

One improvement that was eventually made in the harness was to sew darts between the anterior and posterior Velcro. This is achieved by making a 3-4cm cut in the fabric between the two pieces of Velcro, overlapping the two pieces of fabric to make a shallow cone, and sewing them together (Fig 2.3A and B, arrowheads). This seemed to help the harnesses match the shape of the rat's body better and ultimately allow for a tighter fit. Some rats seemed to run more on the VR after the harnesses were made to fit better. However, after we made this change, we saw a small increase in the number of times the rats got their bottom teeth stuck in one of the arm straps of the harness. It was never explored whether the darts directly caused this increase. While grooming, rats sometimes get their bottom teeth stuck on the fabric that goes over his shoulders and under his neck. If the straps are loose enough, he can release his teeth without difficulty. If the straps are snug, however, he will not be able to do this. The restraint is stressful, and if not released quickly, most rats will try to release themselves by violently arching their backs and pulling their heads up, thus pulling the harness up and over their heads. The amount of force rats can achieve in this maneuver is enough to separate the drive from the skull, so it is a very serious problem. One improvement that was never tried was

to make the arm straps out of neoprene, or another fabric that can easily be ripped if the rat should get his teeth caught. Another method might be to improve the fit of the harness even more so the probability of the rat getting his teeth caught in the first place is diminished.

## 2.3 VR Pretraining Protocol

### 2.3.1 Introduction

David Ho, Jesse Cushman and I played an instrumental role in developing a training protocol to gradually prepare a naive rat to run comfortably in a VR environment. In the lab's first attempt at training a rat on the VR, we tried to put a well-handled rat directly on the VR apparatus without any prior exposure. This was incredibly stressful for the rat, and we were ultimately unsuccessful in training him to explore the virtual environment. There were several problems with this approach. First, the rat was unused to restraint, which is stressful for unhabituated rats. Although the spherical treadmill allows them to walk freely in every direction, thus reducing the feeling of restraint, it does not allow them to turn fully around to face the back of the VR apparatus. Second, even though the rat is held on top of the Styrofoam ball by the harness, there is some degree of freedom due to both the harness and the hinged attachment. This decreases the feeling of restraint and allows for natural behaviors, but requires the rat to be able to balance himself on top of the ball and to feel comfortable rotating it under him. Third, rats dislike being forced into new environments, and restraining a rat within an apparatus he has never seen before was a very stressful experience. Fourth, the main reward for being on the VR is sugar water, but a naïve rat will not necessarily know to expect sugar water from the dispenser, or know that the reward tone signifies its availability. Without this knowledge, the rat will not drink sugar water, and thus will not be able to form a positive association with the VR. To prepare the rat for eventual introduction to the VR, we developed a general pretraining procedure that consisted of several phases. In this order, the rats were habituated to handling,

habituated to wear the harness, trained to associate the reward tone with availability of sugar water, trained to balance themselves and walk while held on top of the Styrofoam ball, and finally introduced to several virtual worlds to allow him to improve his strength and dexterity in manipulating the spherical treadmill.

### 2.3.2 Handling and harness training

Naïve rats are first handled for 30-60 minutes a day for 1-2 weeks. The purpose is to habituate them to all the handling situations they might encounter. Training techniques involve picking the rats up, letting them walk along outstretched arms, and holding them in the various types of manual restraints that will be used throughout training and recording. In most cases, rats that have been previously housed together are handled together. This gives the rats extra enrichment and social interaction. In some cases, single rats or pairs of rats are allowed to explore play arenas set up specifically for that purpose. This was not a very stable part of the protocol; the setups changed a lot over time, but would usually consist of a large box or small open field with a running wheel, plastic tunnel, cardboard box, and plastic house. Sometimes pieces of Froot Loops cereal or standard rat chow are scattered around the arena, or the rats are simply allowed to explore and play freely. From my own observations, the rats that are most likely to perform well in the virtual tasks are both comfortable with being handled and naturally active and curious.

As soon as the rat is comfortable being handled, harness training starts, and usually occurs simultaneously with continued handling. Rats are first trained with the size medium white harness (Braintree Scientific) (Fig 2.3C-D). This harness is more comfortable and easier to put on than the denim one eventually used in the VR, so is suitable for starting habituation. With most rats, the best way to proceed is to put on the harness as quickly as possible the first time. Usually, if the rat is comfortable with being handled, he will not resist harnessing the first time. Once the harness is on, let him rest in his cage and give him sugar water or Froot Loop

rewards. If the rat is not stressed, leave the harness on for only about 5 minutes, then take it off. The goal is to let the rat learn that there is nothing threatening about having the harness on, and that you will take it off. If the rat resists harnessing, it is important to eventually get the harness on at least once during the session, so the resistant behavior is not reinforced.

To put on the harness, I start by placing the rat on my right thigh facing away from me. I cup the rat in my right hand with his front legs extending between my index and middle fingers (Fig 2.5A). Using my right thumb to push the rat's left shoulder to extend his front leg, I use my left hand to put the correct armhole over this leg. With my left thumb, I hold the harness in place on the rat's back (Fig 2.5B). I then use my right thumb to extend the rat's right front leg and use my right fingers to put the arm hole over that leg (Fig 2.5C). Then, using both hands to hold each end of the harness over the rat's back, I can fasten the Velcro (Fig 2.5D-F). Note that in the photographs, the experimenter uses the opposite hands as described above.

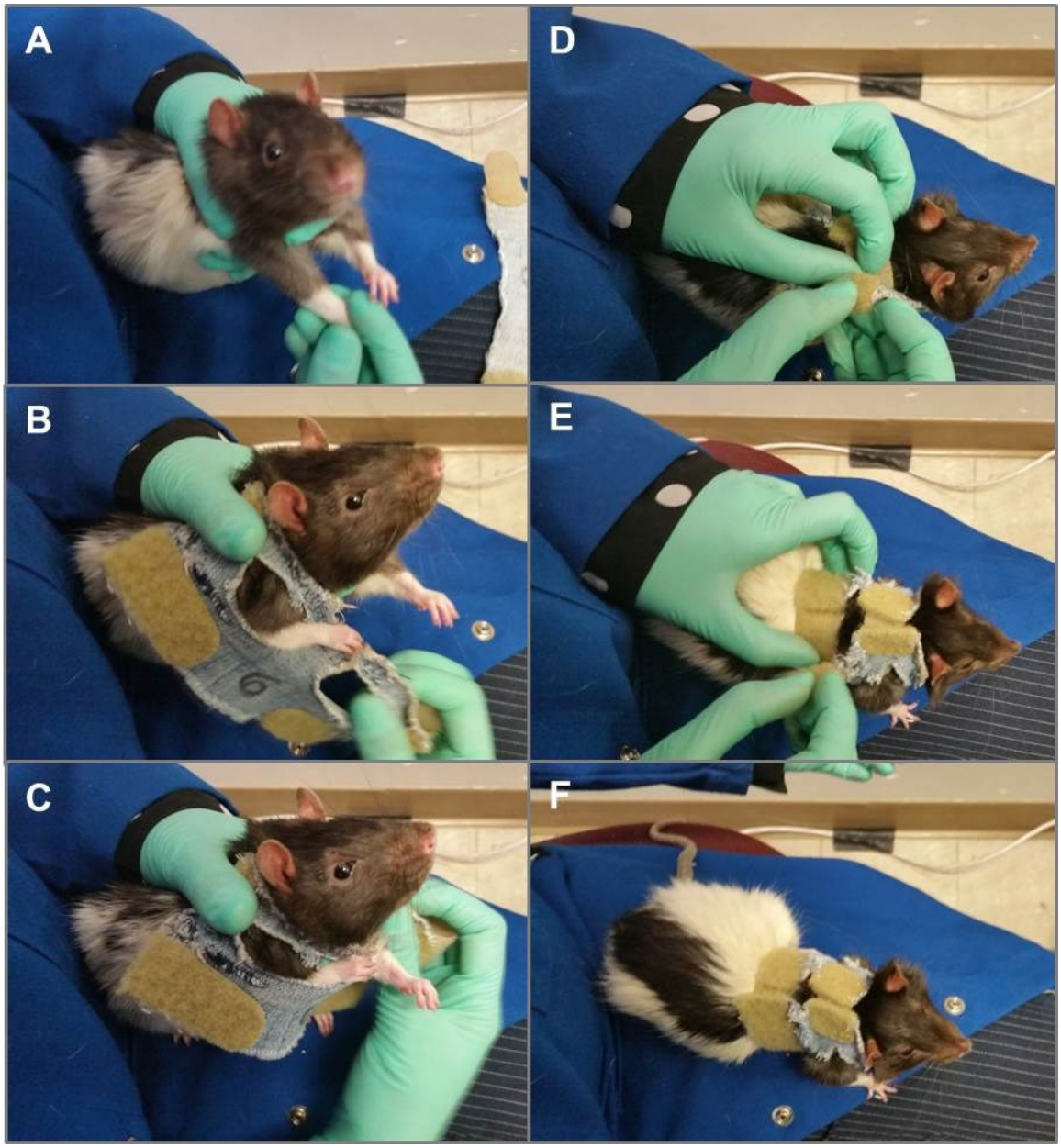


**Fig 2.5:** Harnessing procedure. **A)** Grasp rat in one hand such that forelimbs are extended. **B)** Put one armhole over one forelimb, and hold on rat's back with thumb. **C)** Wrap harness around the rat's chest and put the other forelimb through the remaining armhole. **D)** Using both hands, secure the anterior Velcro. **E)** As in **(D)**, for the posterior Velcro. **F)** Photo of the rat in the harness after completed harnessing procedure.

Once it is possible to put the harness on the rat, the rat should be required to wear the harness for increasing amounts of time. Once the rat is habituated to putting on and wearing the white harness, begin using the denim VR harness. Most rats transition easily between the two harnesses. Harness training, from start to finish, usually takes about 1 week.

### 2.3.3 Reward tone association training

This pretraining phase was mostly developed by Jesse Cushman. The goal of this training phase is to allow the rats to associate the reward tone with availability of sugar water. The set up consists of a rat cage with a small hole in the side. The VR lick tube is detached from the VR apparatus and extended through the hole into the cage (Fig 2.6).

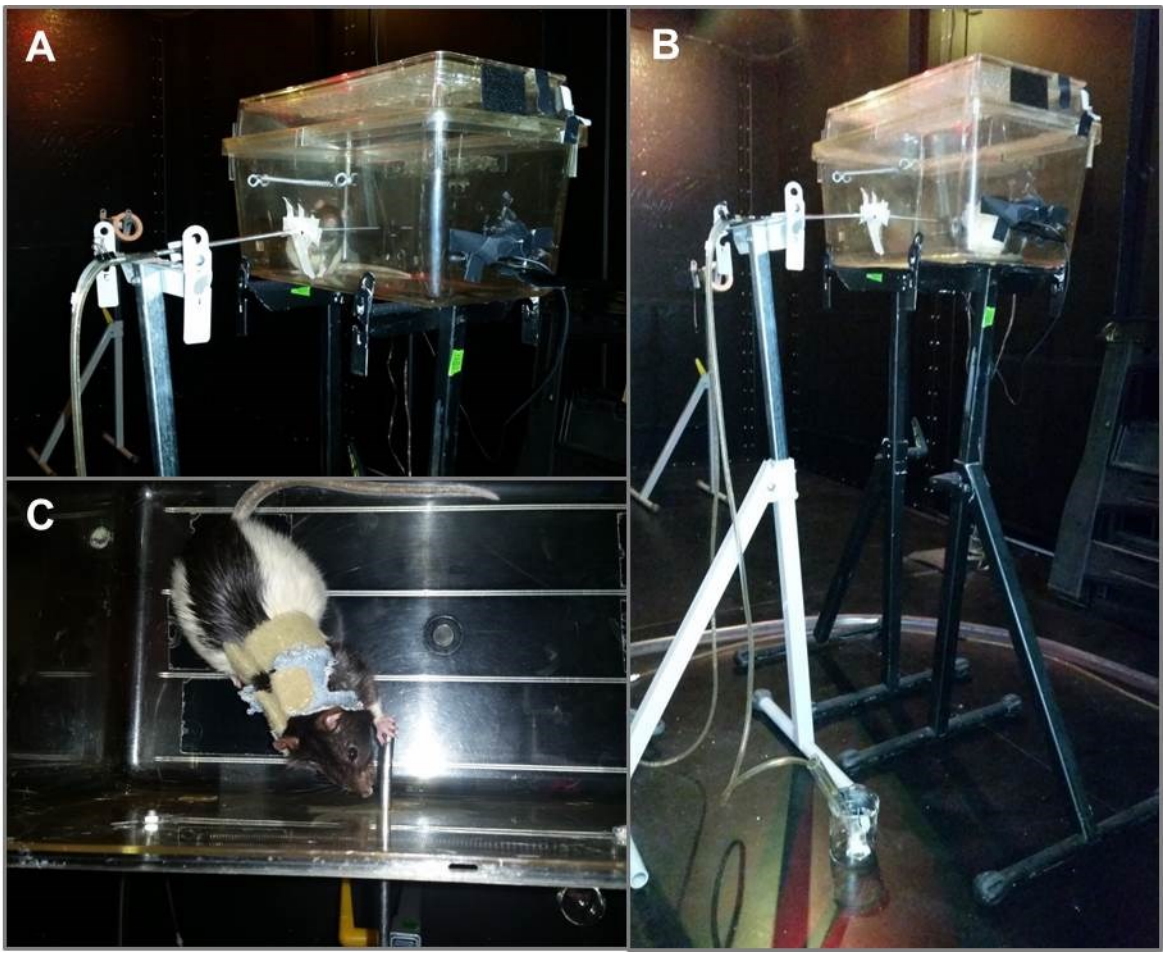


**Fig 2.6:** Reward tone association training apparatus **A and B)** Photographs of the reward tone association training apparatus. **C)** Photograph of a rat in the apparatus. Notice his interest in the lick tube.

To complete the training, first allow the rat to explore the cage for 5 minutes at the beginning of each training session. Then release rewards on a random interval schedule, with an average of one reward each minute for the next 15 minutes. In our setup, each reward consists of 5 reward tones and 5 correlated pulses of sugar water. The reward tone is a 200 ms

1 kHz beep and the sugar water pulse is a 400 ms opening of the valve. The sugar water is a 10% w/v solution of sucrose. Usually, 1 week of this procedure is sufficient for the rats to associate the tone with the availability of sugar water.

### 2.3.4 Ball training

The last phase of pretraining was designed to teach the rat how to balance on the Styrofoam ball and to feel comfortable walking forward. All of these procedures are done with a ball removed from the VR apparatus. First, the rat is placed on top of a ball held steady on the ground, and allowed to explore the surface. Once the rat is comfortable being on top of a stationary ball, the experimenter can pick up the ball and rotate it manually to counteract the rat's movements as he explores. Once the rat is comfortable with this, the next step is to let the rat walk around on top of the ball as it rolls on the floor. This procedure works best with two experimenters. The Styrofoam ball is placed on the floor, and one experimenter holds the rat on top of the ball using the harness and the attachment used in the VR apparatus. The other experimenter holds a syringe filled with sugar water and periodically rewards the rat (Fig 2.7). Some rats will readily follow the sugar water syringe and quickly become comfortable walking on top of the ball, and others will not. With these more cautious rats, it is important to increase the amount of time on the ball gradually, and to hold them so that they are in the most balanced position on the ball. Eventually, pulling them slightly back on the ball will encourage them to walk forward.

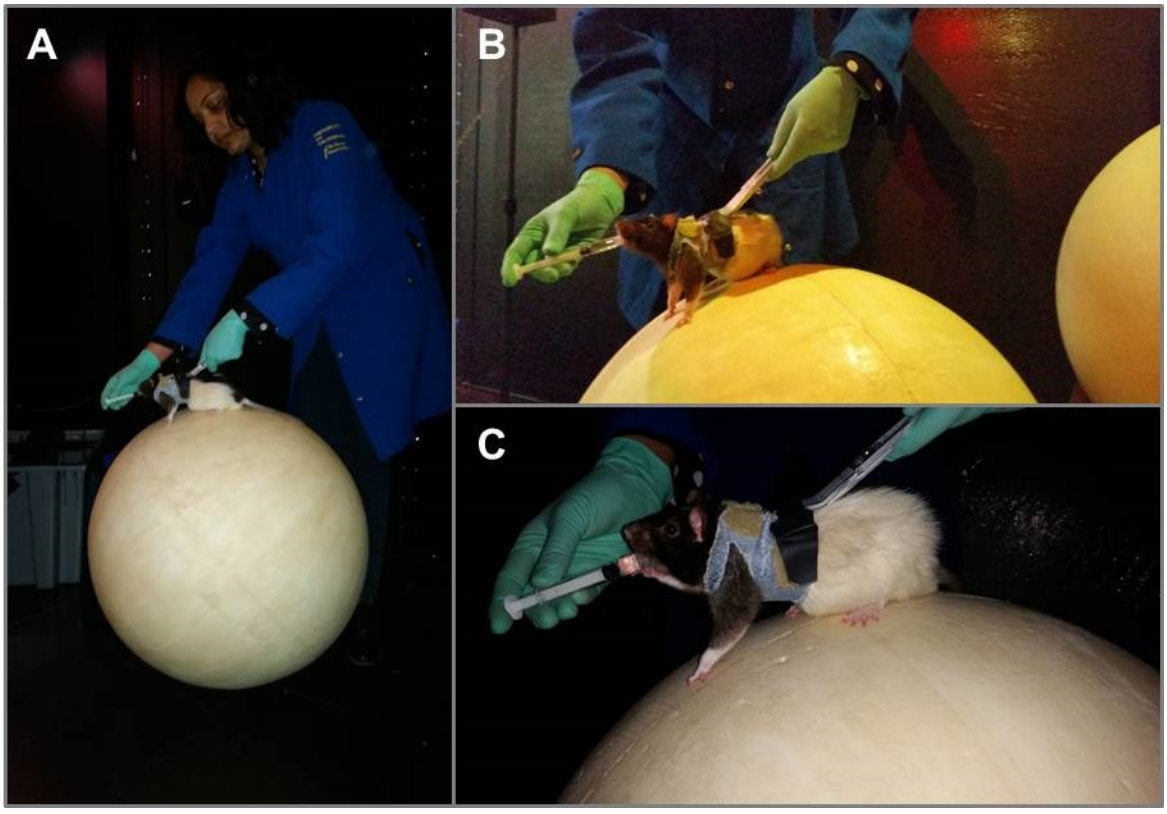


**Fig 2.7:** Ball training protocol. **A)** Full photograph of an experimenter holding a rat on top of the ball and giving him sugar water reward from a syringe. **B and C)** Close-up photographs of same procedure as in **(A)**.

### 2.3.5 VR training envrionments

After pretraining, rats were first run on a suite of training environments in the VR. Jesse Cushman designed these environments, with help from myself, David Ho, and other members of the lab. We developed a shaping procedure designed to train rats to navigate in virtual environments based on navigating to randomly dispersed visual beacons that signify reward. The rat started in the middle of an octagonal table placed in a virtual square room (3 x 3 m). The table was 150 cm above the floor of the room, indicated by a black and white grid pattern. The table consisted of a green pattern designed to provide optic flow feedback without providing any spatial information. The visual beacons were 10 cm wide pillars with vertical black and white stripes, suspended above the virtual table. Immediately below the visual beacons were

20 cm radius white dots. When the rat entered these white dots the reward tone played and sugar water was dispensed for 400 ms. As long as the rat stayed in the dot he could receive up to 5 tone-sugar water pulses per dot. When the rat received all 5 rewards or he exited the white dot the reward was inactivated, the pillar and dot disappeared and the reward was available under a new pillar/dot placed at a random location. A shaping procedure was used, where the first virtual environment consisted of a large table (1.5 m radius) with five pillars at any given time (abbreviated LT5) (Fig 2.8A-C). The rats were advanced to progressively more difficult tasks by reducing the number of pillars and the size of the table. The progression was from a Large Table with 5 pillars (LT5) → Large Table with 3 pillars (LT3) → Small Table with 2 pillars (1 m radius, ST2) → Small Table with 1 pillar (ST1). The rats were allowed to run for up to 35 minutes or until 200 rewards had been dispensed. The criterion for advancement to the next stage was 200 rewards delivered within 30 minutes. Rats rapidly learned to quickly maneuver away from and then avoid the edges of the virtual table, reaching an asymptotic level of performance within five sessions (Fig 2.8D). In addition, they rapidly learned to navigate to the pillars, reaching an asymptotic level of rewards per minute within four sessions (Fig 2.8E). Thus, the majority of improvement in this virtual foraging task occurs during the first four days of experience with the large virtual table and five random reward zones (LT5).

Notably, the edges of the virtual world were defined solely by visual cues and did not provide somatosensory stimulation that typically defines boundaries in the real world. Thus, this task replicates previous findings that rodents can navigate to virtual visual beacons (Holscher et al., 2005) or landmarks (Youngstrom and Strowbridge, 2012) and significantly extends these by showing that rats readily learned to respect virtual edges and can therefore be constrained within finite 2-D virtual environments.

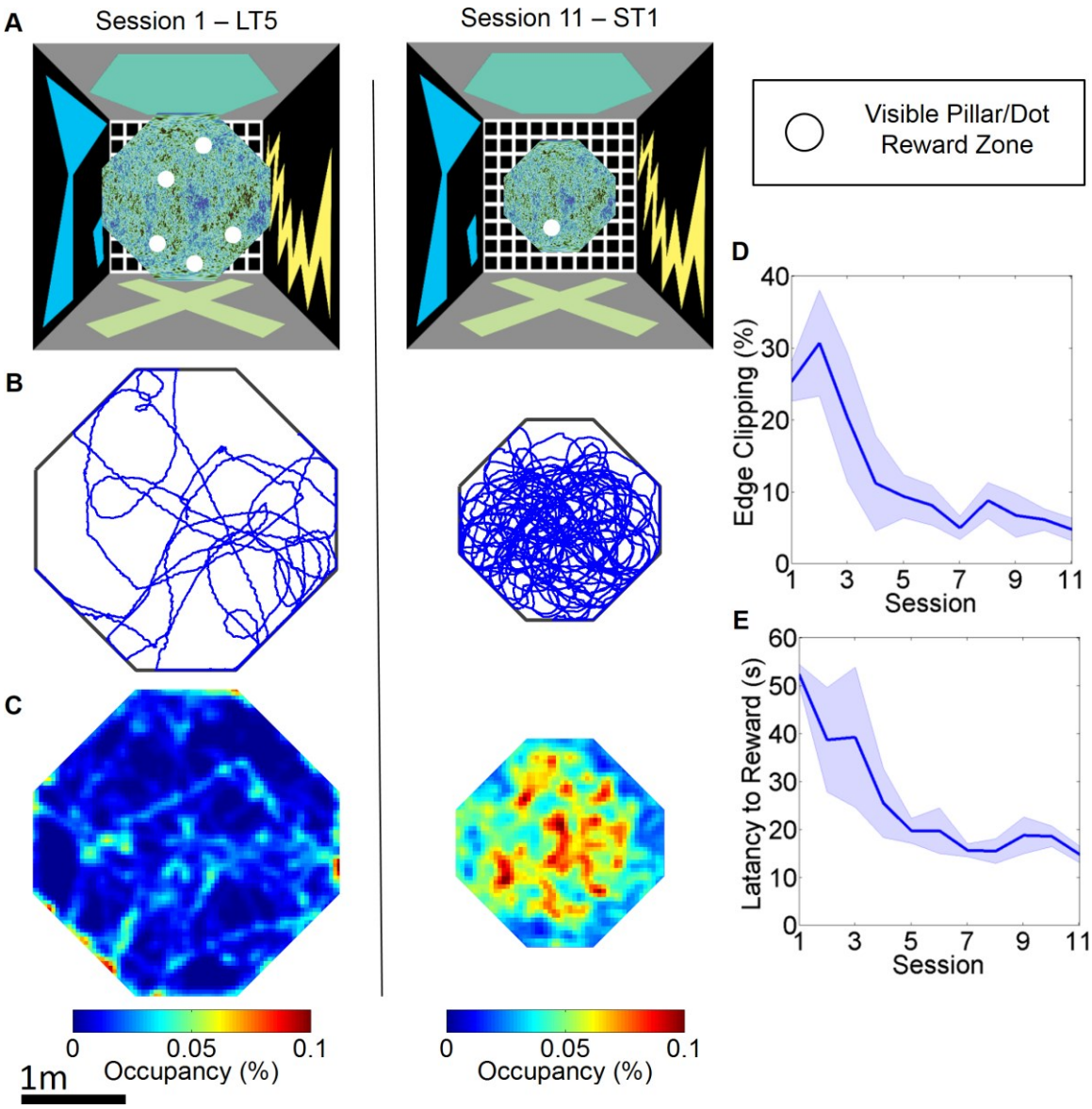


**Fig 2.8:** Initial virtual training environments. Rats rapidly learn to navigate and avoid edges in a finite 2-D virtual environment. **A)** Schematics for: Session 1 in the Large Table with 5 rewards (LT5) virtual environment and Session 11 in Small Table with 1 reward (ST1) virtual environment. **B)** Example of a 30 minute path from a single rat in session 1 and 11 respectively. **C)** Mean Occupancy across all rats in session 1 and 11 respectively. **D)** Acquisition curve of the percentage of distance traveled into the edge of the platform, referred to as edge clipping. Effect of session: $F(2,32) = 4.037$, $p = 0.0038$, First vs. fifth session: $t = 2.812$, $p<0.05$, $N = 4$. **E)** Acquisition curve for latency between rewards. Effect of session: $F(2,32) = 3.913$, $p = 0.0012$, First vs. fourth session: $t = 3.056$, $p<0.05$.

The protocol described above was used for many projects in the lab, including the one published in *Science* in 2013 and described in Chapter 3 of this thesis. For my project in the medial entorhinal cortex (see Chapter 4), however, I needed to modify this training protocol.

Specifically, for this project, it was important to remove the reward zone-indicating pillars. Reviews from the previous paper had raised the concern that perhaps the pillars were influencing the firing of spatially selective cells. In addition, a highly salient but spatially unstable proximal visual cue would have interfered with the project's goal of determining the relative contributions of different classes of cues. Last, the removal of the pillars would make the virtual reality task more similar to that in the real world, where there could be no visible reward-indicating beacon.

To prevent the possible demotivation the rats might experience when switching from an environment with marked reward zones to one without, I decided to train the rats for the MEC project from the beginning without pillars and dots marking the reward zones. In this training protocol, the first training environment was a 1.5 meter radius octagon within a 12 meter square room. The reward zone was invisible and unmarked, 1 meter in radius, and moved in a random order to predetermined, uniformly-spaced locations. In addition, all 5 reward pulses were given every time the rat stepped into the reward zone, regardless of when he exited it. In this initial training task, the reward zone was so large that the rat was rewarded often, even for little running. After the rat was proficient at this task, the next environment was a 1 meter radius circle within a 12 meter square room. The reward zone, still unmarked, was reduced in size to 50cm in radius. Over the rest of the pretraining, the platform and room were kept the same, and only the size of the reward zone was incrementally decreased to 30cm radius.

At first, there were 18 predetermined reward zones that were sampled from equally. However, we saw that some rats were only walking in a ring a certain distance from the edge of the table, corresponding to where 17 of the 18 reward zones could be easily accessed. To counteract this, we later weighted the reward zone locations such that the one in the center occurred 8 times as many as the ones outside the center. This effectively encouraged the rats to explore the center more often, thus making the occupancy more evenly distributed throughout the environment.

## 2.4 Medial Entorhinal Cortex Implantation Surgeries

### 2.4.1 Introduction

One of the main techniques well-known in the lab is how to implant drives and perform extracellular *in vivo* electrophysiology in CA1 of the hippocampus. One aspect of my thesis work was to record from neurons in the medial entorhinal cortex (MEC). The overall technique is similar to that for recording in CA1, but in order to successfully record data in the MEC, I had to adjust the technique. Few other labs have perfected this technique, and the documentation found in peer-reviewed journals was insufficient for me to perform the technique without many optimization experiments, described in more detail below.

### 2.4.2 Determining an MEC implantation coordinate

Several aspects of the MEC and its location make it more difficult to target than CA1. First, it is a posterior structure, and this distance makes bregma a poor landmark. Second, its medial-lateral and anterior-posterior extent is smaller than that of CA1, requiring more precise coordinates to target. Third, the transverse sinus runs just posterior to the MEC. This is a major blood vessel that sits in the groove between the cerebrum and cerebellum. The proximity of the transverse sinus combined with the small cross-sectional area of the MEC makes errors in both the anterior and posterior direction very costly. Placing the craniotomy too far posterior and damaging the transverse sinus during surgery leads to excessive bleeding, compromising the health of the rat. Considering that at the time of surgery rats had already undergone months of VR training, puncturing the transverse sinus and preventing the rat from continuing in the study was a very undesirable outcome. On the other hand, coordinates that were too anterior could put the tetrodes out of the range of the MEC, and months of effort could be wasted trying to record grid cells when in fact they could never be reached.

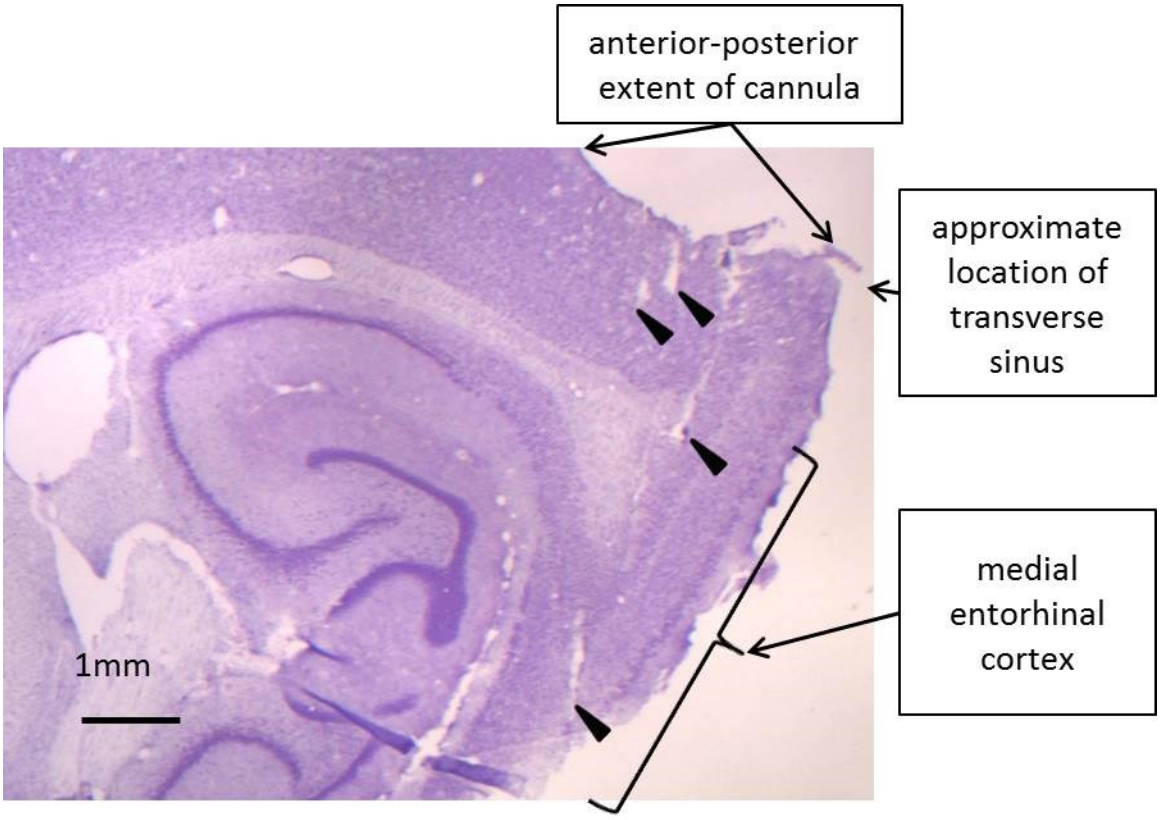


**Fig 2.9:** MEC implantation. Histology micrograph shows a sagittal section from a successful MEC implantation, including approximate locations of MEC, cannula, and the transverse sinus. Arrowheads mark tetrode tip locations. Scale bar: 1mm.

Most MEC *in vivo* literature states that the MEC implantation coordinates are referenced from the transverse sinus itself, rather than the bregma skull marking (Fyhn et al., 2004; Barry et al., 2007; Savelli et al., 2008; Stensola et al., 2012). Since it was not reported in the literature how the transverse sinus was located, I tried various ways of trying to find the transverse sinus (explained below), all to no avail.

At first, since I could not locate the transverse sinus, and bregma was too far, I used lambdoid as the reference point for my implantation coordinates. I performed 12 practice surgeries to determine the relative location between lambdoid and the MEC. Pascal Ravassard was instrumental in conducting these practices. I also collected data from actual implantation surgeries. To perform the practice surgeries, I would drill a hole in the skull where I guessed the MEC was, insert a 27Ga needle into the brain, dissect the brain out of the rat, cut the brain with

a razor blade at the level of the lesion, and observe whether the lesion made by the needle was located in the MEC. (Fig 2.10) Whether or not the lesion ended up in the MEC, I used it to determine the distance between the posterior edge of the MEC and lambdoid (Table 2.1). Unfortunately, I found was that this measurement showed high variability between and even within rats, with a range of 2 to 4 mm. I tried correlating this measurement with other factors, such as the rat's age, weight, distance between bregma and lambdoid, and combinations of these measures. The correlations were all very loose, but perhaps the best one was the relation with age (Fig 2.11). With age, the distance between lambdoid and the posterior edge of the entorhinal cortex decreased. However, for the 5-7 month age range, in which I implanted most of my rats, there was still a measured range of 1.5 mm, much too imprecise for my purposes.

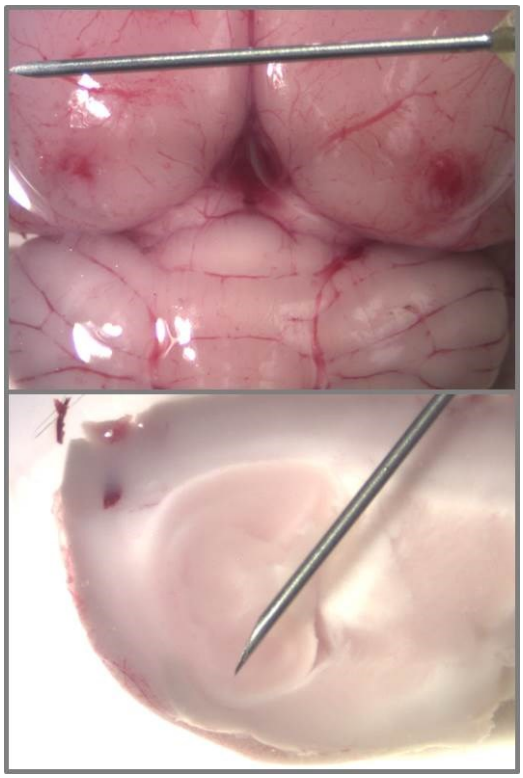

**Fig 2.10:** Practice surgeries to determine a coordinate for targeting the MEC. **Top:** Dorsal view of the whole brain, with 2 bloody lesions above left and right MEC. Transverse sinus has been removed. **Bottom:** Sagittal section, showing lesion in MEC. Needle in both pictures is size 27 Ga, which is the same size as was used to make the lesions.

| Rat ID | Age (months) | Weight (g) | Distance between Bregma and Lambdoid (mm) | Distance Between Lambdoid and Posterior Edge of MEC (mm) | |
|---|---|---|---|---|---|
| | | | | Right hemisphere | Left hemisphere |
| 1 | 3 | 270 | 6.9 | 2.9 | 3.2 |
| 2 | 12 | 420 | 8.3 | 1.9 | 2.2 |
| 3 | 5 | 450 | 7.2 | 3.9 | - |
| 4 | 5.5 | 575 | 7.0 | 3.0 | - |
| 5 | 7 | 365 | 7.8 | 3.7 | 3.4 |
| 6 | 6 | 365 | 7.6 | 2.6 | - |
| 7 | 6.25 | 400 | 7.4 | 3.7 | 4.0 |
| 8 | 10.5 | 400 | 7.8 | 1.9 | |
| 9 | 9 | 375 | 7.3 | 2.4 | 2.3 |
| 10 | 5 | 345 | 7.2 | 3.0 | - |
| 11 | 6 | 370 | 7.1 | 3.1 | - |
| 12 | 7 | 340 | 8.1 | 2.8 | - |
| 13 | 11 | 375 | 7.2 | 3.3 | - |
| 14 | 5.5 | 335 | 7.3 | 3.6 | 4.1 |

Table 2.1: Measurements collected from practice and actual MEC surgeries.

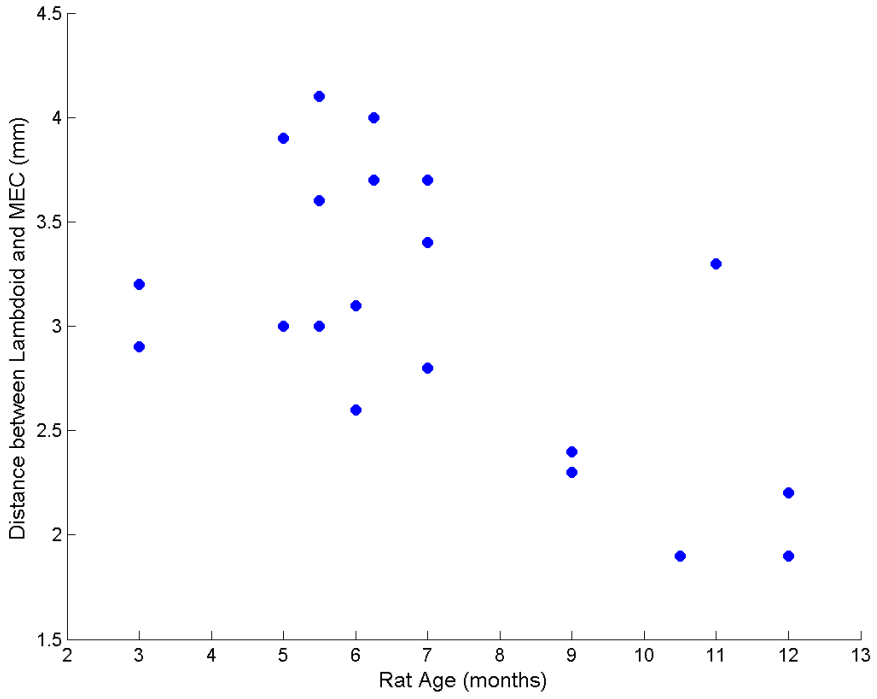


**Fig 2.11:** Determining a coordinate for targeting the MEC. Relationship between the age of the rat in months and the location of the posterior edge of the MEC, expressed in mm posterior to lambdoid.

However, it was the best information I had available. In an attempt to improve my success rate, I tried to refine my coordinates based on measurements taken from littermates. For every rat I implanted, there was a littermate that had undergone the same training procedures and feeding schedule. The two rats were usually therefore well-matched in age and weight. About a week before each implantation surgery, I would perform a practice surgery on the littermate and obtain the distance between lambdoid and the posterior edge of the entorhinal cortex. I would then use this measurement to determine the coordinates for the actual surgery.

In later attempts at implanting in the entorhinal cortex, I tried shaving the skull around the implantation site and watching for bleeding. Heavy skull bleeding would indicate the proximity of the transverse sinus and then cause me to move the implantation coordinates anterior or posterior as needed.

### 2.4.3 Attempts to improve the success rate of MEC surgeries

While working on the MEC part of this thesis, I tried various methods to improve the success rate of the MEC implantation surgeries. All the optimization attempts involved trying to locate the transverse sinus either before or during surgery. Ultimately, nothing worked and all the implantation coordinates of the rats used in the study were relative to lambdoid and an estimate based off the age of the rat and measures taken from littermates.

First, I tried to determine whether the transverse sinus can be seen if the bone above it is shaved very thin. My first attempts to do this were in dead rats. When the skull was very thin, the transverse sinus could clearly been seen because the deoxygenated blood contrasted well with the rest of the brain tissue. When I tried the same procedure on a rat while it was alive, it was very difficult to determine with any level of certainty the exact location of the anterior edge of the transverse sinus (Fig 2.12). Since the literature reports implantation coordinates that are hundreds of microns anterior to the transverse sinus, this edge needed to be located with 100-micron accuracy, something I was not confident to do in such a low-contrast condition. I learned

too late in the process that this actually is how other labs find the transverse sinus. It takes a trained hand to shave the skull, and a trained eye to locate the transverse sinus. This is perhaps why I was unable to do so without being trained by an experienced person.

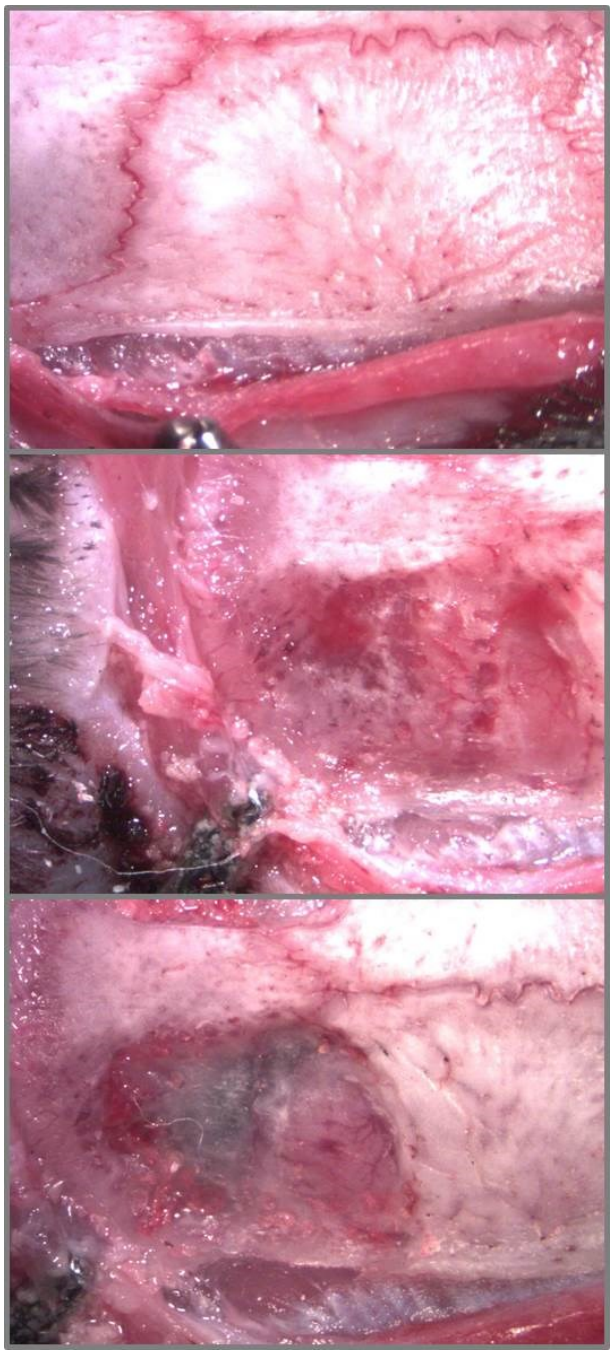

**Fig 2.12:** Attempt to visualize the transverse sinus by shaving the skull. **Top:** Picture of the area over the transverse sinus with the skull wholly intact. **Middle:** Picture of the skull shaved while the rat is alive. Note that the transverse sinus is difficult to locate with a high degree of precision. **Bottom:** Same as above, but after the rat's death. The transverse sinus is the dark region just posterior to the suture.

In the meantime, I tried other methods to locate the transverse sinus. One promising method was laser speckle imaging. This sort of imaging can be used to measure blood flow in vessels under the skin. One paper reported its use through the skull (Li et al., 2006), so I tried to replicate this method. The method is based off the fact that when coherent light reflects off a surface, the interference creates light and dark patches in the reflected light, called speckles. If the surface is moving, the speckle pattern will change in relation to the speed of the surface. This method used 780nm light, which transmits through bone, but reflects off blood. Taking a video and analyzing the change of light intensity of each pixel across time should expose the blood vessels, where the speckle intensity should change more over time than pixels of stationary tissue. This method, however, requires a very stable set up, exact parameters, and a sensitive CCD video camera, a piece of equipment I did not have access to. Ultimately, I could not get the technique working with the available equipment, and could not provide enough guarantee of its eventual success to justify buying new equipment.

Also during this time, I tried to visualize the transverse sinus using bright green light. Green wavelengths transmit through bone. They are absorbed by blood, but reflected by surrounding tissue, resulting in blood vessels showing up as dark regions. This works very well in mice (Barth and Mody, 2011), but not in rats, perhaps due to the thicker skull.

Last, I tried MRI and CT. UCLA has a 7-tesla small animal MRI, and it is capable of showing the location of the MEC for any individual rat. Since MRI only shows soft tissue, it was impossible to have any naturally-occurring external marker that could be used as a zero coordinate during surgery. It would have been easy to place a fatty marker on the rat's head, but getting something small and stable enough to provide 100 micron precision proved difficult. So, I tried microCT. UCLA's microCT is able to give 3D representations of the skull, with enough resolution to see the skull sutures, a very good external marker for referencing coordinates. CT, however, can't resolve soft tissue without a contrast agent, usually an iodine-based injection. The hope was to use a contrast agent appropriate for imaging veins, thus

allowing us to image the skull sutures and transverse sinus in one 3D reconstruction. However, since the safety clearances to start taking such images were long, I simply ran out of time on the project to test whether this method might work.

## 2.5 Spherical Environments in Virtual Reality

### 2.5.1 Introduction

One of the original aims of this thesis was to dissect the functional relationship between border and grid cells. Several studies suggest that the pattern of periodicity in grid cells is influenced by the presence and location of environmental boundaries (Barry et al., 2007; Derdikman et al., 2009; Stensola et al., 2012; Krupic et al., 2015; Stensola et al., 2015). Information about these boundaries is most likely provided to the grid cells by border cells in the MEC (Solstad et al., 2008). The ideal experiment would be to selectively inhibit or activate border cells and observe their influence on grid cells. However, these two cell types are spatially intermingled within the same brain area, so spatially localized pharmacologic interventions would not provide the level of specificity necessary. In addition, no genetic marker has yet been confirmed for either grid cells or border cells. Since these cell types are functionally defined, it is difficult to have both access to the genetic or morphological characteristics, and a measure of the cell's spatial firing properties in the awake, freely moving animal. The only technique that will allow for this level of analysis is *in vivo* patch clamping or juxtacellular recording, and other labs are currently working on this problem (Tang et al., 2014).

In the meantime, while there is no way to pharmacologically or optogenetically control the firing of border cells, the only way to prevent these cells from firing is to have an environment without boundaries. Due to the mechanical restraints and the finite nature of laboratory space, such an environment is impossible to achieve in the real world. Thus, virtual reality was a necessary tool in answering this question. There are two types of virtual

environments that have no boundaries: a flat plane that extends infinitely in every direction, or a sphere. Both types of environments have pros and cons for measuring the activity of grid cells. Planes have a geometry more similar to RW environments, but in an infinite plane, nothing confines the rat to a particular space and thus obtaining sufficiently dense coverage to assess spatial firing properties might be difficult. Small spheres solve this coverage problem, but it is unclear how grid cells would map an environment of this geometry. Ultimately, we decided to first measure grid cell activity in a small spherical environment in virtual reality.

After data collection had begun, it became clear that recording grid cells on a virtual sphere would yield uninterpretable data. First, our own recordings in finite planar environments showed that grid cells do not maintain their spatial selectivity in VR like we had expected (see Chapter 4). Therefore it was unlikely that grid cells would have any discernable spatial activity in spherical environments in VR. Second, another lab shared data through a poster that suggested that even if grid cells were able to map virtual environments, they still would not be able to maintain their periodicity on a sphere. In this experiment, rats that were raised in opaque spherical cages had distorted grid fields when exposed to planar environments. Even over a period of a few weeks, the grid cells were unable to map the environment with a regular pattern (Kruge et al., 2013). Since our rats were raised in standard rectangular cages, it seemed unlikely that their grid cell systems would be able to adapt to a spherical geometry in the VR.

Eventually, data collection was stopped for this project. Some electrophysiological data was recorded but not analyzed. While virtual spherical environments might not be useful for studying the activity of spatially selective cells, it might be useful for other questions. With this potential purpose in mind, included here is a preliminary analysis of the behavioral data collected from spherical virtual environments, and the effects of particular task parameters.

### 2.5.2 Methods

#### *2.5.2.1 Subjects*

Seven adult male Long-Evans rats (rat IDs: N, P, R, Z, B, C, H), approximately 3.5 months old at the start of training, were individually housed on a 12 hour light/dark cycle. Animals were food restricted (15-20 g of food per day) to maintain body weight. Animals were allowed to access a restricted amount of water (25-35 ml of water per day) after the behavioral session to maintain motivation. All experimental procedures were approved by the UCLA Chancellor's Animal Research Committee and were conducted in accordance with USA federal guidelines.

#### *2.5.2.2 Virtual reality apparatus*

The VR system contained a 61cm diameter Styrofoam sphere that floated freely on an acoustically quiet air cushion (Fig 2.1A). The ball rotation was measured by two orthogonally placed laser sensors, merged by a microcontroller, and used by custom software to change the surrounding visual scene. There was one-to-one mapping between the rat's movements and the corresponding changes in the virtual environment. The standard deviation of the ball tracking for one revolution was 1.3% of a revolution. A micro projector projected visual stimuli on a custom made convex mirror, which reflected the stimuli onto a 300°, 68cm diameter, 75cm tall cylindrical screen made of white fabric. Our VR system allowed presentation of an undistorted visual scene in all directions including within 1cm of the rat. A hinged harness held the rat on the sphere. A stainless steel tube mounted in front of the rat dispensed liquid rewards (10% sucrose water, 150µl per reward) controlled by a software driven solenoid valve. The VR software was built in C++ using the Ogre 3D graphics engine and OpenAL. VR data, including the animal's (virtual) speed, position and heading, were recorded by the software at a sampling rate of 60Hz.

#### *2.5.2.3 Virtual spherical environment*

The virtual environment consisted of a virtual sphere with a radius of 32cm floating in a dark space. The white surface of the sphere was covered with a regular pattern of 2cm diameter black dots spaced 4cm apart. This pattern was designed to provide optic flow, but no positional or directional information. Sixteen regularly spaced, flat visual stimuli hung 90cm above the surface of the sphere on all sides. All stimuli were oriented to be parallel to the sphere surface, i.e. all stimuli appeared to be "facing" the rat when he stood directly under them. All 16 stimuli were different shapes and all were asymmetrical in either shape, color, or both.

#### *2.5.2.4 Training*

All rats completed the virtual reality pretraining procedures described previously in this Chapter. All rats were proficient at running on planar environments in virtual reality before they were introduced to the sphere.

#### *2.5.2.5 Task and parameters*

In all versions of the task, the rat was required to forage for sugar water reward. To optimize the behavioral performance, many parameters were changed throughout the course of the study. At first, rats were trained with visibly marked reward zones ("Marked" condition); a pillar hung above the reward zone and could be seen from many parts of the sphere. Then the decision was made to remove the pillar from the environment so cell firing would not be influenced by this salient cue. Subsequently, all rats were trained to run for hidden rewards ("Hidden" condition). This changed the nature of the task and also the rats' performance.

Another thing that was changed was the distribution of the rewards. At first, each reward location was selected at random, in phi and theta spherical coordinates ("Random" condition). Even with a uniform distribution of selection over both phi and theta, this method selects a higher proportion of coordinates near the poles of the sphere. So, to encourage even coverage in the rat's behavior, we wondered if it was better to have an even distribution of reward zones.

The easiest way to ensure this in spherical coordinates was to preselect a finite number of evenly spaced reward zones, and activate them in a random order ("Preselected" condition).

Last, we eventually realized that the rats were not able to attain the same level of performance with hidden rewards as they had with marked rewards. Since we had made the design choice to have hidden rewards, we counteracted this with larger reward zones to increase the chance of the rats walking through them. Eventually, we adopted a shaping procedure where the reward zones started very large, and got smaller as the rats' performance increased.

Table 2.2 summarizes which rats were run on which types of tasks, and for how many sessions total.

| Parameter Combination ID Number | Marked or Hidden Rewards | Selection of Reward Locations | Reward Zone Radius | Rats Trained on this Task | Total Number of Sessions | Color Used to Represent in Figures |
|---|---|---|---|---|---|---|
| 1 | Marked | Random | 10cm | N, R | 5 | **Red** |
| 2 | Marked | Preselected | 10cm | R, Z | 2 | **Pink** |
| 3 | Hidden | Random | 10cm | N, P | 14 | **Orange** |
| 4 | Hidden | Preselected | 10cm | N, R, Z | 59 | **Purple** |
| 5 | Hidden | Preselected | 75cm | Z, B | 4 | **Light Green** |
| 6 | Hidden | Preselected | 50cm | B, C, H | 6 | **Dark Green** |
| 7 | Hidden | Preselected | 25cm | B | 2 | **Light Blue** |
| 8 | Hidden | Preselected | 20cm | B, C, H | 59 | **Dark Blue** |

**Table 2.2:** Summary of behavior data collected on the virtual spherical environment.

#### *2.5.2.6 Statistics*

Resampling statistics were used to compare group data. The median was used intead of mean because many groups were not normally distributed. A modified one-way analysis of variance method was used, where the F statistic was defined as the sum of the N-weighted absolute values of the differences between the group medians and the grand medians, divided by the sum of the absolute values of the differences between each value and its group median. The same F statistic was calculated for 10,000 resampled surrogate data sets. Surrogate data sets were created by first subtracting each value from its group median, then resampling from

each group separately with replacement. Data points were treated as independent, even though each animal contributed many samples to the dataset. Therefore, these statistics do not take into account individual effects, or the effects of learning across sessions.

### 2.5.3 Results

#### *2.5.3.1 Rats were able to complete the task with all parameter combinations*

Rats were able to run to obtain reward in all task types (Fig 2.13-20 top left), but measures of the quality of their behavior differed. When studying spatial cognition, it is important for the rat to be able to obtain dense and approximately even coverage of the area in a reasonable amount of time. There are two important aspects of this. First is average speed over the session. The faster the rat runs the more area he can cover in a shorter amount of time. For this, it was useful to look at the cumulative distance traveled across time in the session (Fig 2.13-20 bottom left). Steeper slopes signified faster running speeds, and flat regions denoted long pauses in running, which could be indicative of inadequate motivation. Inadequate motivation could be caused by satiety due to too much reward, or frustration due to too little. Related to this is the efficiency of the paths the rat takes to obtain reward. Our measure for this was the reward path residual, which is the distance the rat traveled between rewards minus the actual shortest distance between those rewards along the sphere surface (Fig 2.13-20 bottom right). Smaller residuals indicate more efficient paths. Residuals of more than 200cm would suggest the rat traveled more than once around the circumference of the sphere in searching for the reward zone.

A second measure of behavior quality is the density of coverage. Total meters run contributed to this, with a longer total running distance allowing for more dense coverage. However, the spherical geometry of the environment allows the rat to run straight around the circumference indefinitely; so we needed a way to access the relative coverage over the surface

of the sphere. This is more difficult to calculate and to visualize in spherical geometry, so as a crude measure of occupancy, we split the surface of the sphere into 12 equally-sized bins and calculated the percentage of time spent in each bin (Fig 2.13-20 top right). If coverage is completely even, each bin would have an equal occupancy of 8.3%. So, as a proxy measure for evenness of coverage, we used the range of occupancy across these bins, with lower values indicating more even coverage.

Fig 2.13-20 show example sessions from each task type. Examples were selected to most closely match the means of speed, distance per reward, and time per reward of all the sessions for that task type.

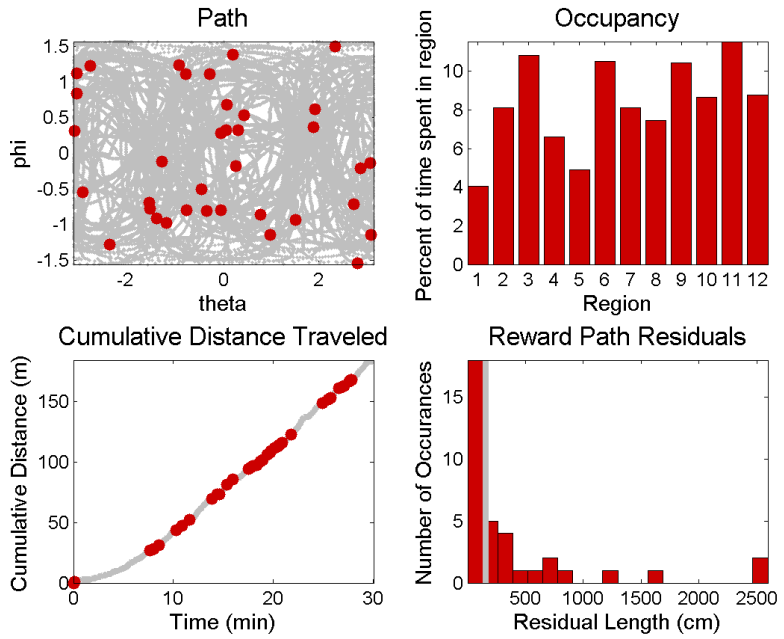


**Fig 2.13:** Example session on a spherical VR environment with maked rewards, random reward locations, and 10cm reward zones (Rat ID: N): In this and all subsequent figures of example sessions: **Top Left:** The rat's path during the session. Grey dots mark his position in theta and phi coordaintes; superimposed colored dots mark his position at reward delivery. The surface of the sphere is distorted to adhere to a rectangular surface, i.e. the top and bottom of the figure appear more stretched out. **Bottom Left:** Cummulative distance traveled over time in grey; superimposed colored dots mark distance and time of reward delivery. **Top Right:** Percent of time spent in each of twelve nonoverlapping regions of equal area. Bins labeled with adjacent numbers are not necessarily adjacent on the sphere surface. **Bottom Right:** Histogram of reward path residuals, or the distance the rat traveled between rewards minus the shortest distance on the sphere between those rewards. A larger residual means a less efficient path was taken to reach the reward. Vertical grey line denotes the median.

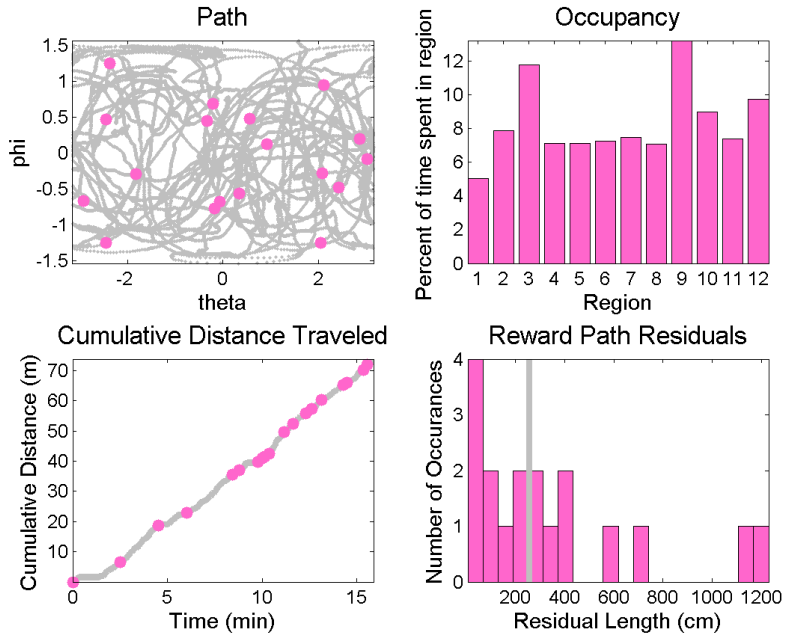


**Fig 2.14:** Example session on a spherical VR environment with maked rewards, preselected reward locations, and 10cm reward zones (Rat ID: R).

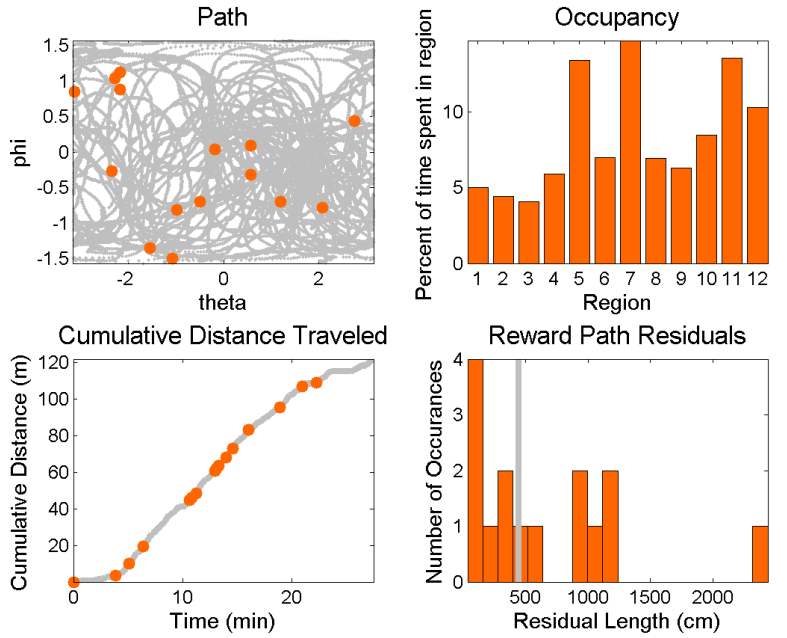


**Fig 2.15:** Example session on a spherical VR environment with hidden rewards, random reward locations, and 10cm reward zones (Rat ID: P).

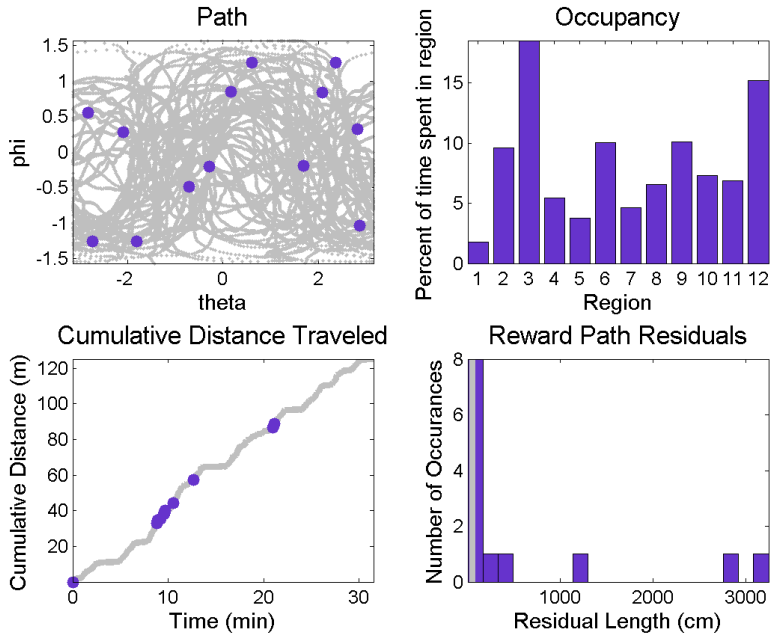


**Fig 2.16:** Example session on a spherical VR environment with hidden rewards, preselected reward locations, and 10cm reward zones (Rat ID: R).

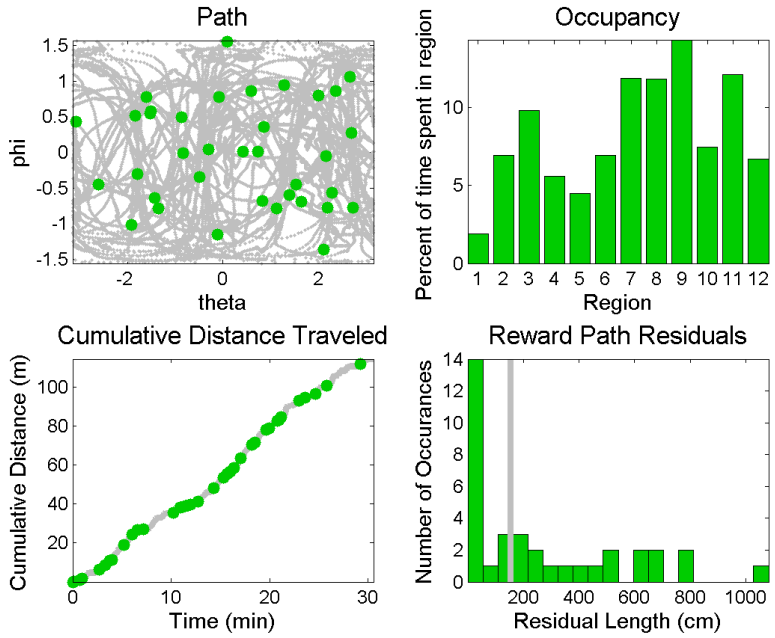


**Fig 2.17:** Example session on a spherical VR environment with hidden rewards, preselected reward locations, and 75cm reward zones (Rat ID: Z).

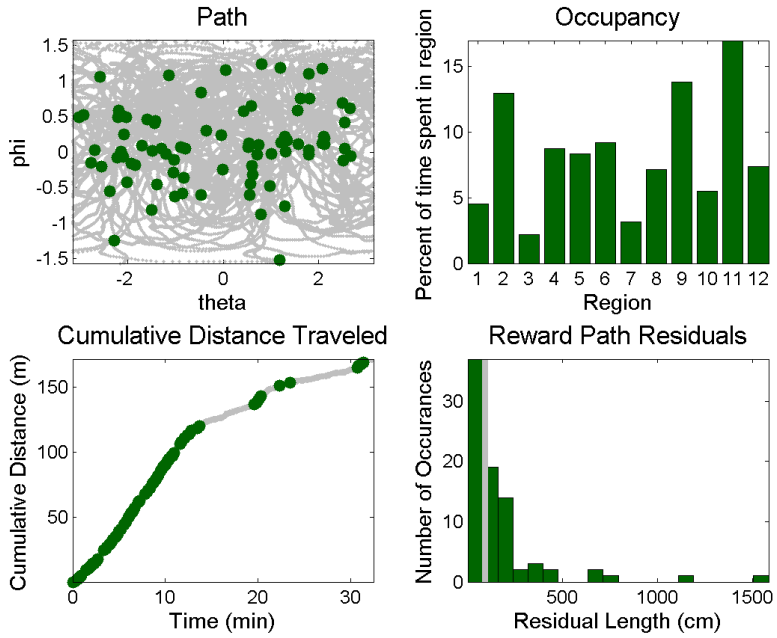


**Fig 2.18:** Example session on a spherical VR environment with hidden rewards, preselected reward locations, and 50cm reward zones (Rat ID: H).

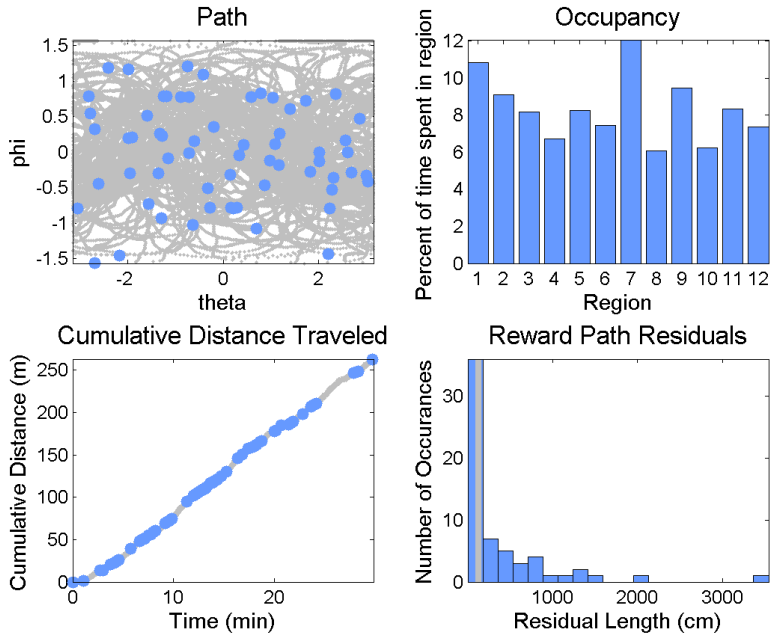


**Fig 2.19:** Example session on a spherical VR environment with hidden rewards, preselected reward locations, and 25cm reward zones (Rat ID: B).

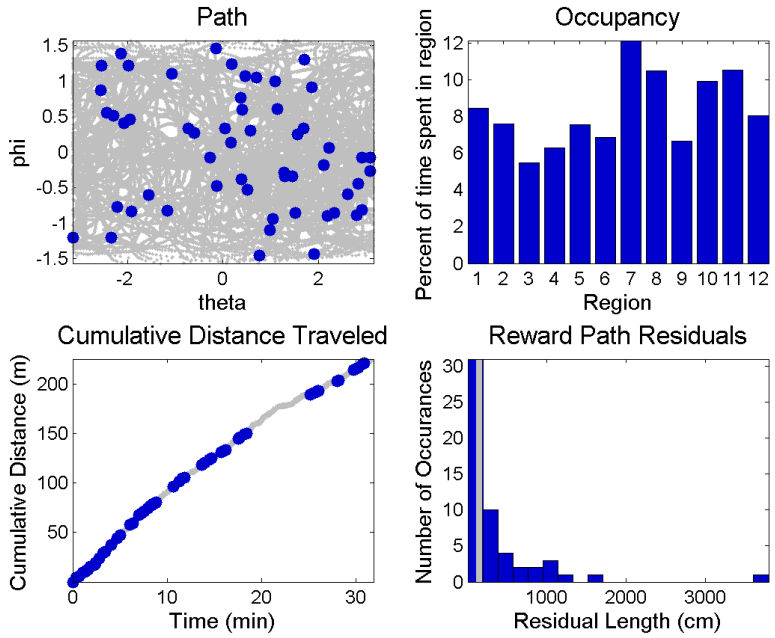


**Fig 2.20:** Example session on a spherical VR environment with hidden rewards, preselected reward locations, and 20cm reward zones (Rat ID: C).

Figures 2.21-23 show the group data from each task type. We looked at the rats' ability to efficiently obtain rewards, both in distance run (Fig 2.21) and time spent (Fig 2.22), as well as their average speed over the sessions (Fig 2.22). Last, we attempted to calculate a measure to succinctly describe the amount of spatial coverage achieved on the sphere. For this, we computed the difference in occupation between the most visited and least visited regions during the session (Fig 2.23). If occupancy was distributed evenly over the 12 regions, then this number would be zero, and greater numbers would indicate less even coverage.

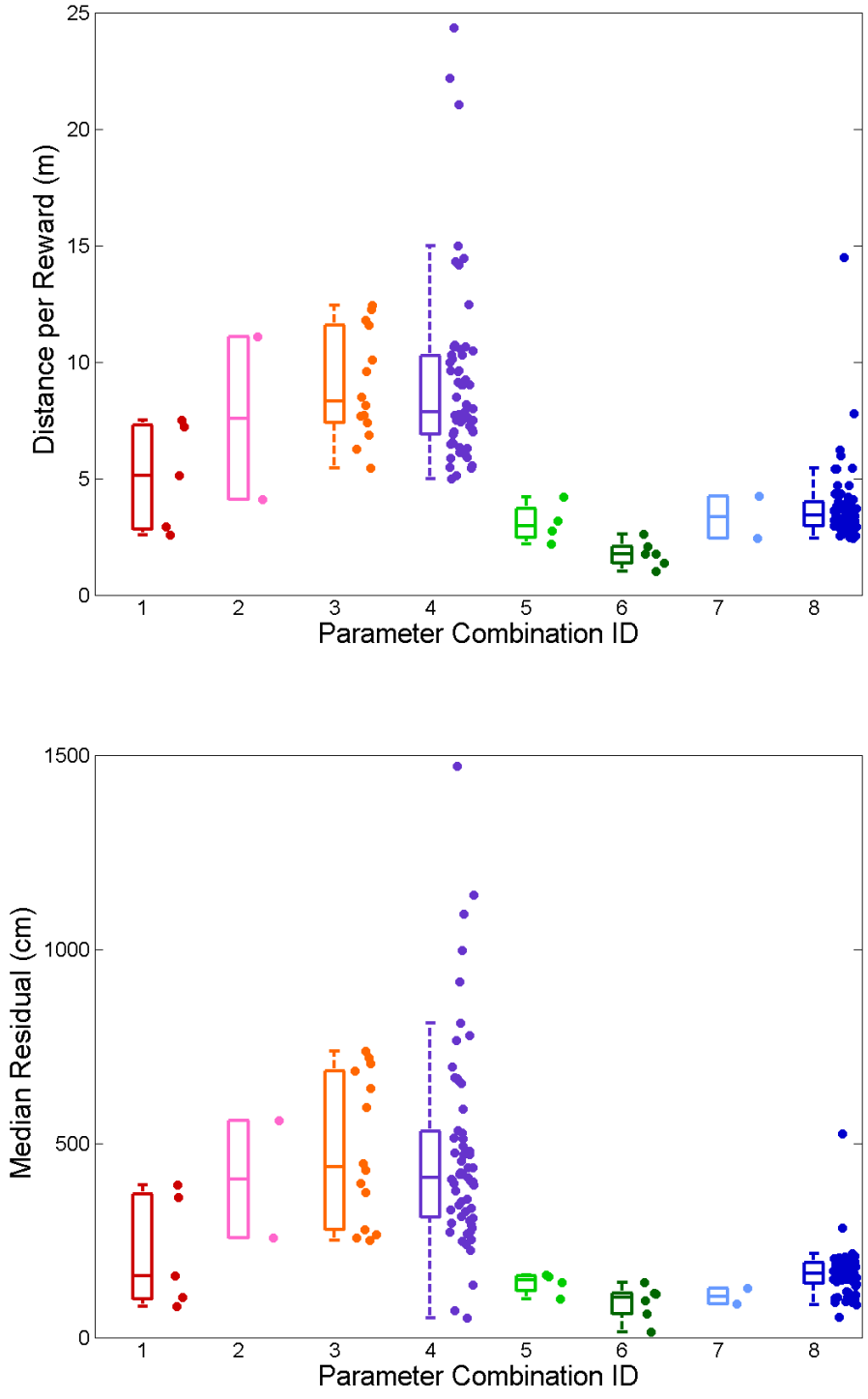


**Fig 2.21:** Rats' efficiency of obtaining reward with respect to distance compared across parameter combinations in the virtual sphere. **Top:** Average distance traveled between rewards, each data point is one session. **Bottom:** Median residual of distance traveled to obtain reward. In this and in all subsequent box and whisker plots, horizontal line is the median, box denotes 25$^{th}$ and 75$^{th}$ percentiles, and whiskers mark the range excluding outliers. Color scheme is same as previous example figures and is continued in all subsequent figures.

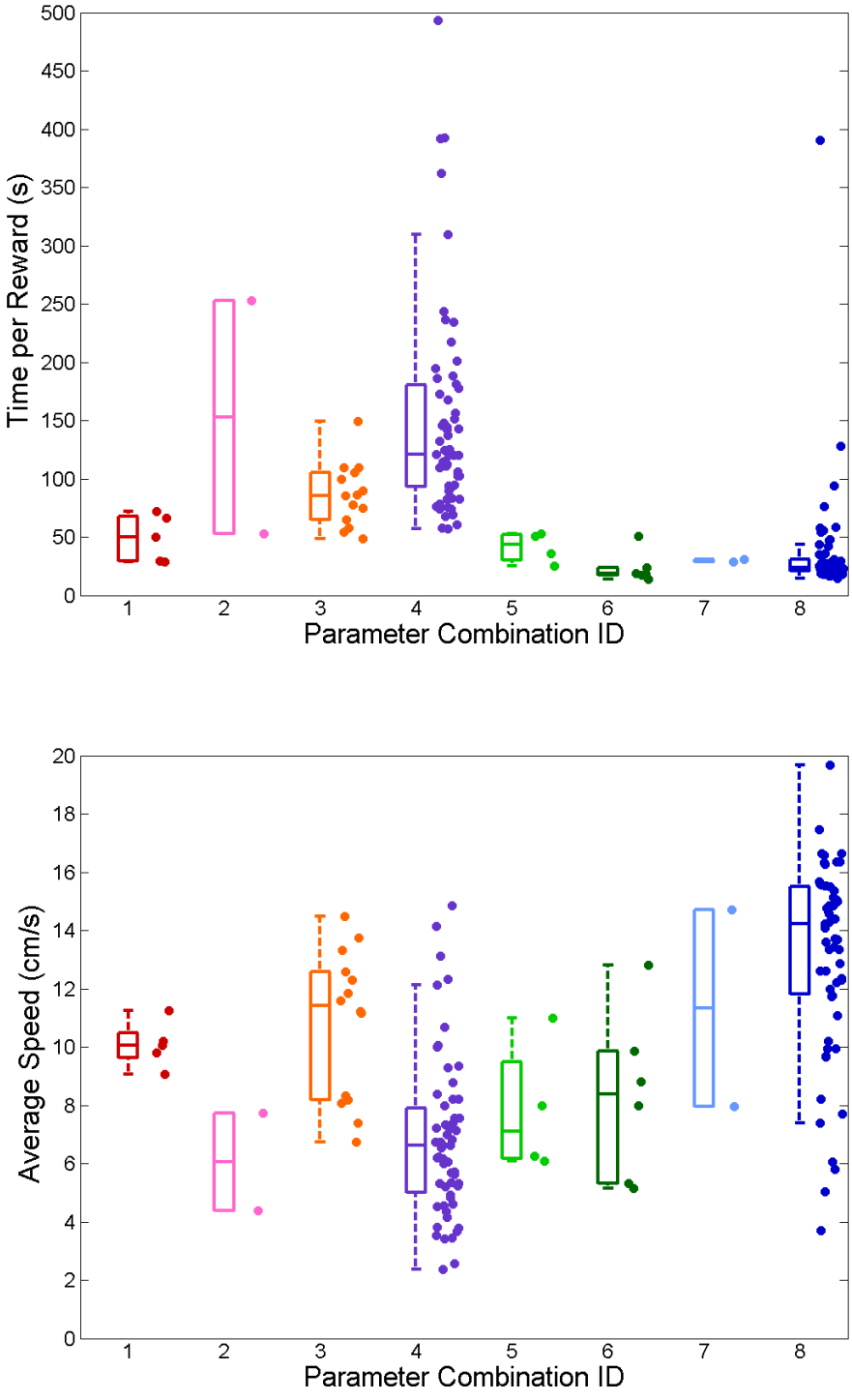


**Fig 2.22:** Rats' efficiency of obtaining reward with respect to time compared across parameter combinations in the virtual sphere. **Top:** Average time between rewards. **Bottom:** Average speed during each session.

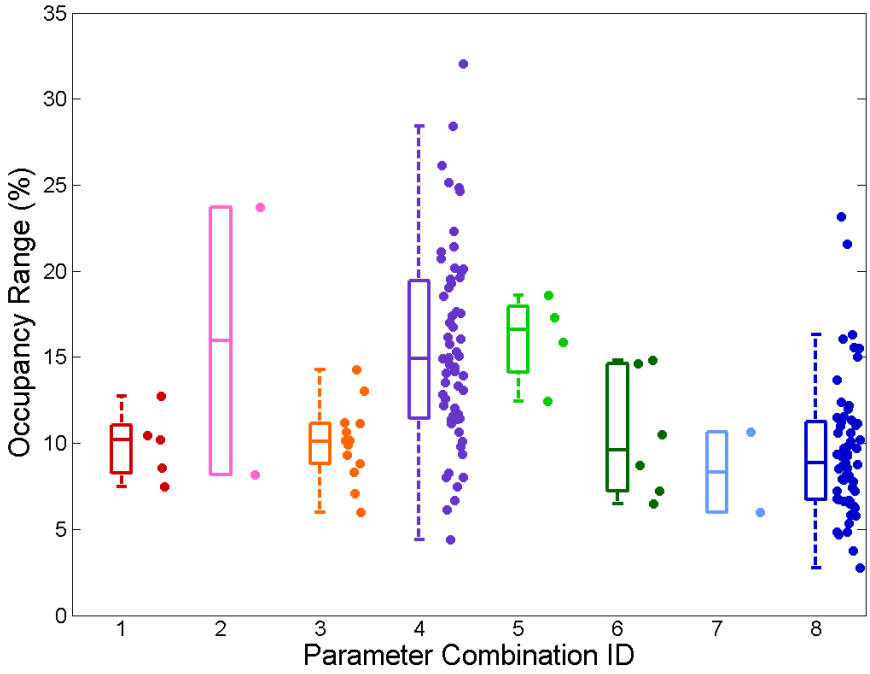


**Fig 2.23:** Rats' coverage of the spherical environment, compared across parameter combinations in the virtual sphere. Shown is difference between minimum and maximum occupancy in 12 spatial bins. Even coverage would have an occupancy range close to zero.

### *2.5.3.2 Behavior improves rapidly when reward zones are marked*

Only rat N was run with a marked reward zone for more than 1 session. In this rat, there was a steady and rapid improvement in his behavior across sessions while the reward was marked (Fig 2.24). He was able to obtain more rewards faster and more efficiently, evidenced by the decreases in distance and time per reward and median residual, despite no change in average speed. The decrease in the median residual below 200cm is particularly striking because it indicates that after training he did not circumscribe the sphere more than once to reach the reward. In contrast, his performance dropped dramatically when he first ran on a task with a hidden reward zone, as can be seen by a decreased speed, and increased distance and time per reward and median residual.

Sessions with marked rewards were not conducted long enough to observe asymptotic levels of behavior, but the rapid improvement across sessions is clear. This rapid improvement in reward efficiency was not observed in tasks with hidden rewards, suggesting marked reward zones are necessary for this learning. This also indicates that even though this rat had never experienced spherical geometry previously, he was able to learn how to traverse the space to reach the marked reward locations efficiently.

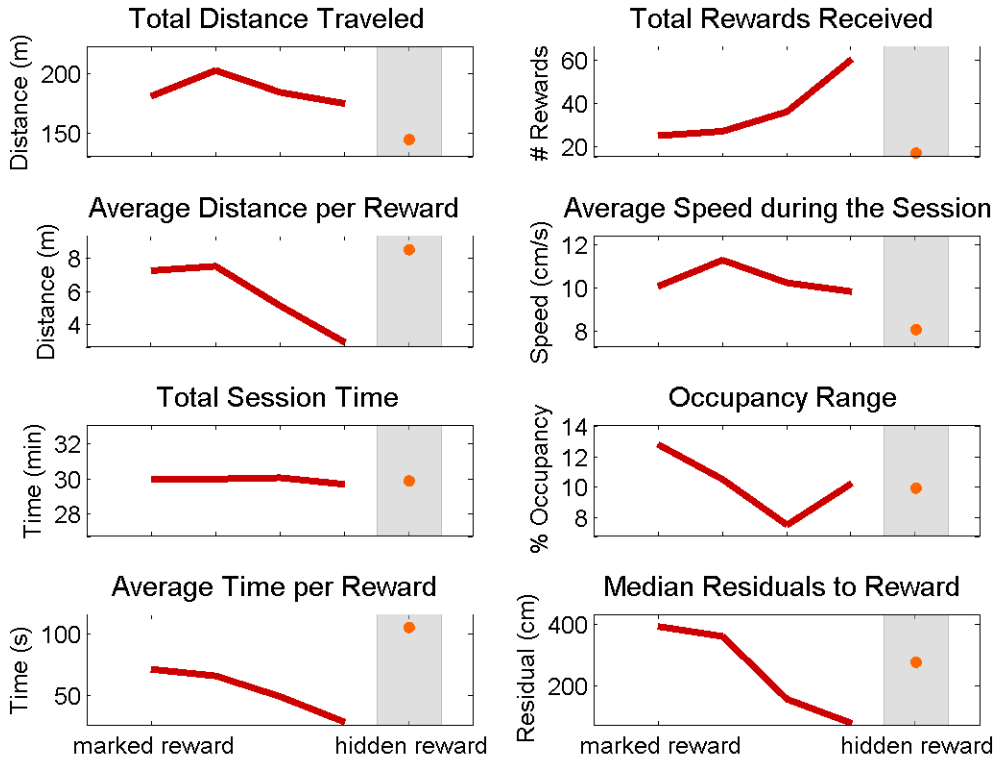


**Fig 2.24:** Performance across sessions in rat N, run with a marked reward for 4 sessions, then with a hidden reward. Gray shading indicates sessions with hidden rewards.

Rat R was switched back and forth between tasks that had marked and hidden rewards. In this case, there was an instant and marked increase in behavioral performance when reward zones were marked (Fig 2.25). Compared to adjacent sessions with hidden rewards, those with

marked rewards have decreased distance and time per reward and median residuals, increased speeds, and more even coverage.

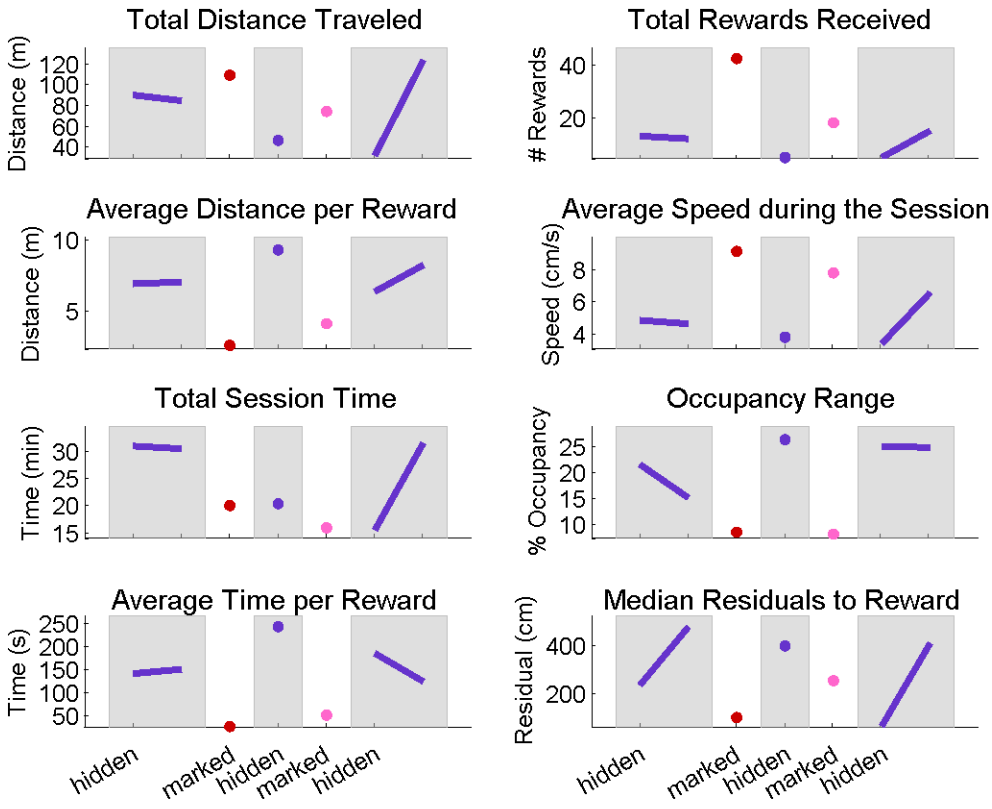


**Fig 2.25:** Performance across sessions in rat R, run with marked and hidden rewards on alternating sessions. Gray shading indicates sessions with hidden rewards.

### *2.5.3.3 Behavior does not improve when reward zones are small and hidden*

After switching from a task with marked reward zones, rat N was run on a task with hidden, 10cm reward zones for 9 sessions. Despite increases in speed, and moderate improvements in evenness of coverage, this rat was unable to improve his efficiency in obtaining reward (Fig 2.26). Qualitatively similar results were found in rat P, run on the same task for 5 sessions. Unlike rat N, this rat showed no improvement in behavior, neither in reward efficiency nor in speed or coverage (Fig 2.27).

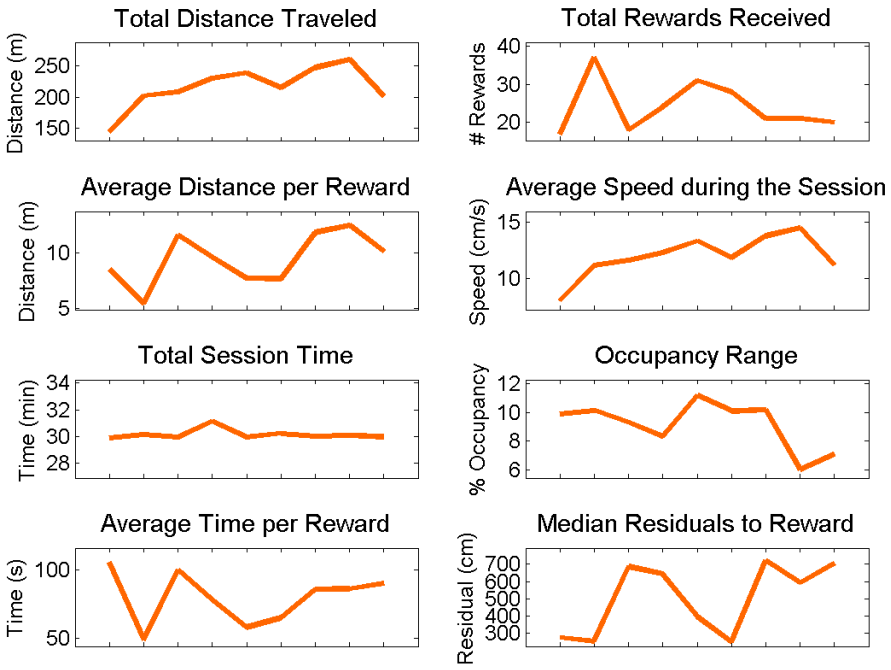


**Fig 2.26:** Performance across sessions in rat N, run with a hidden, 10cm reward for 9 sessions.

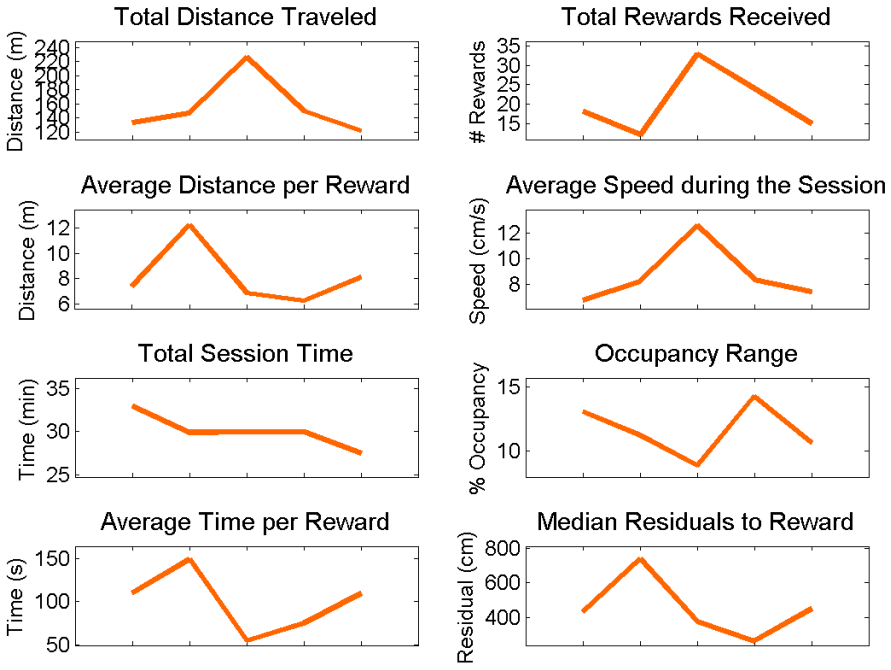


**Fig 2.27:** Performance across sessions in rat P, run with a hidden, 10cm reward for 5 sessions.

### *2.5.3.4 Behavior improves when reward zones are larger and hidden*

More improvement in behavioral performance was seen in rats that were trained with larger reward zones. These rats were first run on a task with very large reward zones (either 75cm or 50cm) and then switched to medium sized reward zones (either 25cm or 20cm). Even though decreases in performance occurred at the time of switching from large to medium sized rewards, rat B showed a subsequent improvement, seen in the decrease in distance and time per reward and an increase in average speed (Fig 2.28). There was no clear trend in median residuals or evenness of coverage, however. In contrast, rat H did show improvement in these areas, though this trend might be misleading due to a small number of sessions (Fig 2.29).

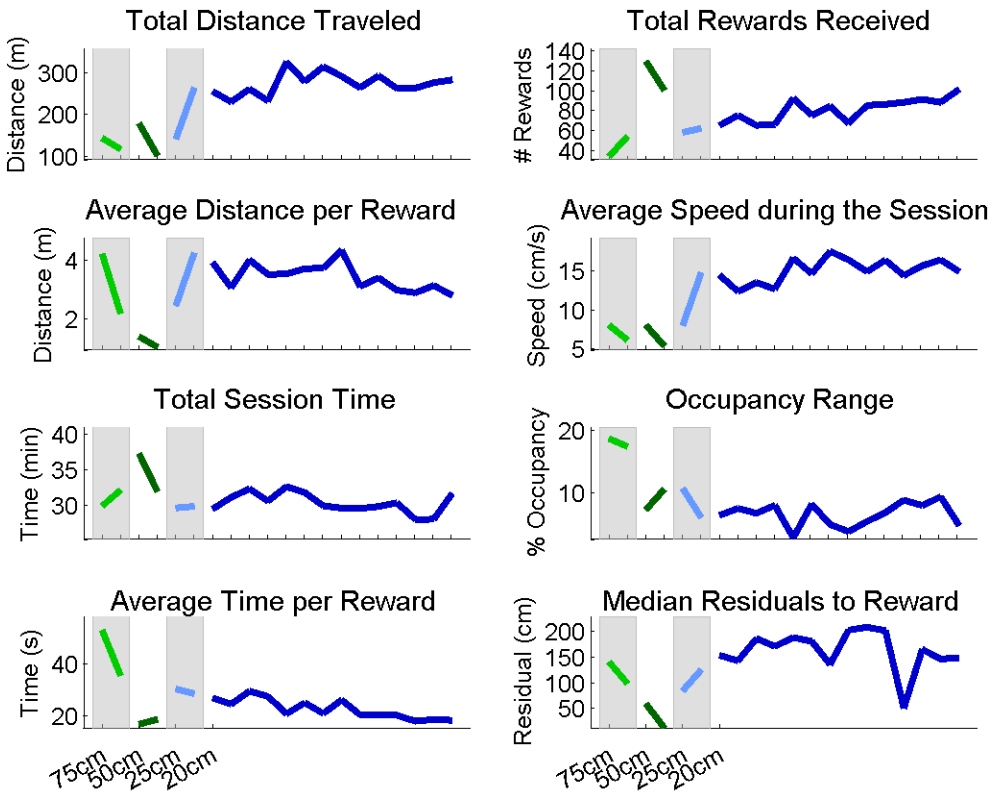


**Fig 2.28:** Performance across sessions in rat B, run with a hidden reward zones that ranged from 75cm to 20cm in radius. Grey shading is included to more clearly denote changes in task type.

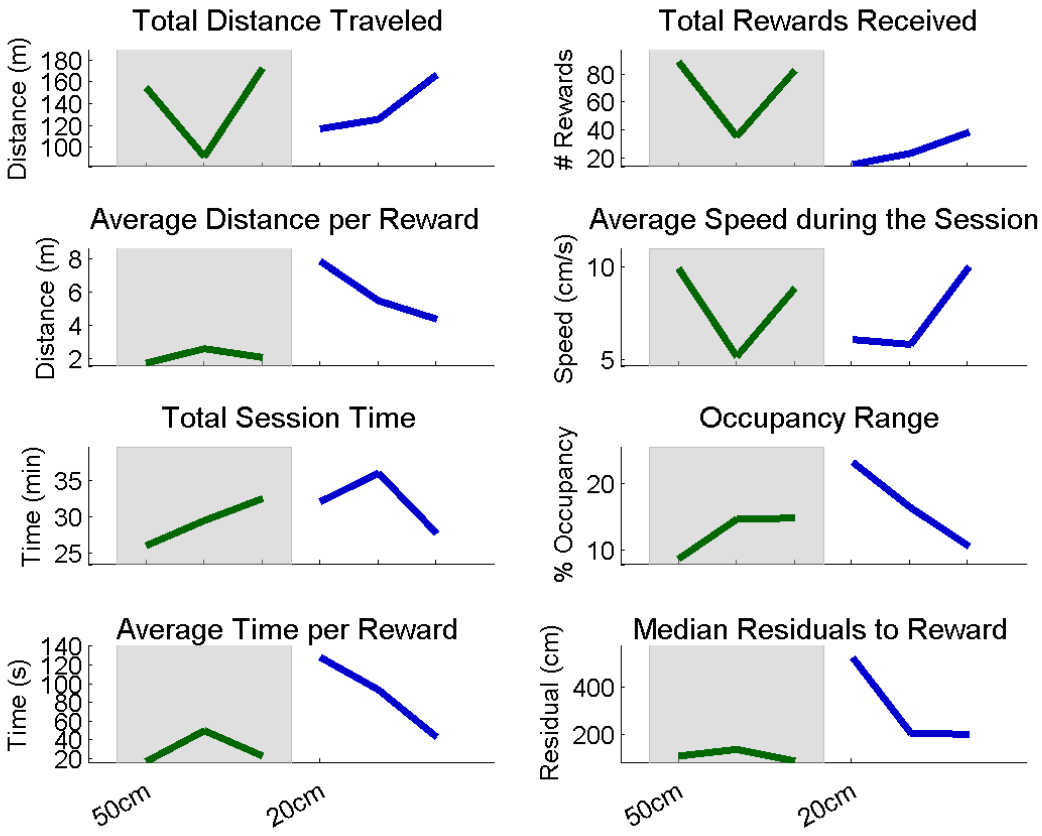


**Fig 2.29:** Performance across sessions in rat H, run with 50cm and 20cm radius hidden reward zones. Grey shading is included to more clearly denote changes in task type.

To further examine the effect of reward zone size, we pooled sessions from different task types across rats and across time. On every measure of behavior, there was a significant effect of reward zone size (Fig 2.30-32). Rats took more efficient paths and took less time to obtain rewards with reward zone sizes larger than 10cm, compared to those that were 10cm. Between all the reward zone size categories, running speed was significantly higher and occupancy range significantly lower with a 20-25cm reward zone, suggesting that this size of reward zone struck a balance between a reward zone that was too small to find, and one that was too large and too easy to find. Overall, all the measures of behavior showed the best performance in the 20-25cm condition.

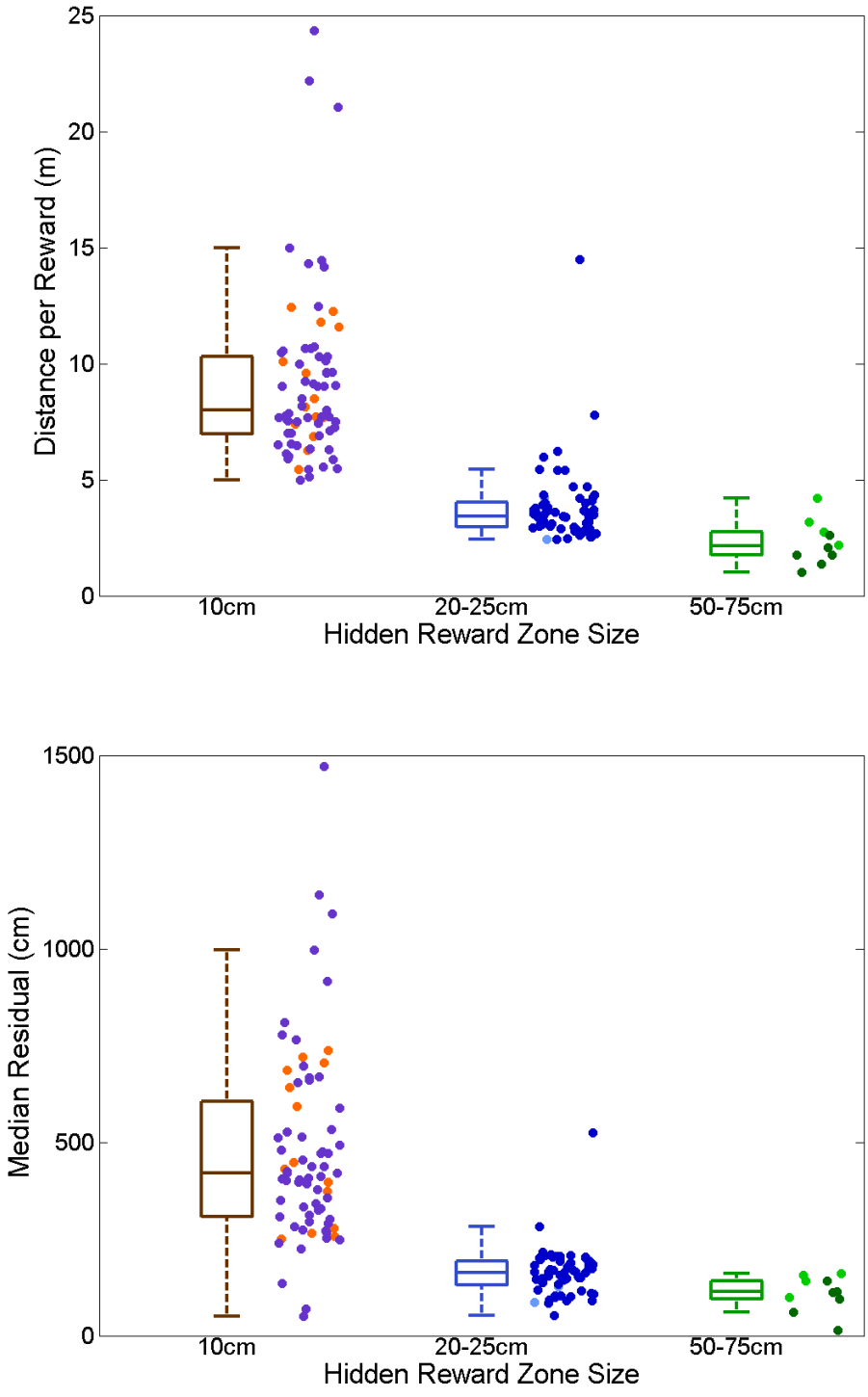


**Fig 2.30:** Effect of reward zone size on efficiency of obtaining reward with respect to distance in the virtual sphere. **Top:** There was a significant effect of reward zone size on the median distance rats ran between rewards (8.0m for 10cm, 3.4m for 20-25cm, and 2.1m for 50-75cm, $F = 1.46$, $p<10^{-4}$). **Bottom:** There was a significant effect of reward zone size on the median residual distance ran to obtain reward (420cm for 10cm, 160cm for 20-25cm, and 110cm for 50-75cm, $F = 1.24$, $p<10^{-4}$).

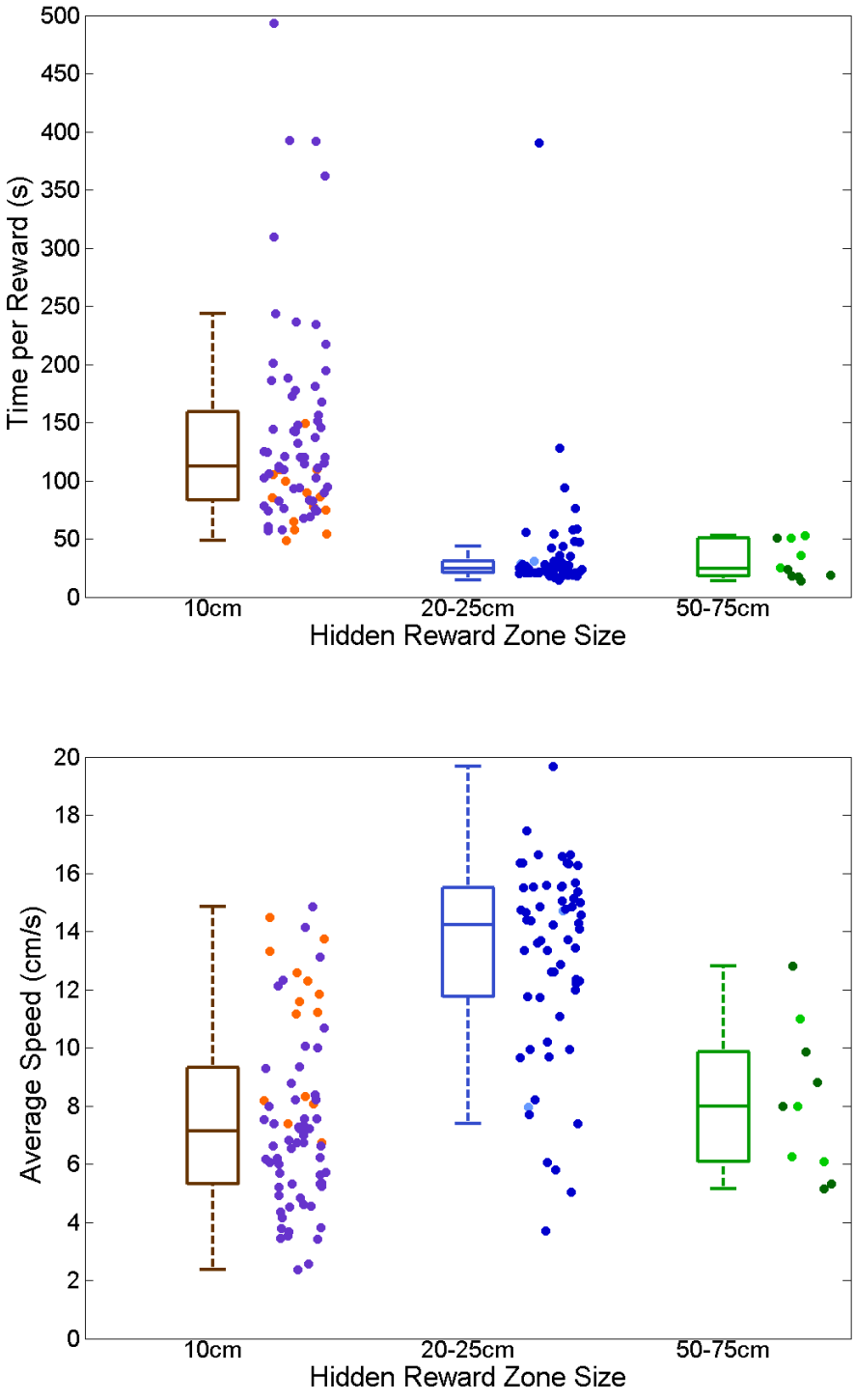


**Fig 2.31:** Effect of reward zone size on efficiency of obtaining reward with respect to time in the virtual sphere. **Top:** There was a significant effect of reward zone size on the median amout of time rats ran between rewards (110s for 10cm, 25s for 20-25cm, and 24s for 50-75cm, $F = 1.09$, $p<10^{-4}$). **Bottom:** There was a significant effect of reward zone size on the the median of the average running speed over the entire session (7.1cm/s for 10cm, 14cm/s for 20-25cm, and 8.0cm/s for 50-75cm, $F = 1.40$, $p<10^{-4}$).

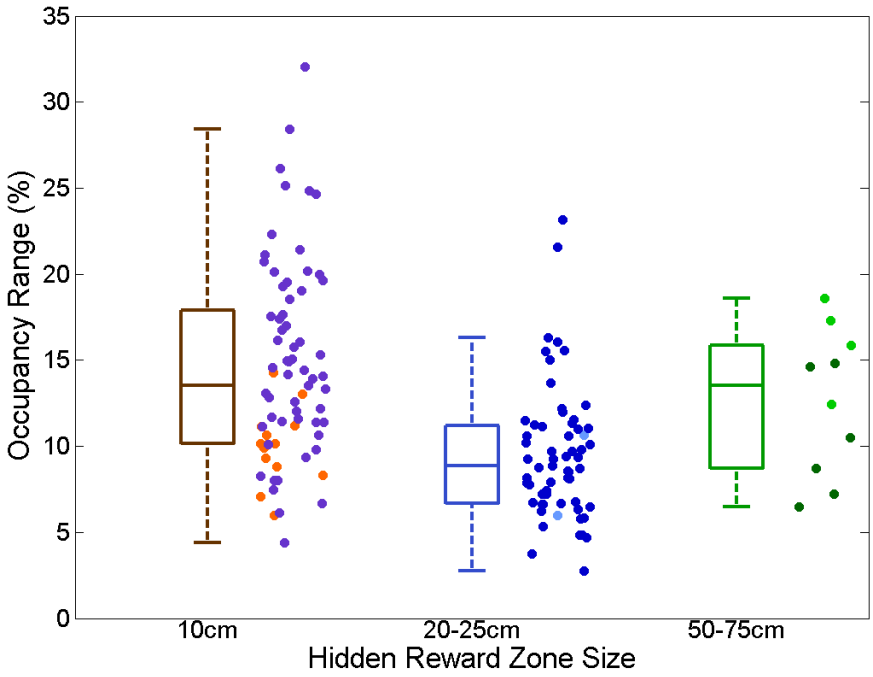


**Fig 2.32:** Effect of reward zone size on coverage in the virtual sphere. There was a significant effect of reward zone size on the median of the range in percent occupancy (14% for 10cm, 8.9% for 20-25cm, and 14% for 50-75cm, $F = 0.633$, $p<10^{-3}$).

### *2.5.3.5 Even distribution of rewards does not increase coverage*

Last, we asked whether the distribution of the reward zones affected the rats' coverage of the environment. Based on our crude measure of coverage, we found that there was no significant difference whether the hidden reward zones were clustered at the poles ("Random") or evenly distributed ("Preselected") (Fig 2.33).

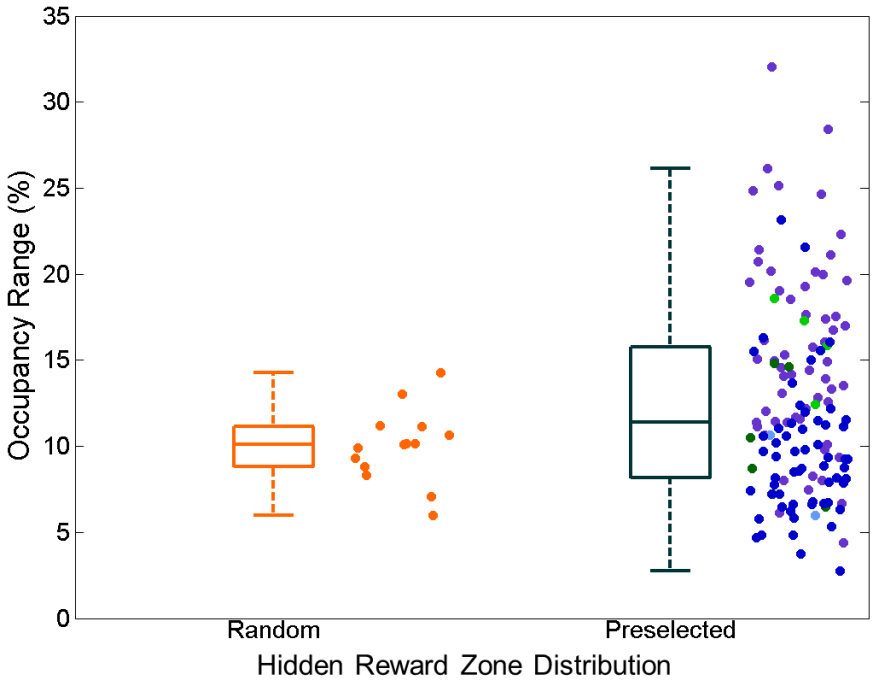


**Fig 2.33:** Effect of reward zone distribution on coverage in the virtual sphere. There was no significant effect of reward zone distribution on the median of the range in percent occupancy (10% for Random, 11% for Preselected, F = 0.08, p=0.15).

### 2.5.4 Summary and conclusions

This pilot study to optimize spatial behavior in virtual spherical environments yielded a few findings. First, one rat showed steady improvement with marked reward zones, suggesting that rats can learn to efficiently navigate spherical environments to reach visible locations. Second, when reward zones are hidden, the best behavior can be obtained when the reward zones are neither too large nor too small. In a spherical environment with a radius of 32cm, we obtained the best results with reward zones 20-25cm in radius. In this condition, the reward zones were large enough for the rats to find in a reasonable amount of time, but small enough that rats had to run a reasonable distance between rewards. Last, we were unable to influence the quality of coverage on the sphere, despite making reward zones more evenly distributed.

## 2.6 References


Barry, C., Hayman, R., Burgess, N., & Jeffery, K. J. (2007). Experience-dependent rescaling of entorhinal grids. *Nature neuroscience*, *10*(6), 682–4.

Barth, A. M. I., & Mody, I. (2011). Changes in hippocampal neuronal activity during and after unilateral selective hippocampal ischemia in vivo. *The Journal of neuroscience : the official journal of the Society for Neuroscience*, *31*(3), 851–860.

Derdikman, D., Whitlock, J. R., Tsao, A., Fyhn, M., Hafting, T., Moser, M.-B., & Moser, E. I. (2009). Fragmentation of grid cell maps in a multicompartment environment. *Nature neuroscience*, *12*(10), 1325–32. Nature Publishing Group.

Fyhn, M., Molden, S., Witter, M. P., Moser, E. I., & Moser, M.-B. (2004). Spatial representation in the entorhinal cortex. *Science (New York, N.Y.)*, *305*(August), 1258–1264.

Harvey, C. D., Collman, F., Dombeck, D. A., & Tank, D. W. (2009). Intracellular dynamics of hippocampal place cells during virtual navigation. *Nature*, *461*(7266), 941–6. Nature Publishing Group.

Hölscher, C., Schnee, A., Dahmen, H., Setia, L., & Mallot, H. A. (2005). Rats are able to navigate in virtual environments. *The Journal of experimental biology*, *208*, 561–9.

Kruge, I.U., Wernle, T., Moser, E.I., Moser, M.-B. (2013). *Grid cells of animals raised in spherical environments.* Program No. 769.14. 2013 Neuroscience Meeting Planner. San Diego, CA: Society for Neuroscience, 2013. Online.

Krupic, J., Bauza, M., Burton, S., Barry, C., & O'Keefe, J. (2015). Grid cell symmetry is shaped by environmental geometry. *Nature*, *518*(7538), 232–235. Nature Publishing Group.

Li, P., Ni, S., Zhang, L., Zeng, S., & Luo, Q. (2006). Imaging cerebral blood flow through the intact rat skull with temporal laser speckle imaging. *Optics letters*, *31*(12), 1824–1826.

Savelli, F., Yoganarasimha, D., & Knierim, J. J. (2008). Influence of boundary removal on the spatial representations of the medial entorhinal cortex. *Hippocampus*, *18*, 1270–1282.

Schmidt-Hieber, C., & Häusser, M. (2013). Cellular mechanisms of spatial navigation in the medial entorhinal cortex. *Nature neuroscience*, *16*(3), 325–31. Nature Publishing Group.

Schnee, A. (2008). *Rats in virtual reality: The development of an advanced method to study animal behavior* (Doctoral dissertation). Retrieved from Eberhard Karls Universitat Tubingen Universitatsbibliothek Publikationssystem http://nbn-resolving.de/urn:nbn:de:bsz:21-opus-35504

Solstad, T., Boccara, C. N., Kropff, E., Moser, M.-B., & Moser, E. I. (2008). Representation of geometric borders in the entorhinal cortex. *Science*, *322*(December), 1865–1868.

Stensola, H., Stensola, T., Solstad, T., Frøland, K., Moser, M.-B., & Moser, E. I. (2012). The entorhinal grid map is discretized. *Nature*, *492*(7427), 72–8. Nature Publishing Group.

Stensola, T., Stensola, H., Moser, M.-B., & Moser, E. I. (2015). Shearing-induced asymmetry in entorhinal grid cells. *Nature*, *518*(7538), 207–212. Nature Publishing Group.

Tang, Q., Burgalossi, A., Ebbesen, C. L., Ray, S., Naumann, R., Schmidt, H., Spicher, D., Brecht, M. (2014). Pyramidal and Stellate Cell Specificity of Grid and Border Representations in Layer 2 of Medial Entorhinal Cortex. *Neuron*, *84*(6), 1191–1197.

Youngstrom, I. A., & Strowbridge, B. W. (2012). Visual landmarks facilitate rodent spatial navigation in virtual reality environments. *Learning & Memory*, *19*, 84–90.

# Chapter 3

# Hippocampal Place Cells on Virtual Linear Tracks

## 3.1 Introduction

The first project of this thesis was aimed to determine the relative contributions of sensory cues on place cell firing. Input to the hippocampus can be divided into three broad categories of stimuli: distal visual cues (O'Keefe and Dostrovsky, 1971; Muller and Kubie, 1987); self-motion cues (Gothard et al., 1996a; Gothard et al., 1996b; Pastalkova et al., 2008), e.g. proprioception, optic flow, and vestibular cues (Stackman et al., 2002); and other sensory cues (Battaglia et al., 2004), e.g. olfaction (Wood et al., 1999; Save et al., 2000), audition (Itskov et al., 2012), and somatosensation (Young et al., 1994). The cognitive map is thought to be primarily driven by distal visual and self-motion cues (O'Keefe and Nadel, 1978). Evidence for this relies on the fact that place cells will rotate their fields to match the rotation of a salient distal visual cue (Muller and Kubie, 1987; Muller et al., 1987), but can also maintain their spatial selectivity when there are no visual cues, i.e. in the dark (Quirk et al., 1990), or in blinded rats (Save et al., 1998). The prevailing hypothesis is that the internal representation of space is primarily determined by self-motion information, but is then anchored to and periodically updated by distal visual information. Indeed, place cells lose their spatial selectivity when the vestibular organ is lesioned, suggesting that vestibular information is necessary (Stackman et al., 2002). There is evidence, however, for at least some influence of the other sensory modalities mentioned above. For example, the place cell map rotates when the environment is

cleaned, suggesting place cells can anchor to particular olfactory cues that may be removed or altered during cleaning (Save et al., 2000).

It is difficult to study each sensory modality in isolation because they are all spatially correlated in real world environments. Olfactory and tactile cues, while usually not specifically manipulated in most studies, are difficult to control, and may play an unknown role in place cell firing. Some sensory modalities, such as self-motion cues, are impossible to eliminate in the real world without lesions or pharmacological interventions. Thus it is difficult to determine the relative influence of each sensory modality in real world environments.

To avoid these difficulties, we developed a noninvasive VR (Fig 3.1) for rats where vestibular and other sensory cues did not provide any spatial information. Place cells have been measured in VR in head fixed mice (Harvey et al., 2009; Dombeck et al., 2010) and are thought to be similar in VR and RW but this has not been tested.

Because rats were body fixed and could not turn themselves around on the ball, vestibular information for angular acceleration did not always correlate with the visual information for angular acceleration. Vestibular cues for linear acceleration were mostly eliminated due to the body fixation. Thus, any path integration computations the brain might use would have to function in the absence of accurate vestibular information.

Other sensory cues, such as local visual, olfactory, and tactile cues, were not eliminated in the VR; rather, these cues were either on the ball the rat walked on, the surrounding VR apparatus, or the room in which the apparatus was located. In all of these conditions, none of these uncontrolled cues could be correlated with the virtual environment, and thus could not be used by the hippocampus to determine the rat's location. Thus, presence of spatially selective firing fields in the virtual environment would support the hypothesis that the spatial information provided by these cues in RW is not necessary for spatial selectivity.

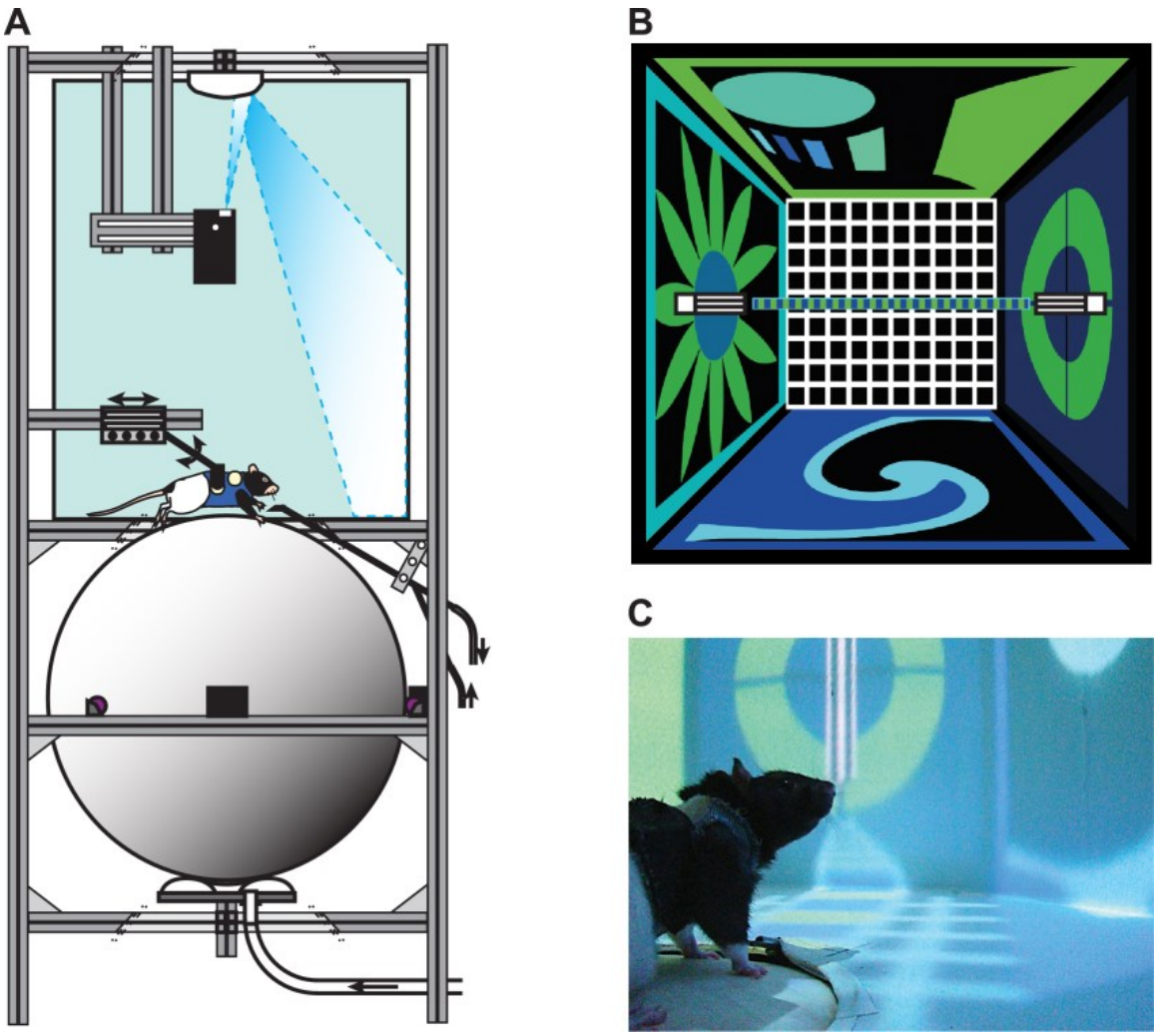


**Fig 3.1:** Virtual reality apparatus and environment. **A)** Schematic of the virtual reality system, reward delivery tube, hinged and adjustable harness, spherical treadmill, micro projector, distortion mirror and cylindrical projection screen. **B)** Top down view of the environment, consisting (both in RW and VR) of a 2.2m linear track in the center of a 3x3m room with unique distal visual cues on each wall. Pillars, present in some of the experiments, indicated the active reward location. **C)** A rat in the virtual reality apparatus.

Therefore, in the virtual environments used in this study, the only spatial information came from distal visual cues, optic flow and proprioception of the rat's own movements. Consequently, we will refer only to proprioception and optic flow as 'self-motion cues', and vestibular inputs will be treated separately, as they are not spatially informative in the VR.

The question we sought to answer with this manipulation was thus: For what place cell firing properties are distal visual and self-motion cues sufficient? Any differences between place

cell firing in RW and VR environments would suggest a role of the other sensory cues in these properties.

To answer this question, we used tetrodes to measure neural activity from the dorsal CA1 of six rats while they ran in VR or RW environments consisting of a linear track in the center of a square room with distinct distal visual cues on each of the four walls (Fig 3.1B). The visual scene was passively turned when rats reached the end of the virtual track. The distal visual cues were nearly identical in VR and RW, but rats were body fixed in VR which eliminated spatially informative other sensory cues and minimized both angular and linear vestibular inputs (see methods).

## 3.2 Methods

### 3.2.1 Subjects

Six adult male Long-Evans rats (approximately 3.5 months old at the start of training) were individually housed on a 12 hour light/dark cycle. Animals were food restricted (15-20 g of food per day) to maintain body weight. Animals were allowed to access a restricted amount of water (25-35 ml of water per day) after the behavioral session to maintain motivation. All experimental procedures were approved by the UCLA Chancellor's Animal Research Committee and were conducted in accordance with USA federal guidelines.

### 3.2.2 Virtual reality apparatus

The VR system contained a 61cm diameter Styrofoam sphere that floated freely on an acoustically quiet air cushion (Fig 3.1A). The ball rotation was measured by two orthogonally placed laser sensors, merged by a microcontroller, and used by custom software to change the surrounding visual scene. There was one-to-one mapping between the rat's movements and the corresponding changes in the virtual environment. The standard deviation of the ball tracking for

one revolution was 1.3% of a revolution. A micro projector projected visual stimuli on a custom made convex mirror, which reflected the stimuli onto a 300°, 68cm diameter, 75cm tall cylindrical screen made of white fabric. Our VR system allowed presentation of an undistorted visual scene in all directions including within 1cm of the rat. A hinged harness held the rat on the sphere. A stainless steel tube mounted in front of the rat dispensed liquid rewards (10% sucrose water, 150µl per reward) controlled by a software driven solenoid valve. The VR software was built in C++ using the Ogre 3D graphics engine and OpenAL. VR data, including the animal's (virtual) speed, position and heading, were recorded by the software at a sampling rate of 60Hz.

### 3.2.3 Task and environment

The virtual environment consisted of a 220x10cm linear track floating 1m above the floor and centered in a 3x3x3m room. Alternating 5cm-wide green and blue stripes on the surface of the track provided optic flow. A 30x30cm white grid on the black floor provided parallax-based depth perception. Distinct distal visual cues covered all 4 walls and provided the only spatially informative stimuli in the VR (Fig 3.1B). In RW, rats ran back and forth on a 220x6cm linear track that was placed 80cm above the floor. The track was surrounded by four 3x3m curtains that extended from floor to ceiling. The same stimuli on the walls in the virtual room were printed on the curtains, thus, the distal visual cues were similar in RW and VR.

### 3.2.4 Behavioral training

All experiments were conducted in identical acoustically- and EMF-shielded rooms. After pretraining (for a detailed description, see Chapter 2), animals were trained to run back and forth in a virtual linear track with the same dimensions as those described above, but with different visual stimuli. This was done to control for the amount of experience on the final version of the task. Due to the relatively short training period needed, rats were trained in the same RW environment as the experimental environment. Total training time in RW and VR was

approximately one week and four weeks, respectively, and training sessions for the two environments were interleaved.

A 10cm wide and 100cm tall visual pillar indicated the reward locations at the end of the track in both VR and RW (Fig 3.1B-C). In some experiments, the pillars were eliminated at one or both ends in VR (Fig 3.17) to determine their influence on neural activity. In both VR and RW, entrance into the active reward location triggered a reward tone and the sugar water delivery, followed by activation of the reward location at the opposite end of the track. To further reduce vestibular inputs in VR the virtual scene was automatically and instantaneously rotated 180° at the end of each lap while the rats were consuming the reward, so the rat faced the opposite reward location. The rats had the ability to rotate the environment at any point of the track, but they were body-fixed in VR which would generate minimal vestibular inputs even if they did turn around. To determine whether passive rotation played a role in position versus disto-code, two rats were also trained to actively rotate the virtual environment at the end of the track. This did not impact the results (Fig 3.19).

Of the six rats studied, three performed VR passive turn and RW tasks. One rat was trained only in the VR passive turn task to determine the degree of interference between the two environments. Cells recorded from this animal exhibited results consistent with those of other animals, including disto-coding, an absence of bidirectional position coding, and a low proportion of baseline cells active in the VR task. In these four rats, other VR experiments were carried out after the first 15 trials. Hence, for consistency, only data from first 15 trials were used from both VR and RW. One rat performed VR passive and active turn tasks and the RW task. The last rat performed only VR passive and active turn tasks. Qualitatively similar results were obtained in all rats.

### 3.2.5 Surgery

Rats showing sufficient performance in the VR task were implanted with 25-30g custom-built hyperdrives containing up to 22 independently adjustable tetrodes (comprised of four 13μm nichrome wires) positioned over both dorsal CA1 areas (-4.0mm A.P., 2.4mm M.L. relative to bregma). Surgery was performed under isoflurane anesthesia and heart rate, breathing rate, and body temperature were continuously monitored. Analgesia was achieved by using Lidocaine (0.5mg/kg, sc) and Buprenorphine (0.03mg/kg, ip). Two 2mm-diameter craniotomies were drilled using custom software and a CNC device with a precision of 25μm in all 3 dimensions. Dura mater was removed and the hyperdrive was lowered until the cannulae were 100 μm above the surface of the neocortex. The implant was anchored to the skull with 7-9 skull screws and dental cement. The occipital skull screw was used as ground for recording. Rats were administered 40mg sulfamethoxazole and 8mg trimethoprim in drinking water and ~10mg/kg carprofen (Rimadyl bacon-flavored pellets) one day prior to surgery and for at least 10 days during recovery.

### 3.2.6 Electrophysiology

The tetrodes were lowered gradually after surgery into the hippocampus and allowed to stabilize above the CA1 hippocampal subregion. Positioning of the electrodes in CA1 was confirmed through the presence of sharpwave ripples during recordings, and through histology after experiments (Fig 3.2).

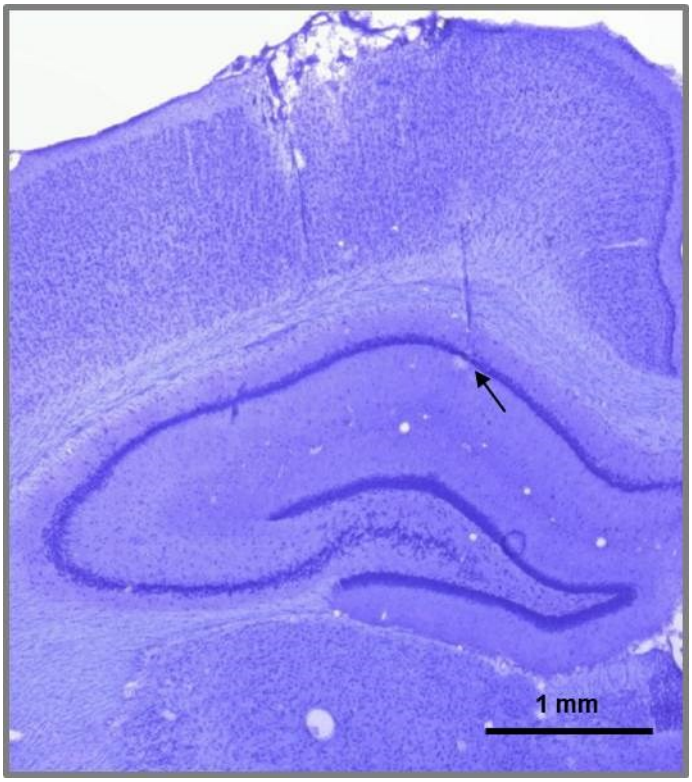


**Fig 3.2:** Histology showing tetrode tracks in hippocampus. We implanted tetrodes to record CA1 cells in both hippocampi and cells in the parietal cortex. Histology micrograph of a coronal section shows a tetrode track ending in CA1. Arrow marks the tetrode tip location. Scale bar: 1mm.

Signals from each tetrode were acquired by one of four 27-channel headstages, digitized at 32kHz, bandpass-filtered between 0.1Hz and 9kHz, and recorded continuously. Each recording session in VR and RW included hour-long baselines pre- and post-task to ensure stability of units. During baseline sessions, rats were allowed to rest in a box outside the task apparatus. By the time the first place cell was detected (3 to 5 weeks after surgery), rats were fully habituated to run the VR and RW tasks with their implant. From this point on, rats ran the VR task in the final environment as described above. At the time of recording, the rats had experienced both the RW and VR environments for at least one week.

Given that the fraction of baseline cells active during the task session was significantly lower in VR, in order to record comparable numbers of track active cells in RW and VR we recorded more task (and hence corresponding baseline) sessions in VR than RW.

We recorded 106, 62, 55, 136, and 73 track active cells in the five rats in VR, and 125, 72, 22 and 21 track active cells in the four rats in RW.

### 3.2.7 Spike sorting

Spikes were detected offline using a nonlinear energy operator threshold (Gibson et al., 2008), after application of a noncausal 4th order Butterworth band pass filter (600-6000Hz). After detection, 1ms spike waveforms were extracted, upsampled fourfold using cubic splines, aligned to their peaks and downsampled back to 32 data points. Spike sorting was performed manually using a modified version of the MClust software package (MClust-3.5, A.D. Redish, http://redishlab.neuroscience.umn.edu/MClust/MClust.html).

For classification of single unit type, each unit's average (energy normalized) waveform was computed. Units with a peak-to-trough fall time less than 0.4ms and mean firing rate during running epochs of at least 5Hz were classified as interneurons (Fig 3.3). Units with a peak-to-trough fall time greater than 0.4ms were classified as pyramidal. This classification was verified in two ways: first, we verified that principal component analysis on the single unit waveforms revealed two clear clusters which agreed with the fall time classification. Second, we verified that units classified as pyramidal had high complex spike index (Mehta et al., 2000) and high information content; while interneurons had low values for both measures.

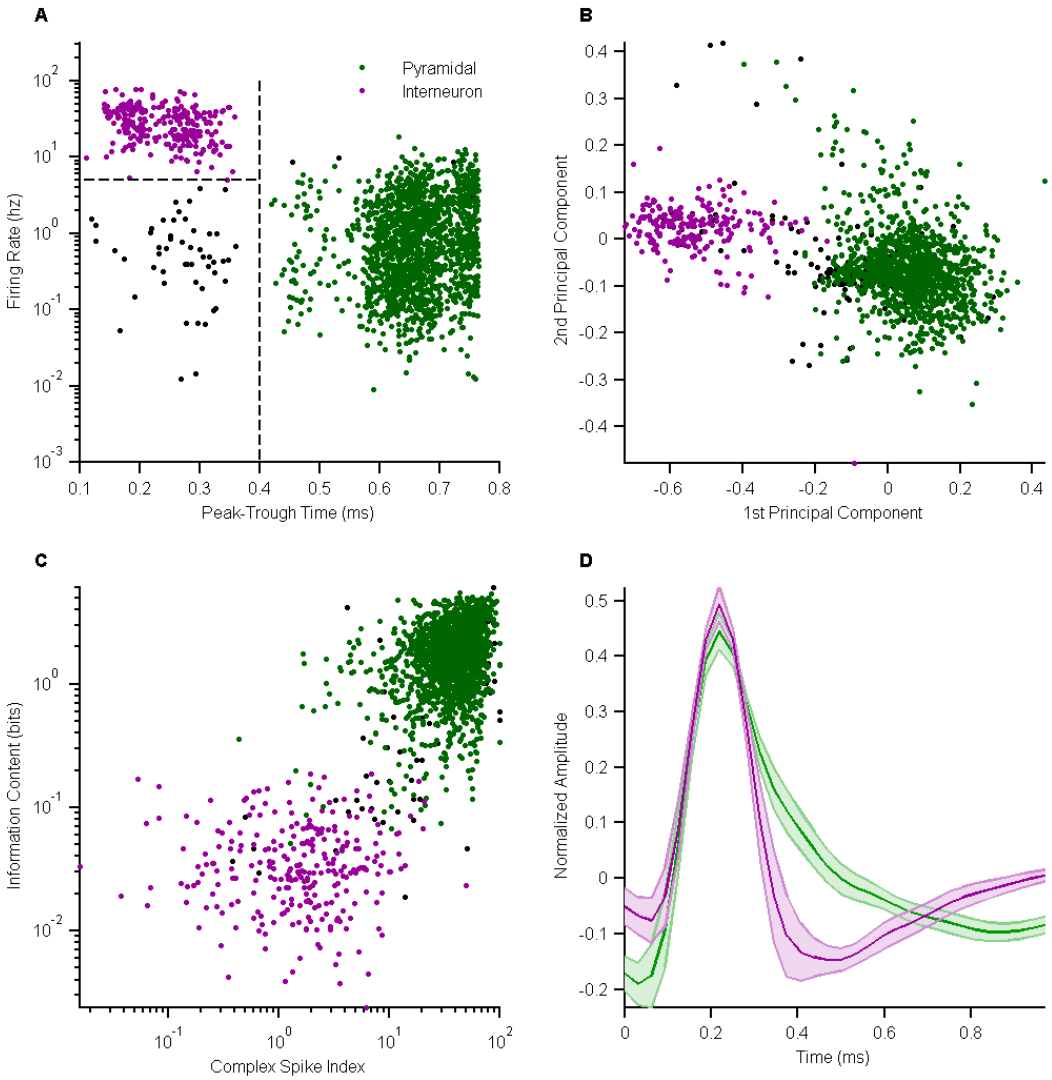


**Fig 3.3:** Classification of pyramidal cells and interneurons. **A)** Units with peak to trough time greater than 0.4ms were classified as pyramidal, and units with peak to trough time shorter than 4ms and mean rates greater than 5Hz were classified as interneurons. In all subsequent panels waveforms are colored according to this classification. **B)** Principal component analysis of the energy normalized waveforms considered in A confirms the existence of two distinct groups of waveforms. **C)** Examination of complex spike index and information content values confirms the identification of pyramidal and interneuron groups. **D)** Average (energy normalized) waveforms of the two unit groups. Shaded areas indicated standard deviations.

Cluster quality was assessed using the isolation distance metric (Schmitzer-Torbert et al., 2005), as well as the false positive and negative estimates (Hill et al., 2011). While there was a correlation between the unit quality metrics and the instability metric, four-way ANOVA

found the difference between VR and RW stability values could not be explained by unit quality metrics (Fig 3.9).

On days when rats ran in both VR and RW, the same cells were identified by overlaying cluster boundaries from one recording session onto data from the other, and identifying clear overlaps. If cell identities were unclear due to electrode drift the data were discarded from the same cell analysis.

### 3.2.8 Statistics

All analyses were performed using custom code written in MATLAB. Circular statistics were computed using the CircStat toolbox (Berens, 2009). Unless otherwise stated, significance tests between two distributions of linear variables were performed using the nonparametric Wilcoxon rank-sum test, and tests between circular variables were performed using the Kuiper test. Tests for populations significantly different from zero were performed using the nonparametric Wilcoxon signed-rank test. Values are reported in the text in the form mean ± s.e.m. unless otherwise stated.

### 3.2.9 Rate maps and place fields

A trial was defined as a continuous run from one end of the track to the other, followed by a continuous run back to the starting position. Start and end times for trials were determined by a minimal speed threshold (5cm/s), data during times while the rat was stationary were not included in the analysis, except for the calculation of goal-cell activity. A unit was considered track (goal) active if its mean firing rate on track (goal) was at least 1Hz.

Spatial firing rates were computed using a 5cm Gaussian smoothing kernel on occupancy and spike histograms with 0.5cm wide bins. Opposite directions of the track were treated as independent and linearized. The stability coefficient for a single unit was calculated as the correlation between the rate map obtained from the even numbered trials and the firing

rate map obtained from odd numbered trials. This definition avoids spurious contribution of any time dependent, systematic changes of rate maps to the instability measure. Units with a stability coefficient exceeding 0.5 were labeled as stable.

A place field was defined as a region where the firing rate exceeded 5 Hz for at least 5cm. The boundaries of a place field were defined as the point where the firing rate first drops below 10% of the peak rate (within the place field) for at least 5cm. To avoid misidentifying single spike bursts as place fields, it was further required that a place field exhibit significant activity on at least five trials. A unit was defined to be significantly active in a trial if the number of spikes fired in that trial was not below the 5th percentile of $\mathrm{Poisson}\left(\sum_i \lambda_i^{T\backslash t} o_i^t\right)$, where $\lambda_i^{T\backslash t}$ is the firing rate in the $i$-th bin, computed over all trials (T) except the one under consideration (t), and $o_i^t$ is the occupancy time in the $i$-th bin on the trial under consideration.

### 3.2.10 Single unit measures

The information content of a single unit rate map (in bits) was defined as

$$I = \sum_i^L P_i \frac{\lambda_i}{\bar{\lambda}} \log_2 \frac{\lambda_i}{\bar{\lambda}}, \text{ where } P_i = \frac{o_i}{\sum_j^L o_j}, \text{ and } \bar{\lambda} = \sum_i^L P_i \lambda_i$$

Significance of spatial information for each unit was assessed using a trial shuffling procedure. Spiking and occupancy information was circularly shuffled by a random amount for each of the fifteen trials, and the information content of the resulting rate map computed. This procedure was repeatedly and independently applied to the two running directions, to generate a null distribution of 500 information content values for each direction. A unit was considered to have significant spatial information if the information content of its true rate map exceeded that of 95% of values in the null distribution for at least one of the two running directions.

The sparsity of a single unit rate map was defined (with L the number of spatial bins) as

$$S = \left(1 - \frac{1}{L}\frac{\left(\sum_i^L \lambda_i\right)^2}{\sum_i^L {\lambda_i}^2}\right)\left(\frac{L}{L-1}\right)$$

Thus defined, S ranges between zero (for a uniform rate map) and 1 (for a delta function rate map).

The directionality index of a cell was defined (with ${\lambda_i}^F$ as the rate in the $i$-th bin in the forward running direction and ${\lambda_i}^B$ the rate in the $i$-th bin in the backward running direction) as

$$D = \left|\frac{\sum_i^L({\lambda_i}^F - {\lambda_i}^B)}{\sum_i^L({\lambda_i}^F + {\lambda_i}^B)}\right|$$

For bidirectional units (D < 0.5) with at least one clear place field the boundaries of the largest place field of each unit, in position and distance space, defined a position zone, $Z_P$, and a disto zone, $Z_D$, in the opposite travel direction. The disto ($I_D$) and position ($I_P$) indices were then defined as:

$$I_P = \frac{\sum_{i\in Z_P}\lambda_i - \sum_{i\notin Z_P}\lambda_i}{\sum_{i\in Z_P}\lambda_i + \sum_{i\notin Z_P}\lambda_i}, I_D = \frac{\sum_{i\in Z_D}\lambda_i - \sum_{i\notin Z_D}\lambda_i}{\sum_{i\in Z_D}\lambda_i + \sum_{i\notin Z_D}\lambda_i}$$

To compare the closely coupled distance and time parameters, time rate maps were computed for each trial in a similar manner as the spatial rate maps, with the initiation of running as the time reference point. Trials were ordered by speed, and temporal and distal rate maps were computed for the fastest and slowest half of the trials. The correlation coefficient between the fastest and slowest rate maps over time or space thus yielded temporal and distal stability coefficients respectively (Fig 3.15).

### 3.2.11 Population vector

The population vector overlap (PVO) between the forward and backward directions at linear positions $(x, y)$ for a population of N single units over a track of length L was defined (with ${\lambda_j}^F(x)$ the rate of unit j at position x in the forward direction, and similarly for ${\lambda_j}^B(L-y)$ in the backward direction) as

$$\mathrm{PVO}(x,y) = \frac{\sum_j^N {\lambda_j}^F(x){\lambda_j}^B(L-y)}{\left(\sum_j^N {\lambda_j}^F(x){\lambda_j}^F(x)\right)\left(\sum_j^N {\lambda_j}^B(L-y){\lambda_j}^B(L-y)\right)}$$

An alternate population vector computed using linear correlation coefficients rather than a vector dot product yielded qualitatively similar results. Significance values for the PVO were computed using a shuffling and sorting bootstrap method.

### 3.2.12 Theta frequency and phase precession

A multi taper power spectrum for each LFP was calculated during running behavior. To avoid potential contamination from noise, only LFPs exhibiting clear theta, defined as a theta (4-12Hz) to delta (0.01-4Hz) power ratio exceeding 1/3, were considered for analysis of either theta frequency or phase precession. Each LFP was then filtered (4-12Hz, 4th order Butterworth), and theta frequency computed using four methods: cycle detection using Hilbert transformed phase jumps; the derivative of Hilbert transform phase; the short time Fourier transform; and a method based on the Kalman filter (Nguyen et al., 2009). The cycle method results are reported in the main text, and the alternate methods in Fig S14. Results from all four methods are qualitatively similar. The quality of phase precession was measured using the circular linear correlation coefficient (Zar, 1999):

$$\rho_{cl} = \sqrt{\frac{r_{cx}^2 + r_{sx}^2 - 2r_{cx}r_{sx}r_{cs}}{1 - r_{cs}^2}}\ , r_{cx} = \mathrm{corr}(x, \cos\alpha), r_{sx} = \mathrm{corr}(x, \sin\alpha), r_{cs} = \mathrm{corr}(\sin\alpha, \cos\alpha)$$

Spiking frequency of single units was calculated by detecting the peak in filtered spike train autocorrelations.

## 3.3 Results

### 3.3.1 Behavior

During recordings rats ran consistently along the track and reliably slowed before reaching the track end in both VR and RW (Fig 3.4, see methods). There was no requirement for the rat to slow or even stop running in the reward zone, so this anticipatory behavior indicates the rats' involvement in the virtual task was not entirely passive. Although their running speed was somewhat lower in VR than RW perhaps due to differences in effort requirements, their behavioral performance was otherwise similar.

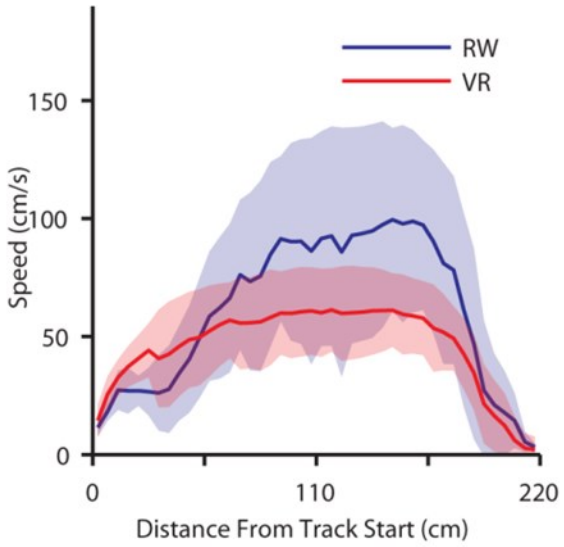


**Fig 3.4:** Rat running speed in RW and VR. Running speed (mean± STD) of rats as a function of position on a 2.2m long linear track for RW (blue) and VR (red). Similar color scheme is used throughout. While the rats were faster in RW, their behavior was similar, reliably reducing speed prior to reaching the end of the track (n=49 sessions in RW, n=128 sessions in VR).

### 3.3.2 Firing rate properties of place cells in VR

#### *3.3.2.1 A smaller proportion of cells are active in VR than in RW*

Clear, spatially focused and directionally tuned place fields, commonly found in RW (Fig 3.5 left), were also found in VR (Fig 3.5 right) (Harvey et al., 2009). Almost all track active

putative pyramidal cells had significant spatial information in VR (96 %) and RW (99 %). Thus, distal visual and self-motion cues are sufficient to generate the hippocampal rate code. We then examined whether the cognitive maps were similar in VR and RW.

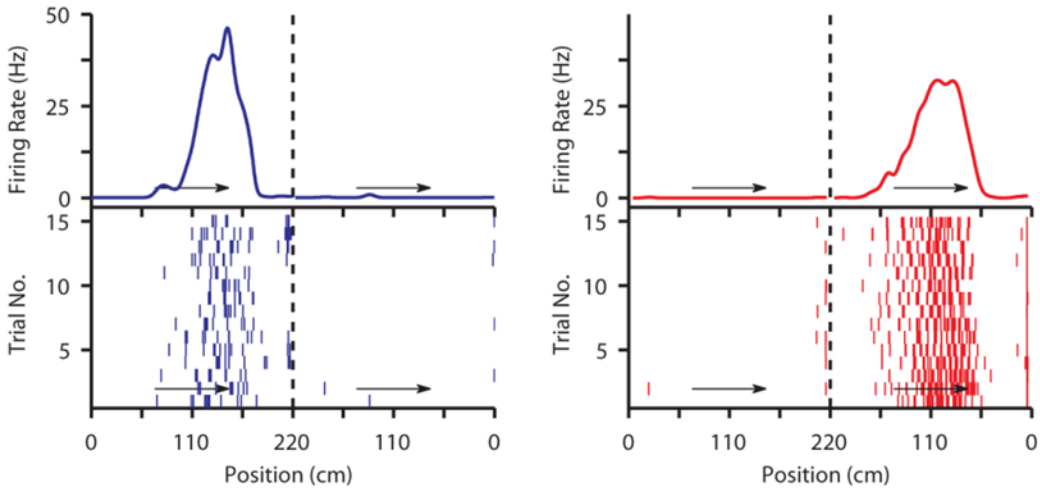


**Fig 3.5:** Example place cells in RW and VR. **Left:** Example of a directional, stable place cell recorded in RW with firing rate (top panel), and raster plot (bottom panel). Arrows indicate running direction. **Right:** A similar place cell recorded in VR.

We measured the activities of 2119 and 528 putative pyramidal neurons in the baseline sessions, conducted in a sleep box, preceding the VR and RW tasks respectively (see methods). Of these, 45.5% were track active in RW. This result is consistent with previous studies, which show that only some hippocampal cells are active within a given environment (Thompson and Best, 1989). The others are silent, and can only be detected when all the cells are active during sleep. In contrast with RW, only 20.4% were track active in VR (Fig 3.6, 3.7), meaning that a far smaller proportion of cells was activated in the VR. The VR track active cells had only slightly smaller mean firing rates (VR: 2.71 ± 0.08 Hz, n=432, RW: 3.06 ± 0.12 Hz, n=240, $p<0.05$), which is likely due to lower running speed (McNaughton et al., 1984). The smaller proportion of activation indicates that in the RW, many sensory modalities contribute to place cell activation. Distal visual and self-motion cues, by themselves, are not sufficient to activate the maximum number of place cells, perhaps because different place cells are driven

by different subsets of sensory cues. While the track active cells were measured during locomotion, we also investigated the place cell activation during periods of immobility at the goal locations, where a similar twofold reduction was seen in the proportion of active cells in VR, with no significant change in firing rates (Table 3.1, Fig 3.6 and 3.8). The similarity between firing rates in RW and VR during immobility supports the hypothesis that the slightly decreased rates during running in VR are due to decreased running speeds rather than a general property of the VR. This further supports the hypothesis that different hippocampal cells are tuned to different subsets of sensory cues. If all cells were tuned to similar inputs, we would expect a global decrease in firing rates in the VR, rather than intact firing rates in some cells and inactivation of others.

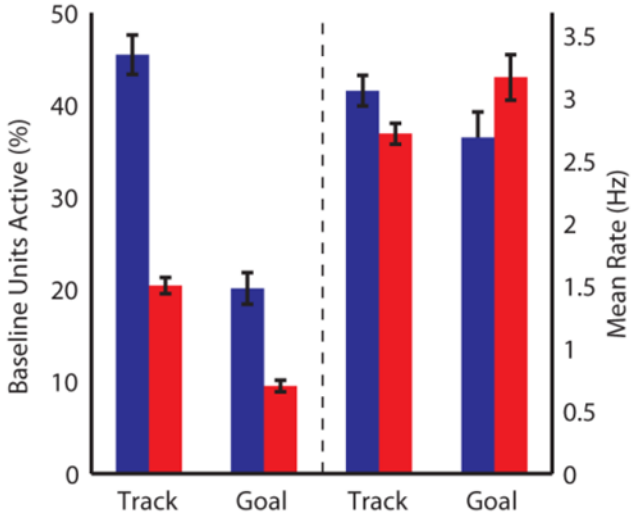


**Fig 3.6:** Comparison of activation ratio and firing rates of active cells on track (RW: 45.5%, 3.06 ± 0.12 Hz, VR: 20.4%, 2.71 ± 0.08 Hz) and at goal (RW: 20.1%, 2.68 ± 0.20 Hz, VR: 9.5%, 3.16 ± 0.18 Hz).

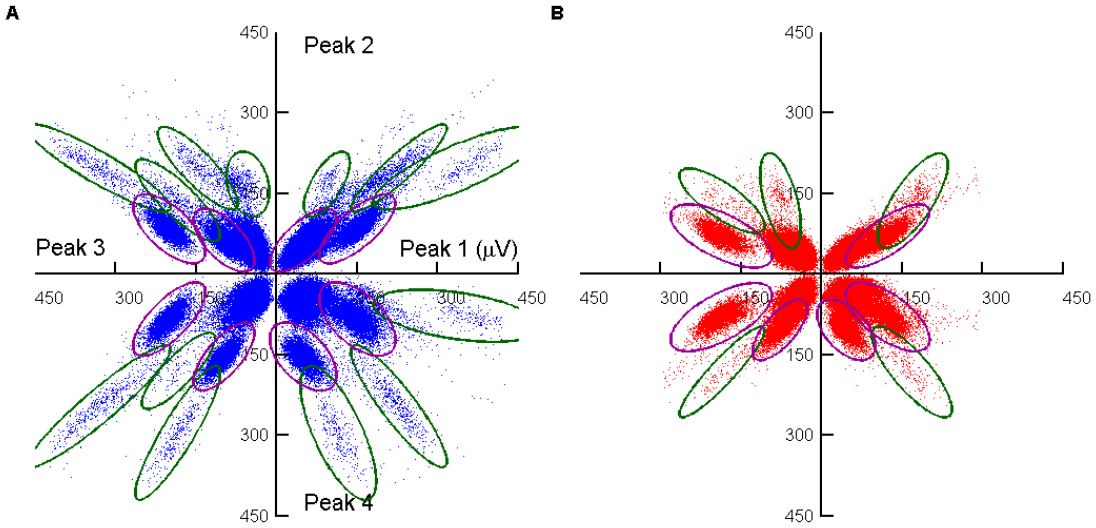


**Fig 3.7**: Fewer pyramidal units are active in VR than RW. **A)** Four projections of spike waveform peaks recorded from a tetrode in the RW. The dense cloud of low amplitude spikes belong to either unclustered multi-unit spikes (no outline), or isolated interneuron spikes (purple outline). The less dense, high amplitude, well isolated and elongated clouds belong to single pyramidal unit spikes (green outlines). **B)** As in A, for data recorded from the same tetrode on the same day in VR. Note the reduced number of pyramidal unit clusters.

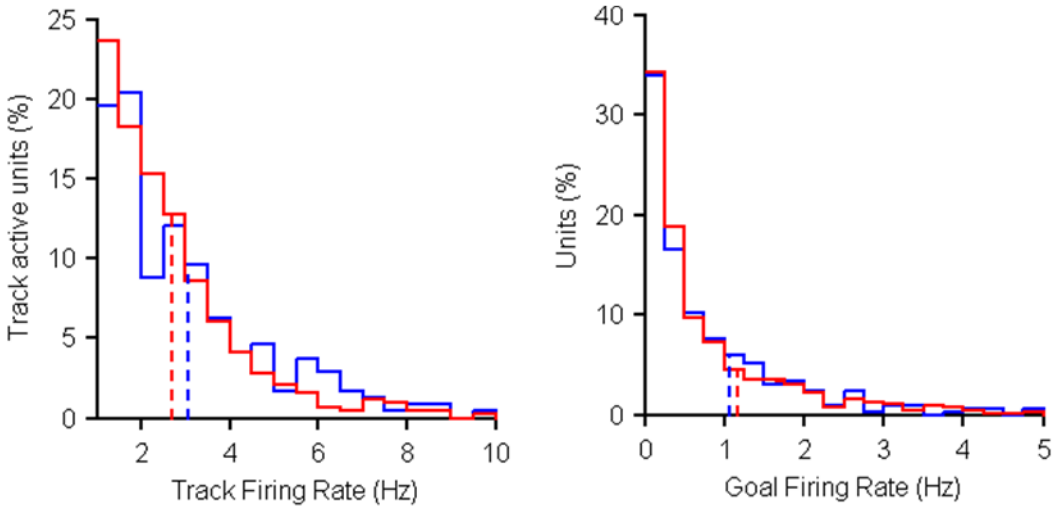


**Fig 3.8** Comparison of firing rates in RW and VR**: Left** Mean firing rates on the track were slightly greater in RW (3.06 ± 0.12 Hz) than in VR (2.72 ± 0.08 Hz), $p<0.05$. **Right** Mean firing rates at the goal locations were similar in RW (1.07 ± 0.09 Hz) and in VR (1.18 ± 0.08 Hz), $p=0.78$.

*3.3.2.2 Place fields in VR are wider and thus have lower spatial selectivity*

The firing rate maps of place cells were slightly less stable in VR (stability index 0.80 ± 0.01, n=432) than RW (0.87 ± 0.01, n=240) (Fig 3.9A). The decrease of stability in the VR was not due to poor clustering; the stability coefficient did not correlate with isolation distance of clusters, or with estimates of false positive and false negative spikes (Fig 3.9B-D). Instead, the decrease in stability could be caused by the lack of coherency between cues in the VR. It is possible that the inconsistency of olfactory or tactile cues encountered on the ball during different traversals of the virtual track caused the instability in the place cell representation. Further work is being done to investigate this phenomenon.

All subsequent comparisons were made across only the 392 and 227 track active, stable cells (Fig S6, see methods) in VR and RW respectively. Place fields were 26% wider ($p<10\text{-}10$) in VR (55.8 ± 1.2 cm, n=482) compared to RW (44.3 ± 1.4 cm, n=365). As a result, spatial selectivity was 22% lower in VR (Table 3.1, Fig 3.10). From these data we hypothesize that the cues that are not spatially informative in the VR are important for fine-tuning the place field in the RW. Triangulating position from distal visual cues does not have high resolution, and path integration from self-motion cues accumulates error over distance. These data support the hypothesis that distal visual and self-motion cues are sufficient to produce spatial selectivity in place cells, but that local cues such as olfactory and tactile cues serve to fine-tune the place field, resulting in higher information content.

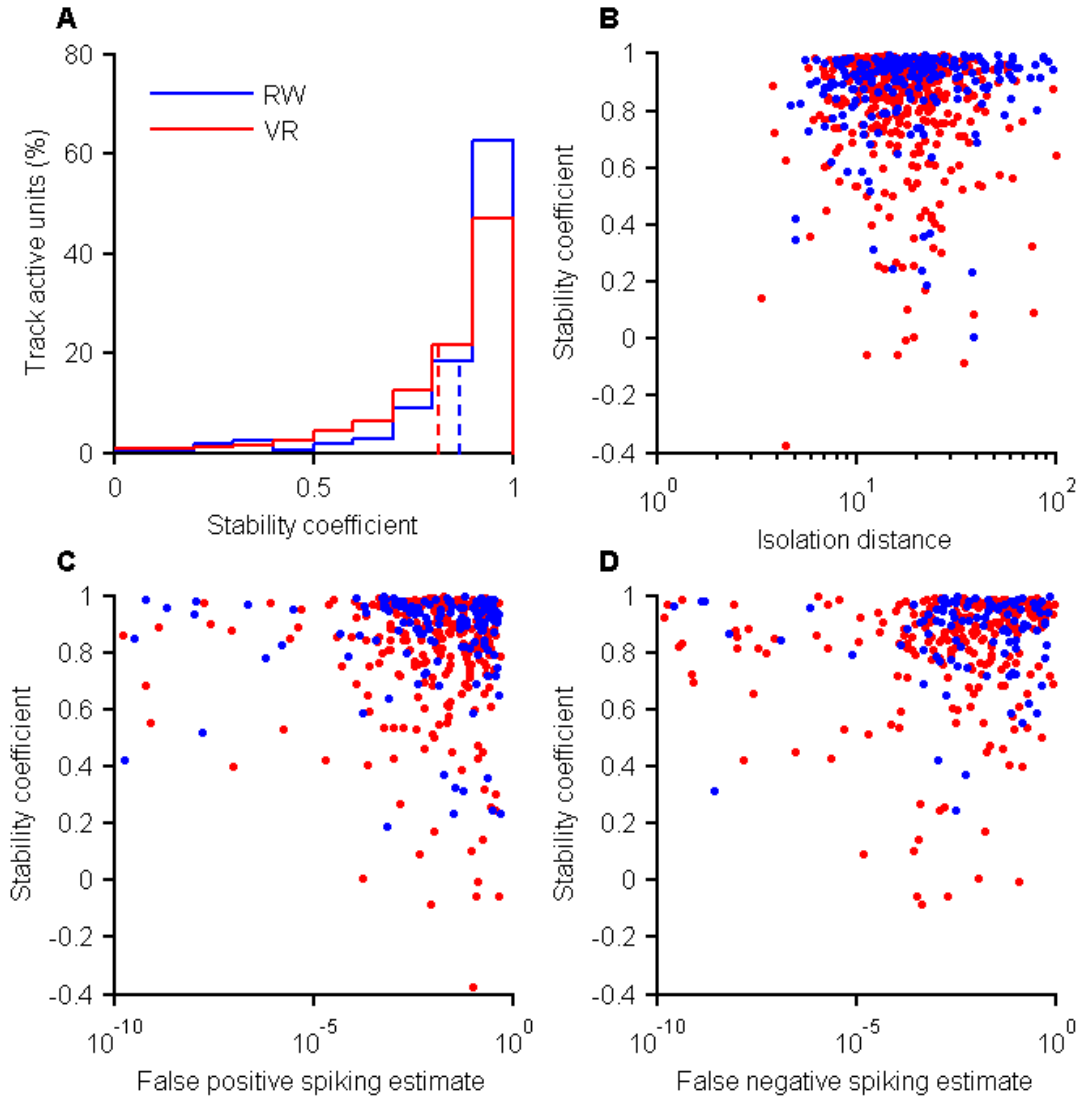


**Fig 3.9:** Instability of VR firing rate maps is not caused by poor cluster quality. **A)** Distribution of stability coefficients for track active units in RW (0.87 ± 0.01) and VR (0.81 ± 0.01). **B)** Unit stability plotted against cluster isolation does not suggest the difference in stability is due to poor unit isolation in VR **C)** As in B, but with false positive spiking estimate instead of isolation distance. **D)** As in B, but with false negative spiking estimate instead of isolation distance. Four way ANOVA shows that stability cannot be explained purely by cluster quality metrics, but that recording in VR has significant effect on unit stability (isolation $p=0.056$, false positive $p<0.05$, false negative $p=0.6$, VR $p<0.001$).

| | VR | | | RW | | | |
|---|---|---|---|---|---|---|---|
| | **Mean** | **Std. Dev.** | **n** | **Mean** | **Std. Dev.** | **n** | **P-value** |
| Track Firing Rate (Hz) | 2.71 | 1.74 | 432 | 3.06 | 1.90 | 240 | $< 0.05$ |
| Goal Firing Rate (Hz) | 1.18 | 1.93 | 671 | 1.07 | 1.63 | 333 | 0.8 |
| Stability Coefficient | 0.80 | 0.23 | 432 | 0.87 | 0.17 | 240 | $< 10^{-3}$ |
| Spatial Information (bits) | 1.32 | 0.67 | 392 | 1.66 | 0.73 | 227 | $< 10^{-7}$ |
| Sparsity | 0.65 | 0.17 | 392 | 0.73 | 0.15 | 227 | $< 10^{-8}$ |
| Directionality | 0.56 | 0.32 | 392 | 0.59 | 0.31 | 227 | 0.2 |
| Position Coding Index | -0.11 | 0.49 | 127 | 0.27 | 0.52 | 91 | $< 10^{-7}$ |
| Disto-Coding Index | 0.14 | 0.48 | 127 | -0.25 | 0.54 | 91 | $< 10^{-6}$ |
| Infield Mean Rate (Hz) | 6.73 | 3.98 | 482 | 8.15 | 4.95 | 365 | $< 10^{-4}$ |
| Infield Peak Rate (Hz) | 14.33 | 7.84 | 482 | 18.39 | 10.63 | 365 | $< 10^{-7}$ |
| Place Field Width (cm) | 55.84 | 28.09 | 482 | 44.40 | 26.91 | 365 | $< 10^{-10}$ |
| Place Field Skewness | -0.10 | 0.57 | 482 | -0.11 | 0.56 | 365 | 0.4 |
| Infield Theta Frequency (Hz) | 7.53 | 0.36 | 251 | 8.25 | 0.39 | 204 | $< 10^{-10}$ |
| Phase Precession Corr. | 0.33 | 0.15 | 251 | 0.33 | 0.14 | 204 | 0.8 |

**Table 3.1:** Summary of place cell properties in VR and RW.

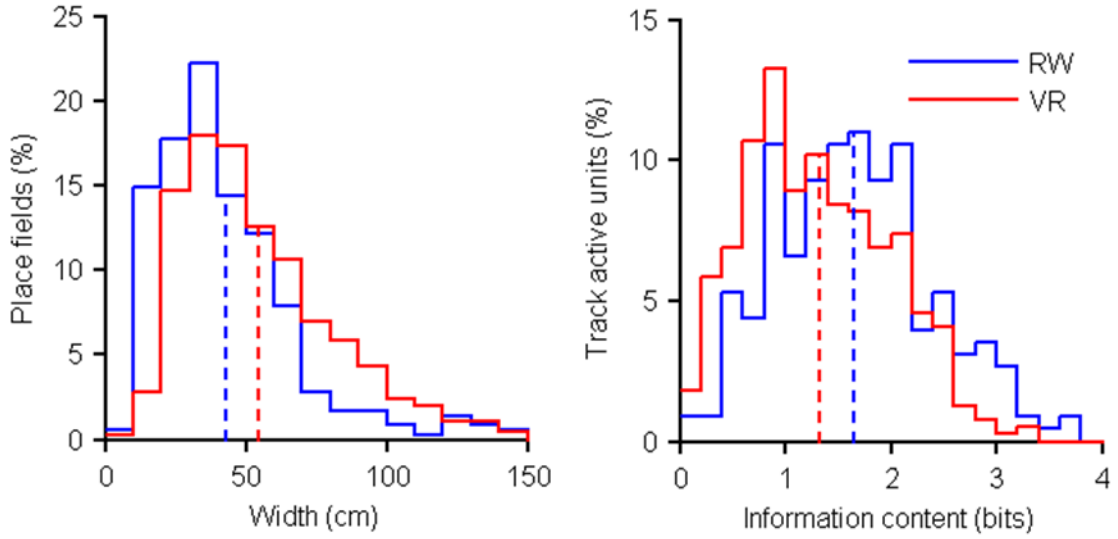


**Fig 3.10:** Place fields are wider and have lower information content in VR. **Left** Place fields were narrower in RW (42.8 ± 1.3 cm) than in VR (54.5 ± 1.2 cm), $p<10^{-11}$. **Right** Spatial information content across 432 track active cells in VR (1.23 ± 0.03 bits, n=432) was significantly lower (22%, $p<10^{-7}$) than in 240 RW cells (1.58 ± 0.05 bits, n=240).

Further, 90% (75%) of track active cells had at least one place field in RW (VR) (Table 3.1). This means that even though comparable percentages of track active cells had information contents significantly greater than zero, slightly fewer cells in VR had true place fields.

In addition, place fields had comparable and significantly asymmetric shapes in both VR and RW such that the firing rates were higher at the end of a place field than at the beginning (Table 3.1) (Mehta et al., 2000; Mehta et al., 2002; Harvey et al, 2009). Place field asymmetry is a measure of anticipatory firing, hypothesized to be caused by strengthened connections between place cells with adjacent firing fields. Since these are similar in VR and RW, we can conclude that the VR itself does not interfere with normal cell firing properties and synaptic plasticity.

*3.3.2.3 Place cells in VR and RW are similarly directional*

It is known that in RW linear tracks some place cells will fire at the same position in both running directions, but others will be highly directional, meaning they will fire in one running direction but not the other (McNaughton et al., 1984). Therefore, we investigated the directionality of place cells in VR. As in RW (McNaughton et al., 1984), the majority of place cells were directional (directionality index close to 1), spiking mostly in one running direction (Fig 3.5). In fact, the distributions of directionality index were identical (Fig 3.11 and Table 3.1). If we set an arbitrary threshold at 0.5 for the directionality index, then there were 43% bidirectional cells in RW and 40% in VR. This is interesting because a previous study showed that in RW linear tracks, the proportion of bidirectional cells increases with increased number of local cues (Battaglia et al., 2004). Presumably, in this experiment, the VR has fewer spatially informative local cues than the RW, but the fact that the directionality did not decrease is perhaps due to a floor effect.

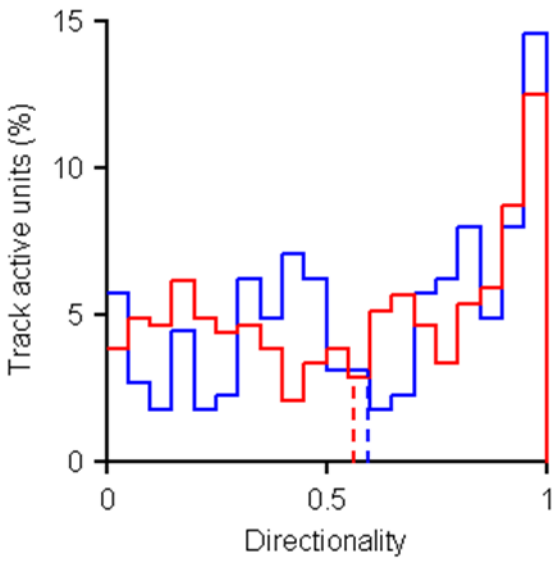


**Fig 3.11:** Ensemble directionality was similar in RW (0.59 ± 0.02) and in VR (0.56 ± 0.02), p=0.21.

The identical directionality distributions do tell us something very important about how the hippocampus encodes the VR environment. In most of the experiments, the visual scene was passively and instantaneously flipped at each end of the track after the reward was delivered. Since this condition removes the ambulatory and optic flow cues associated with a 180-degree turn, the brain could interpret the rat's behavior as running in the same direction on an infinite track, rather than back and forth on a finite one. Given the data, the former condition is unlikely, since place cells do tend to fire in the same location on every traversal of the track in the same direction. If the hippocampus treated each lap as a new section of an infinite track, such periodicity would be difficult to explain. Another possibility is that the brain interprets the change in visual scene as a teleportation between two independent environments, instead of running back and forth in the same environment. As explained in the calculations below, the proportion of bidirectional cells in VR is higher than what we would expect if the place cells were treating the two running directions as independent environments. Thus, the identical distribution

of directionalities is more consistent with the hypothesis that the hippocampus encodes the two directions as a single environment, rather than two independent ones.

We define a cell as active if its firing rate exceeds a threshold T, and make only one basic assumption: the probability of a cell being active in one environment (p) is the same as the probability of it being active in the other, and these activations are statistically independent. This assumption is reasonable considering that the saliency and intensity of cues in the two 'environments' (which are in fact different directions along the same track) are comparable, and that the existing literature has shown the subset of cells active in different environments is largely independent (Mehta et al., 2000).

Define $F_1(r)$ as the cumulative distribution function of firing rates *r* in the first environment, similarly $F_2(r)$ for the second environment, and $F_{1,2}(r)$ for the joint environment. From our definition of active cells (above), and the assumption of equal probability, it then follows that the probability of activation is given by $p = 1 - F_1(T) = 1 - F_2(T)$. Let $\eta$ indicate the fraction of time spent in the first environment, so that the fraction of time spent in the second is $1 - \eta$. In the data these occupancy fractions are typically very close to 0.5, but we do not need to assume any particular value in this treatment.

It follows that the mean rate observed in the joint environment will be $r_{1,2} = \eta r_1 + (1-\eta) r_2$, which we can view as a random variable drawn from a two component mixture distribution, so $F_{1,2}(r) = \eta F_1(r) + (1-\eta) F_2(r)$. We therefore see that the probability of a cell being active in the joint environment is:

$$p_{1,2} = 1 - F_{1,2}(T) = 1 - \eta F_1(T) - (1-\eta) F_2(T) = 1 - \eta(1-p) - (1-\eta)(1-p) = p$$

So our estimate of the activation probability in the joint environment (0.2 in VR, 0.45 in RW) is also an estimate of the activation in the distinct environments, so we set $p_{VR} = 0.2, p_{RW} = 0.45$.

Suppose there are N cells in the baseline that may be activated according to these probabilities in any given track. We then expect $n_1 \sim Binomial(N, p)$ to exceed threshold rate in the first environment, and similarly $n_2 \sim Binomial(N, p)$ to exceed threshold in the second. Further, we expect $n_{1\cap2} \sim Binomial(N, p^2)$ cells to exceed threshold in both in both environments. We therefore get that the fraction of active cells that are directional (i.e. active in only one of the two environments) is predicted to be

$$d(N, p) = 1 - \frac{n_{1\cap2}}{n_1 + n_2 - n_{1\cap2}}$$

Confidence intervals are determined by numerical simulation of 100,000 samples from the above distributions, and computing the one tailed 95% confidence limit. The resulting distributions are presented in Fig S20 below. The results are as follows:

| | **N** | **P** | **Predicted d** | **95% confidence limit** | **Observed d** |
|---|---|---|---|---|---|
| VR | 2119 | 0.2 | 0.89 | 0.86 | 0.62 |
| RW | 528 | 0.45 | 0.71 | 0.65 | 0.59 |

The observed fractions of cells that are directional (bidirectional) are thus significantly lower (higher) than would be predicted by independent activation based on the hypothesis that place cells treat the two movement directions as distinct environments. In fact, the distinct environments prediction is closer to the RW value than that of the VR. Based on these results, together with the identical directionality index distributions (Fig 3.12), and similarity of visual cues in both movement directions, we conclude that the cells are not treating the two running directions as different environments.

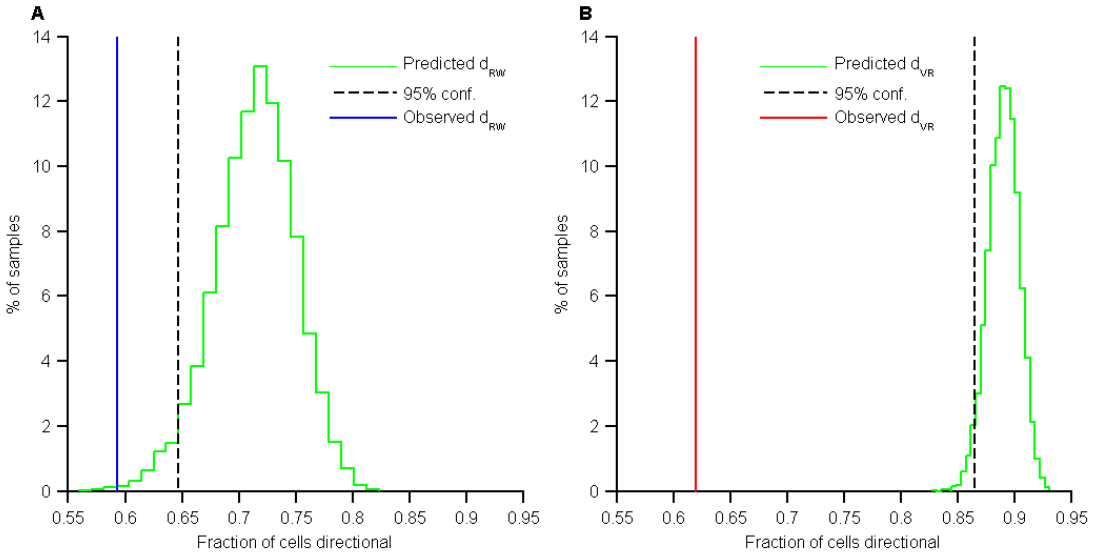


**Fig 3.12:** Two running directions are not treated as different environments by place cells. **A)** The fraction of cells that exhibit directional firing in RW is significantly below the range predicted by the interpretation that cells respond to the two running directions as different environments. **B)** As in A for VR. The directionality observed in the data is significantly lower than the prediction of the different environment interpretation.

### *3.3.2.4 Bidirectional cells in VR encode distance run rather than absolute position*

Although there were similar proportions of bidirectional cells in RW and VR, these cells showed different behavior in the two environments (Fig 3.13). Bidirectional cells fired around the same absolute position on the track in both running directions in RW (Fig 3.13) (Battaglia et al., 2004; Resnik et al., 2012), expressing a position code. In contrast, bidirectional cells in VR fired around the same distance from the start position in both running directions (Fig 3.13), indicative of a disto-code. The position code index (see methods) was significantly positive in RW but significantly negative in VR, indicating a position code in RW and its absence in VR (Fig 3.14). Exactly the opposite was true for the disto-code (Fig 3.14). Analysis of trials run at different speeds showed that spiking was more correlated with distance along the track than the duration of running, suggesting that it is distance run rather than time that determined these cells' activity (Fig 3.15).

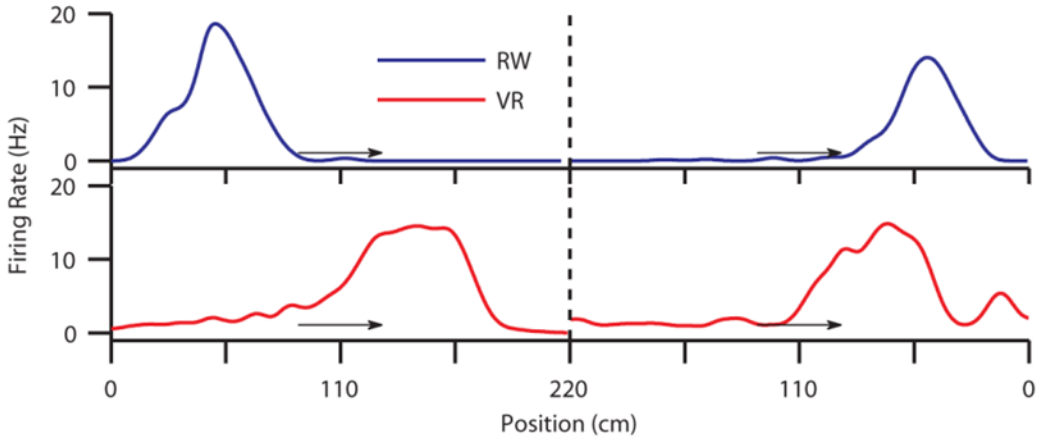


**Fig. 3.13:** Firing rate maps along both running directions for bidirectional cells in RW (top) and VR (bottom). Top panel depicts a position coding cell firing at the same position in both running directions. Bottom panel depicts a disto-coding cell firing at the same distance in both directions.

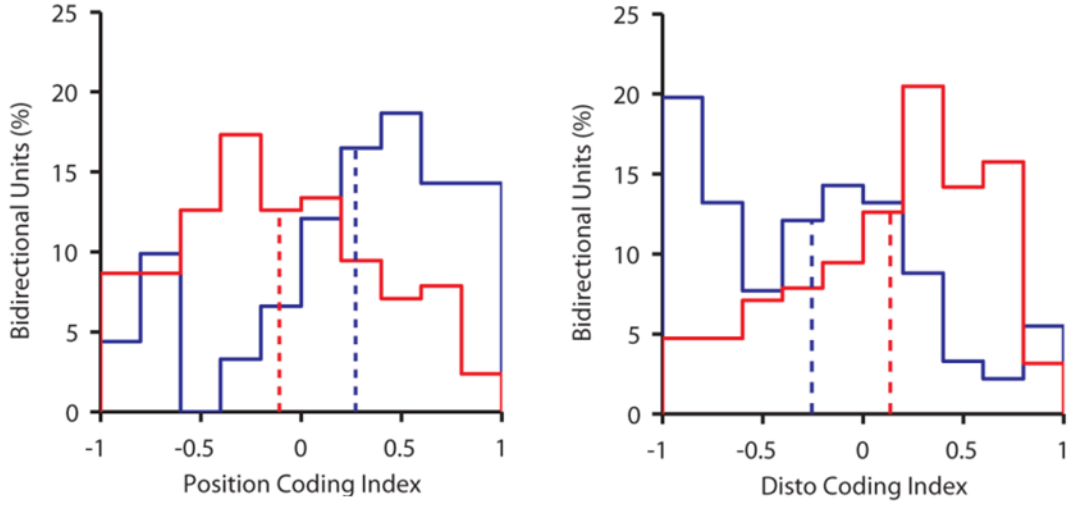


**Fig. 3.14:** Comparison of position and disto coding indices in RW and VR. **Left** Position code index is significantly positive in RW (0.27±0.05, $p<10^{-6}$, n=91) but significantly negative in VR (-0.11±0.04, $p<0.05$, n=127). **Right** The disto-code index is significantly positive in VR (0.14±0.04, $p<0.001$, n=127) but significantly negative in RW (-0.25±0.06, $p<10^{-4}$, n=91). The position code index is significantly greater in RW than VR ($p<10^{-7}$) while disto-code index is significantly greater in VR ($p<10^{-6}$).

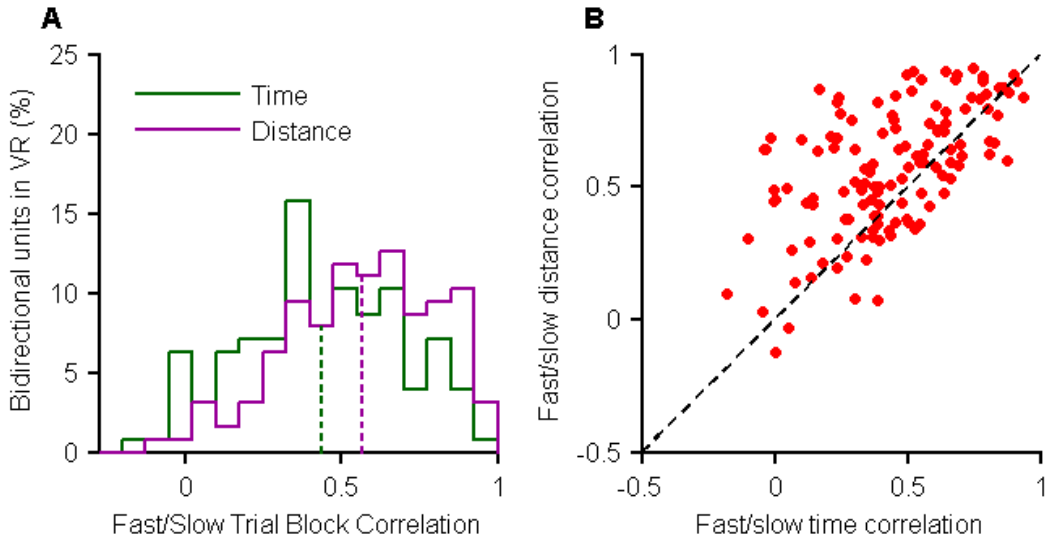


**Fig 3.15:** Disto-cell spiking is more correlated with distance along the track than the duration of the journey. **A)** Correlation between rate maps (computed as a function of either the distance traveled or the duration of journey) between fast and slow trial blocks shows greater correlation with distance (0.57 ± 0.02) than time (0.44 ± 0.02), $p<10^{-4}$. **B)** Time and distance correlations are, as expected, strongly correlated due to the rats' stereotyped speed profile. Cell-by-cell analysis shows that for a majority of cells, firing rate was more correlated with distance than time.

To assess these results at the population level, we performed population vector overlap analysis (Fig 3.16, see methods). The population of bidirectional cells spiked around the same absolute position on the track in two movement directions in RW, indicated by a significant increase in population vector overlap along the -45$^{o}$ diagonal (Fig 3.16A and C). There was no significant overlap along +45$^{o}$ (at the same distance along two directions) in RW. The opposite was true in VR (Fig 3.16B and D), with significant overlap along +45$^{o}$ and no significant overlap along -45$^{o}$. Thus the disto and position codes were present at the population level in VR and RW respectively, but not vice versa.

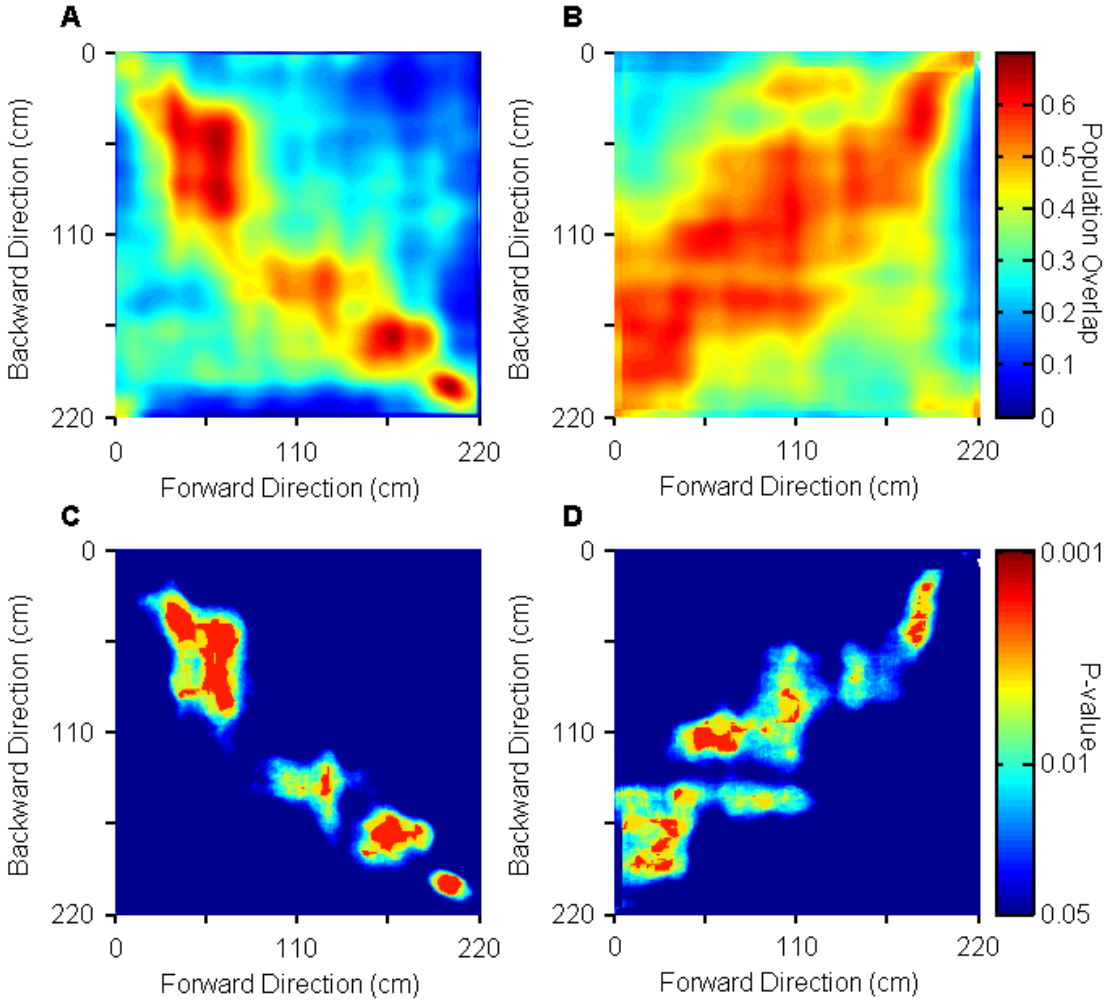


**Fig 3.16:** Population vector overlap. **A)** Similarity of the population of 91 bidirectional cells in RW between two movement directions was computed using the population vector overlap (see methods). Each colored pixel shows the vector overlap between two positions in opposite running directions. Note the clear increase in overlap along the -45º diagonal indicating spiking at the same position. **B)** As in A, for the population of 127 bidirectional cells in VR. Note the clear increase in overlap along the +45º diagonal, indicating spiking at the same distance in both running directions. **C)** P-values (cut off at 0.05) for the population vector in A under the null hypothesis that the rate map profile is independent of position along the track. Note the significant -45° diagonal, indicating position coding by the bidirectional ensemble in RW. **D)** P-values for the population vector in B. Note the significant 45° diagonal, indicating distance coding by the bidirectional ensemble in VR.

What is the likely cause of the disto-code? Besides the removal of spatially informative local cues, two parameters of the VR task could have created the disto-code: the reward-indicating pillar and the passive instantaneous scene reversal at the ends of the track. In the

VR, and not always in the RW, there was a large pillar that was suspended above the rewarded end of the track. When the rat received the reward at one end, the pillar disappeared and reappeared at the other end of the track. Since the rat is always running toward this salient cue, the "bidirectional" cells in the VR could merely be coding distance to the pillar. However, place fields from bidirectional cells do not exhibit any obvious clustering around the pillar at the end of each run (Fig 3.17), casting doubt on this hypothesis. To address this more directly, we performed a control experiment in which one rat was trained to run on the virtual track where he was rewarded at both ends but a reward indicating pillar was present at only one end. The rat's behavior was unaltered by this manipulation. The disto-code index of this rat's bidirectional cells in VR was not significantly different than that of cells from rats that ran with pillars present at both ends ($p=0.5$). The disto-code index was still significantly greater in VR than in RW ($p < 0.05$) in the control animal, and the position code index was significantly greater in RW than VR ($p < 0.05$). This suggests the disto-code was not driven by the reward indicating visual cue. As a further confirmation, disto-coding cells were observed when we ran another animal on a virtual track with no pillars. Sample bidirectional cells recorded under the single pillar and zero pillar conditions are shown in Fig 3.18. Further, directional place cells and bidirectional cells were distributed throughout the track and not clustered only at the track ends.

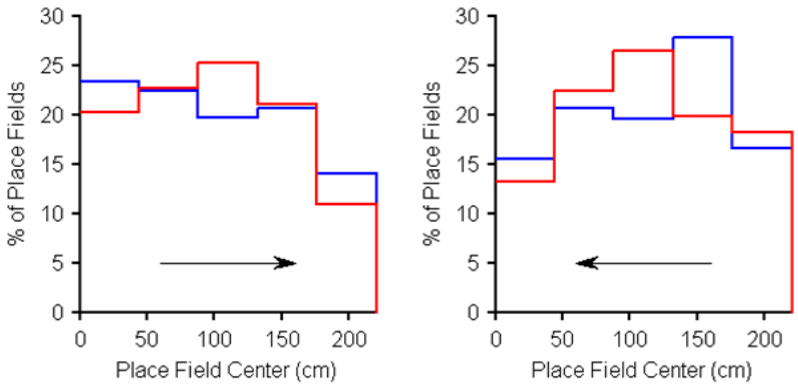


**Fig 3.17:** Distribution of place fields along the track. Arrows indicate running direction. **Left** Place fields from bidirectional cells in the forward running direction. **Right** Place fields from bidirectional cells in the return running direction.

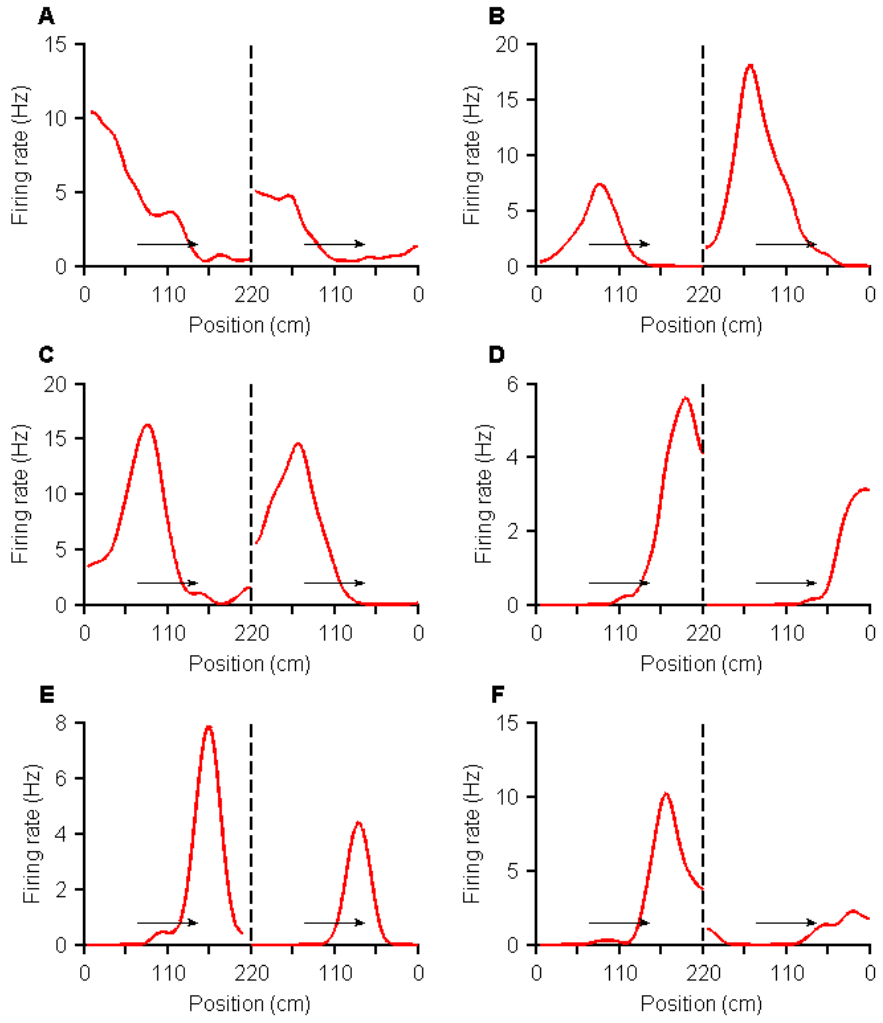


**Fig 3.18:** Sample bidirectional cells recorded during single and zero pillar conditions in VR. Panels **A**, **C**, and **E** show cells recorded with the reward pillar present at only one end of the track, and panels **B**, **D**, and **F** show cells with the reward pillar completely removed from both ends of the track. Disto-code was found in both control experiments.

To test whether the protocol choice of passive scene reversal in VR generated the disto-code, we performed a control experiment in which two rats were trained to run on the virtual track where the scene was not passively reversed, but the rats actively rotated the spherical treadmill to turn the environment. Bidirectional cells recorded under this protocol still exhibited clear disto code, with the position-code index significantly lower than the disto-code index ($p < 10^{-5}$) (Fig 3.19).

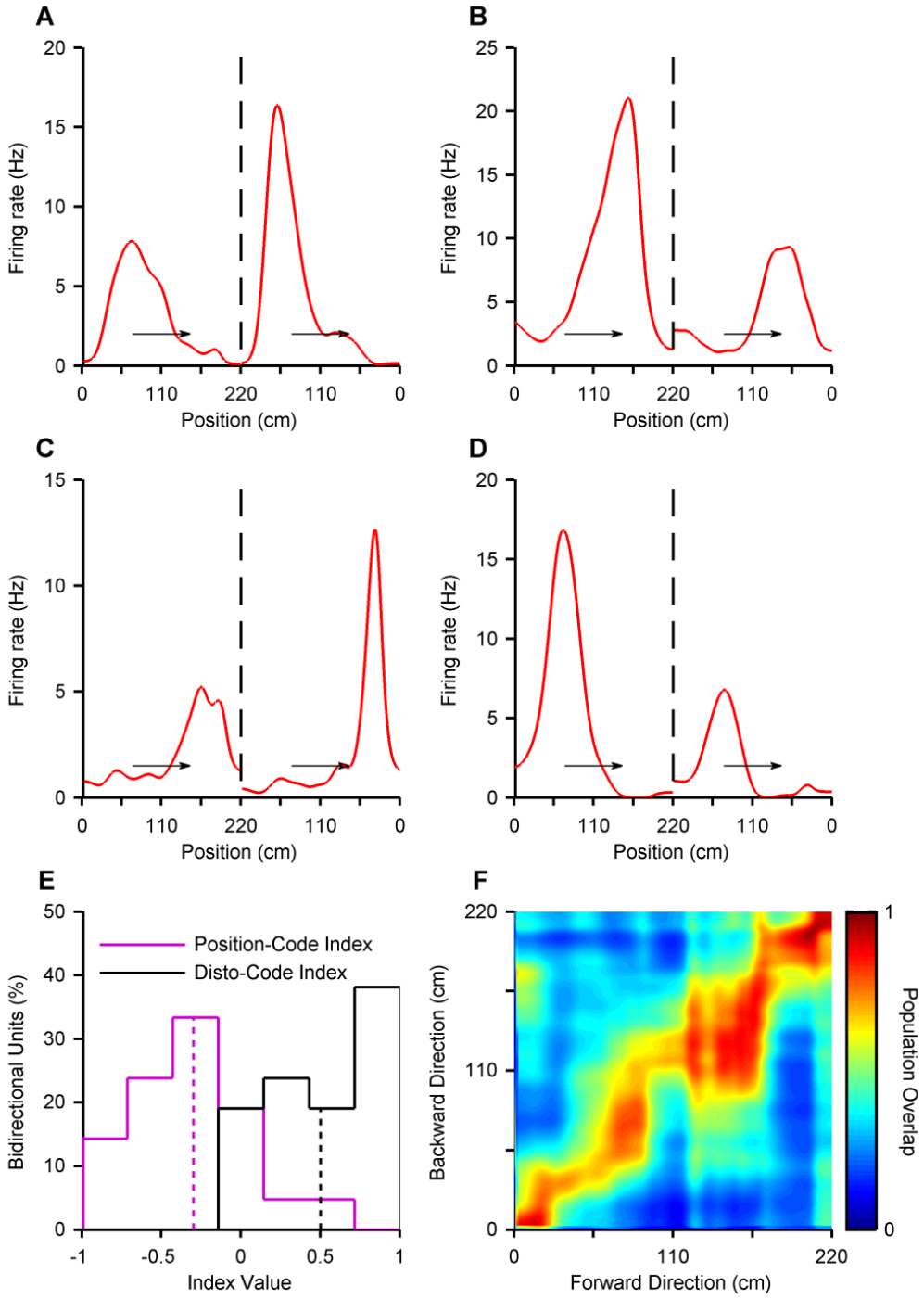


**Fig 3.19**: Passive scene reversal does not generate the disto-code. **A-D)** Sample bidirectional cells recorded in the active rotation protocol. **E)** Position-code index is significantly negative (-0.3±0.08, $p < 0.01$) and disto-code index significantly positive (0.5±0.07, $p<10^{-3}$) for the n=21 bidirectional cells recorded in the active turn condition. **F)** Population vector overlap of data in E.

Clearly, the distal visual and self-motion cues available in the VR are insufficient to support absolute position coding in bidirectional cells. Is the disto-code evidence that the hippocampus is not integrating information from distal visual cues in the VR? Indeed, rats running on a stationary linear treadmill will have reproducible firing fields defined in time or distance (Pastalkova et al., 2008; Kraus et al., 2013). Under these conditions, there is no change in distal visual cues, meaning that time or proprioception cues alone are sufficient to elicit selective firing in hippocampal neurons. If the distal visual cues in our VR were not contributing to hippocampal activity, we would expect all the place cells to be bidirectional and disto-coding. Instead, our data show a significant number of directional cells. Since the self-motion cues are identical in the two directions of running, it must be the distal visual cues that cause this differential firing. Moreover, as described above, the identical distributions of directionalities show that distal visual cues in the VR are sufficient for the hippocampus to bind the two running directions into a single environment.

What we strive to explain, then, is how the hippocampus can differentiate and integrate the two directions of running as being opposite running directions on the same track, yet fail to code absolute position in a view-invariant manner. One hypothesis is the lack of spatially informative local cues. From these data, we hypothesize that the hippocampus requires cues other than distal visual and self-motion to bind a representation to a particular location in space. Work done by other members in the lab in open field virtual environments speaks to this issue (Aghajan et al., 2014), but is outside the scope of this dissertation to be discussed here.

#### *3.3.2.5 Comparisons of the same cells in RW and VR*

The above analyses were on the entire population of cells, taken across rats and sessions. Next we compared the activity of the same cell in RW and VR. For VR and RW sessions that were recorded on the same day, we compared the spike projections of the two recording sessions. Clustered units that appeared in the same location in all 6 peak projections

and that had similar waveforms were considered to be from the same cell. We employed very stringent criteria for cell-matching; any ambiguous data was not included in the analysis. This resulted in a small dataset of 40 cells we were confident we had recorded in both RW and VR.

Examination of the same cells recorded in both VR and RW revealed that their mean firing rates and spatial information were correlated between the environments (Fig 3.20). Furthermore, roughly equal proportions of cells increased and decreased their firing rates in the VR, with a slight bias for cells to decrease, most likely due to slower running speeds. The roughly equal distribution about the unity line supports the hypothesis that specific cells are either activated or deactivated in VR, instead of a general decrease in firing rate across all cells due to a lack of spatially informative cues. This is consistent with the hypothesis that different hippocampal cells are tuned to different sensory inputs, such that some can maintain spatially selective activity in VR and others become silent.

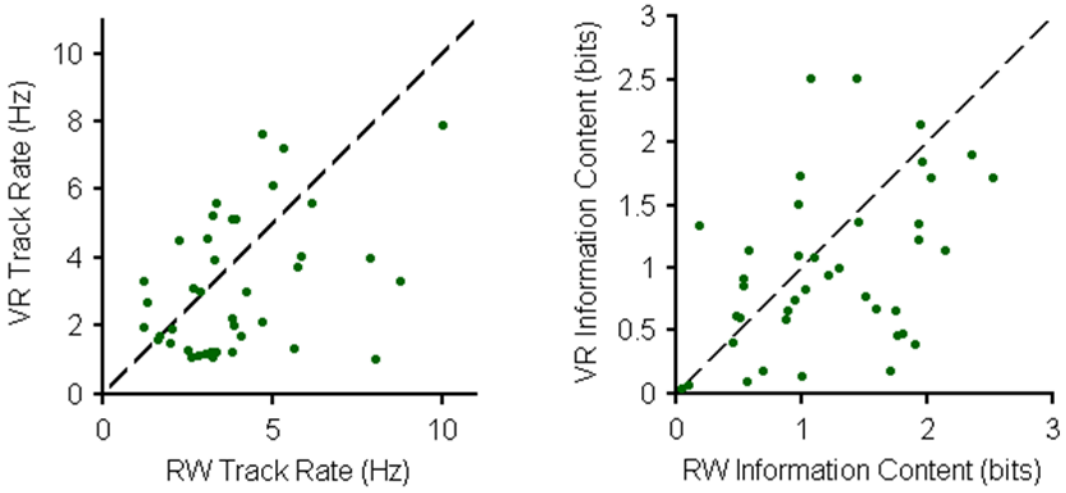


**Fig 3.20:** Comparison of pyramidal cells active in both RW and VR (n=40). **Left** Track firing rate in RW and VR (correlation coefficient r=0.40, $p<0.05$). **Right** Information content in RW and VR (r=0.43, $p<10^{-2}$).

Directionality index was also correlated between the environments (Fig 3.21), but there were several examples of cells that were highly directional in RW but highly bidirectional in VR,

and no examples of the opposite, which is seemingly at odds with the population data showing equal distributions of directionalities. However, this could simply be due to a small sample size.

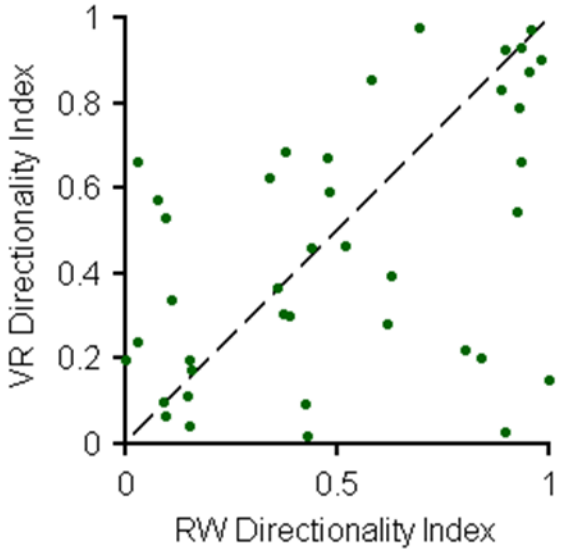


**Fig 3.21:** Comparison of pyramidal cells active in both RW and VR (n=40). Directionality index in RW and VR ($r=0.49$, $p<0.01$).

A clear result was that the position of their place fields was unrelated between the two environments (Fig 3.22, 3.23). This further supports the idea that the hippocampal representation of space is defined by more than distal visual cues. Contrast this result with previous studies involving two very similar environments in the RW (Skaggs and McNaughton, 1998; Spiers et al., 2013). In these cases, place cells maintain the same mapping of the two environments, sometimes even when it is apparent that they are independent environments. Our data from the VR suggests that the distal visual cues alone cannot be wholly responsible for this similar mapping. Alternatively, this could mean that the differences in the distal visual cues between the RW and VR, even though they were designed to be very similar, were sufficient for place cells to differentiate between the two environments.

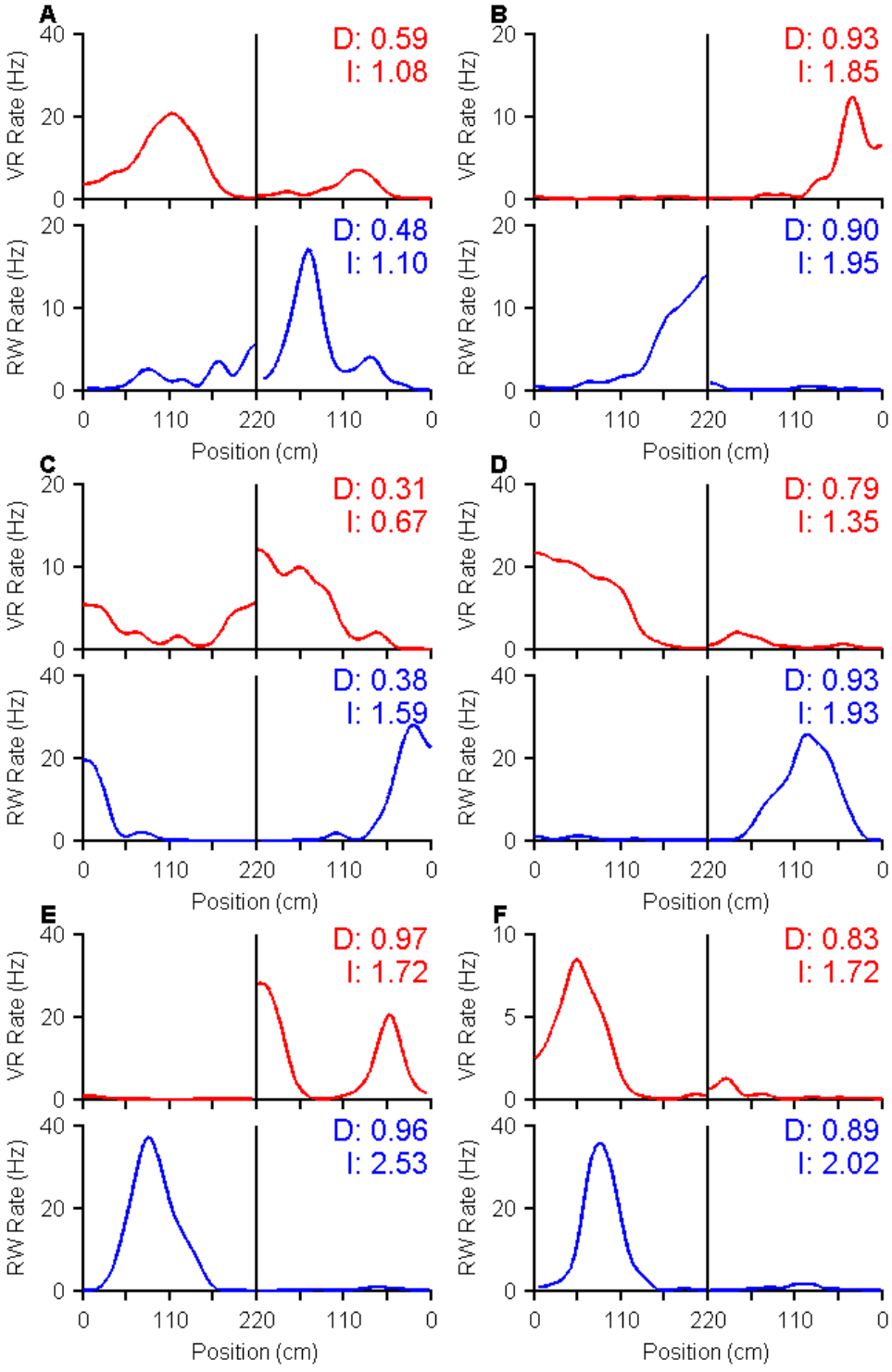


**Fig 3.22: A-F)** Ratemaps from six sample pyramidal cells active in both VR (upper panel, red) and RW (lower panel, blue). Directionality index and information content indicated for each.

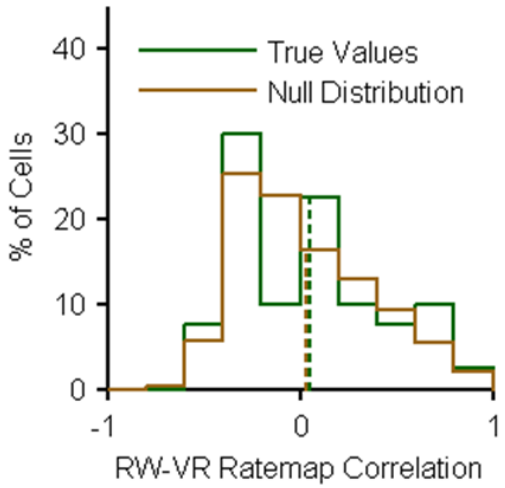


**Fig 3.23:** Comparison of pyramidal cells active in both RW and VR (n=40). Distribution of correlations between the RW and VR ratemaps of the same cell, together with null distribution obtained by shuffling cell identities, p=0.67.

As expected, in cells that were bidirectional in both environments, the disto-code index was greater in VR than in RW, and the position code index was greater in RW than VR (Fig 3.24). From this small sample set of 15 cells, it seems that most place cells switch between the two coding regimes in RW and VR. This suggests a global coding switch in the hippocampus.

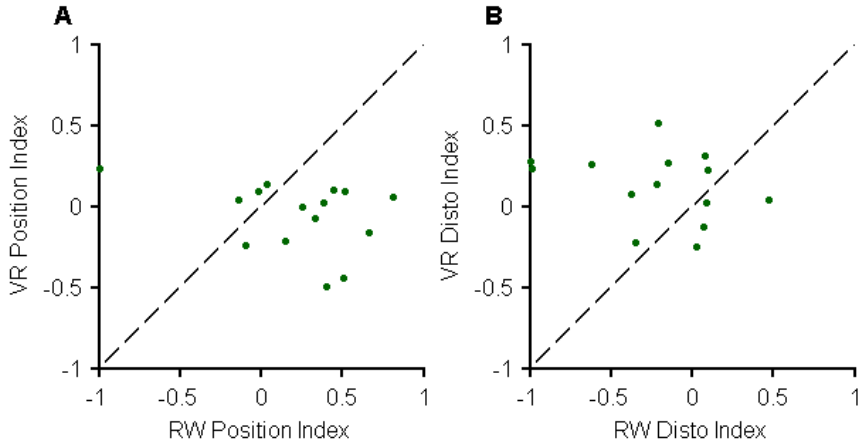


**Fig 3.24:** Position and disto-coding in the same bidirectional cells active in both RW and VR. **A)** Position code index is significantly greater ($p<0.05$) in RW than VR (correlation= -0.36 p=0.19). **B)** Disto-code index is significantly greater ($p<0.05$) in VR than RW (correlation= -0.30 p=0.3).

### 3.3.3 Temporal firing properties of place cells and hippocampal LFP in VR

#### *3.3.3.1 Theta frequency is reduced in VR*

Having examined the rate-code, we investigated the temporal features (O'Keefe and Recce, 1993; Tsodyks et al., 1996; Mehta et al., 2002; Hafting et al., 2008; Harvey et al., 2009) of place cells. The frequency of theta rhythm (see methods) in the local field potential (LFP) during locomotion was reduced in VR compared to RW (Fig 3.25, 3.26). Indeed, across the ensemble of data, the LFP theta frequency within place fields was 8.7% lower in VR compared to RW. Theta frequency was significantly lower in VR than RW at all running speeds (Fig 3.30A-B). A previous study showed that lesions of the vestibular organs caused a decrease in the frequency of theta measured through EEG (Russell et al., 2006). This suggests that vestibular inputs are involved in setting the frequency of theta, and could explain why theta frequency was lower in the VR. Vestibular inputs were not absent, but they were much reduced and did not correlate with the rat's movements in the virtual environment.

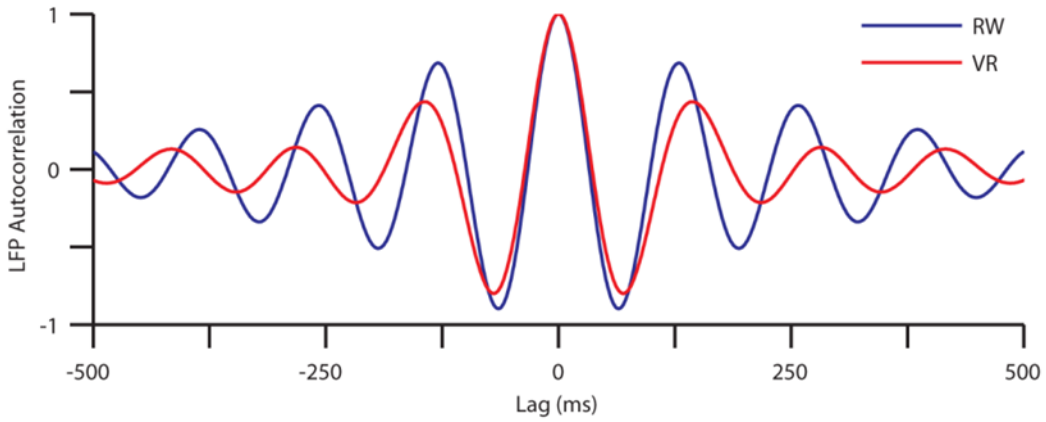


**Fig. 3.25:** Reduced theta frequency in VR. Autocorrelation function of sample hippocampal LFPs in RW and VR showing significant increase in theta period in VR. Both LFPs are recorded from same electrode on the same day.

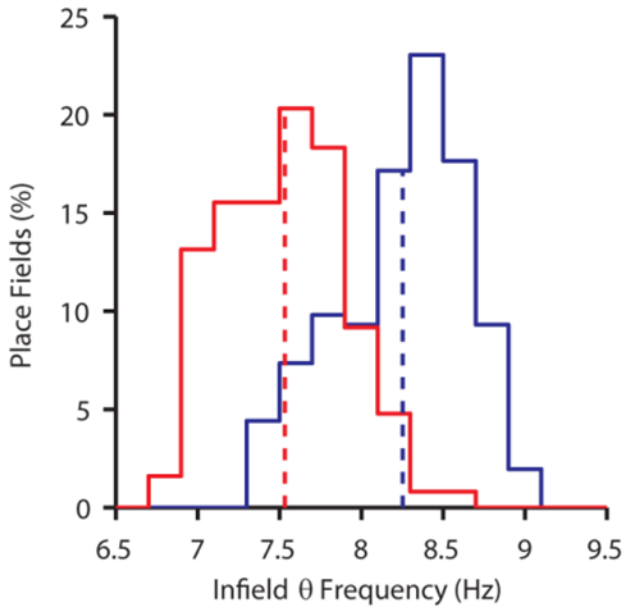


**Fig. 3.26:** Reduced theta frequency in VR. Infield theta frequency of place fields in VR (7.53 ± 0.02 Hz, n=251) was significantly less (8.7%, $p<10^{-10}$, n=204) than that of place fields in RW (8.25 ± 0.03 Hz, n=204).

### *3.3.3.2 Phase precession is preserved in VR*

Despite this, VR cells showed clear phase precession, comparable to RW (Fig 3.27, 3.28). Taken with the previous finding of lower theta frequency, this meant that the frequency of theta modulation of spiking of place cells (O'Keefe and Recce, 1993; Tsodyks et al., 1996; Mehta et al., 2002; Geisler et al., 2007; Hafting et al., 2008; Harvey et al., 2009) must also be significantly reduced in VR (Fig 3.29), which we confirmed. This decrease in firing oscillation frequency cannot be explained solely by lack of vestibular input, as this is not seen with vestibular organ lesions. Instead, this is an encouraging result that LFP frequency and spiking frequency are endogenously linked, and that phase precession is not merely an epiphenomenon. In addition, because phase precession remained intact despite the global change in theta frequency shows that phase precession is independent of the exact frequency of theta.

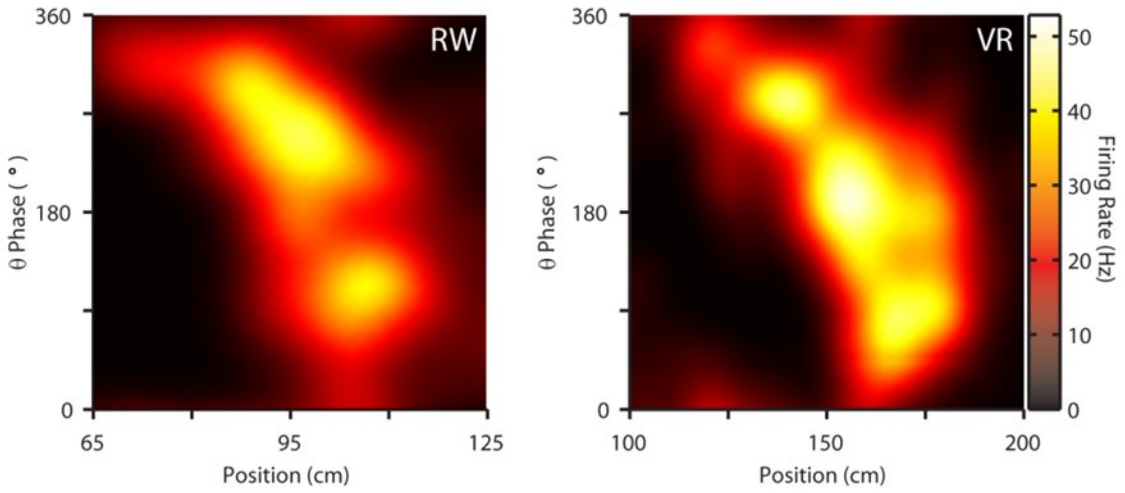


**Fig. 3.27:** Preserved phase precession in VR. . **Left** Representative place field in RW showing clear phase precession. **Right** Representative place field in VR showing clear phase precession.

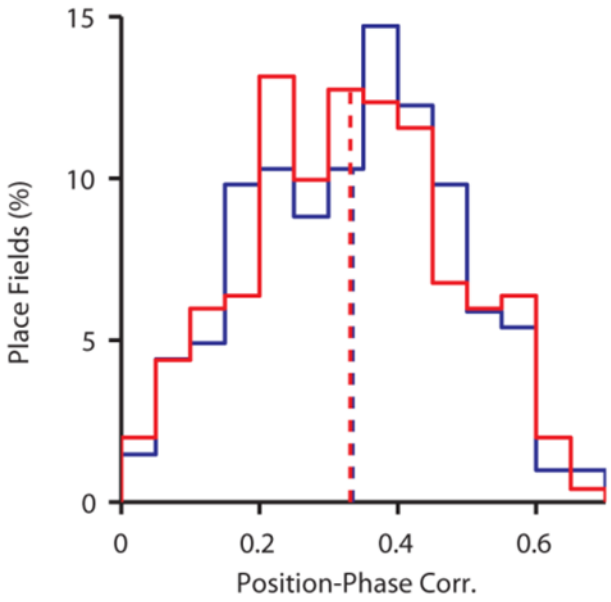


**Fig. 3.28:** Preserved phase precession in VR. Quality of phase precession, measured by position-phase linear-circular correlation, in RW (0.33 ± 0.01) was not significantly different (p=0.8) from precession in VR (0.33 ± 0.01).

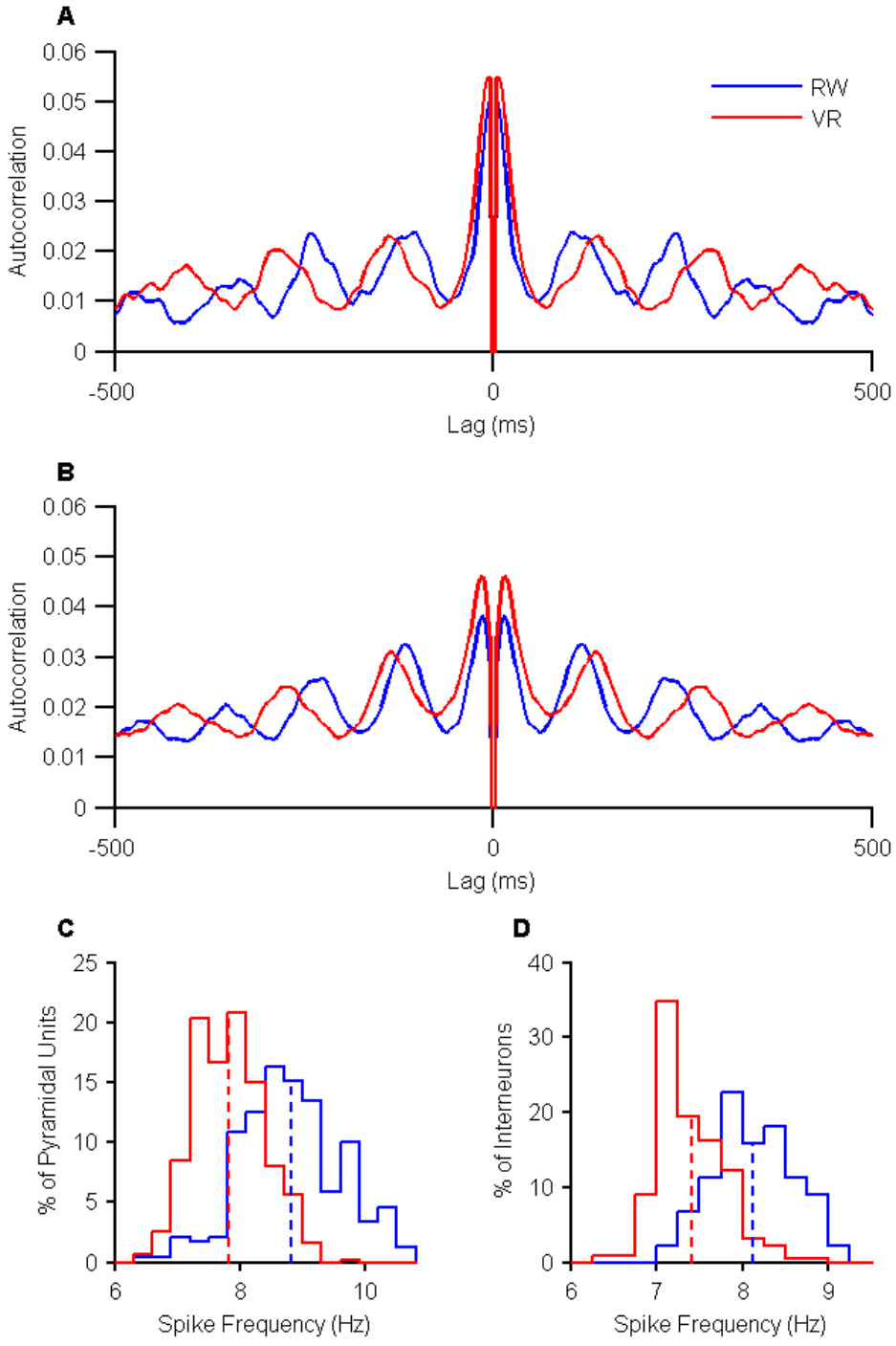


**Fig 3.29:** Spike oscillation frequency is lower in VR than RW for both pyramidal neurons and interneurons. **A)** Spike train autocorrelations from a sample pyramidal cell recorded in both RW and VR. **B)** Spike train autocorrelations from a sample interneuron recorded in both RW and VR. **C)** Spike train autocorrelation peak frequencies for pyramidal units in RW (8.81±0.05 Hz, n=240) and VR (7.83±0.03 Hz, n=432), $p<10^{-10}$. **D)** As in C, for interneurons in RW (8.13±0.07 Hz, n=44) and VR (7.40±0.03 Hz, n=221), $p<10^{-10}$.

*3.3.3.3 Speed dependence of theta is absent in VR*

Across the ensemble, theta frequency increased with running speed in RW but this was abolished in VR (Fig 3.30A-B), matching results from previous studies (Czurko et al., 1999). We thus computed the speed dependence of theta frequency for each electrode within each session (see methods). Noisy but clear speed dependent increase in theta frequency was found within single LFP data in RW (Fig 3.30C), but not in VR (Fig 3.30D). These calculations of the single cycle theta frequency could be influenced by noise, which could especially distort the low amplitude theta and provide erroneous results. Hence, we restricted the analysis to only high amplitude theta cycles (see methods). A large majority (85.4%) of LFPs in RW showed significant correlation between running speed and theta frequency but this was abolished in VR (Fig 3.30E). In contrast, theta amplitude showed identical correlation with running speed in both conditions (Fig 3.30F).

Since this abolishment of the speed-dependency of theta is also found on running wheels (Czurko et al., 1999), we can conclude that the optic flow provided in our VR is insufficient to rescue this effect. From this, we hypothesize that linear vestibular cues might be responsible for the increase of theta frequency with running speed.

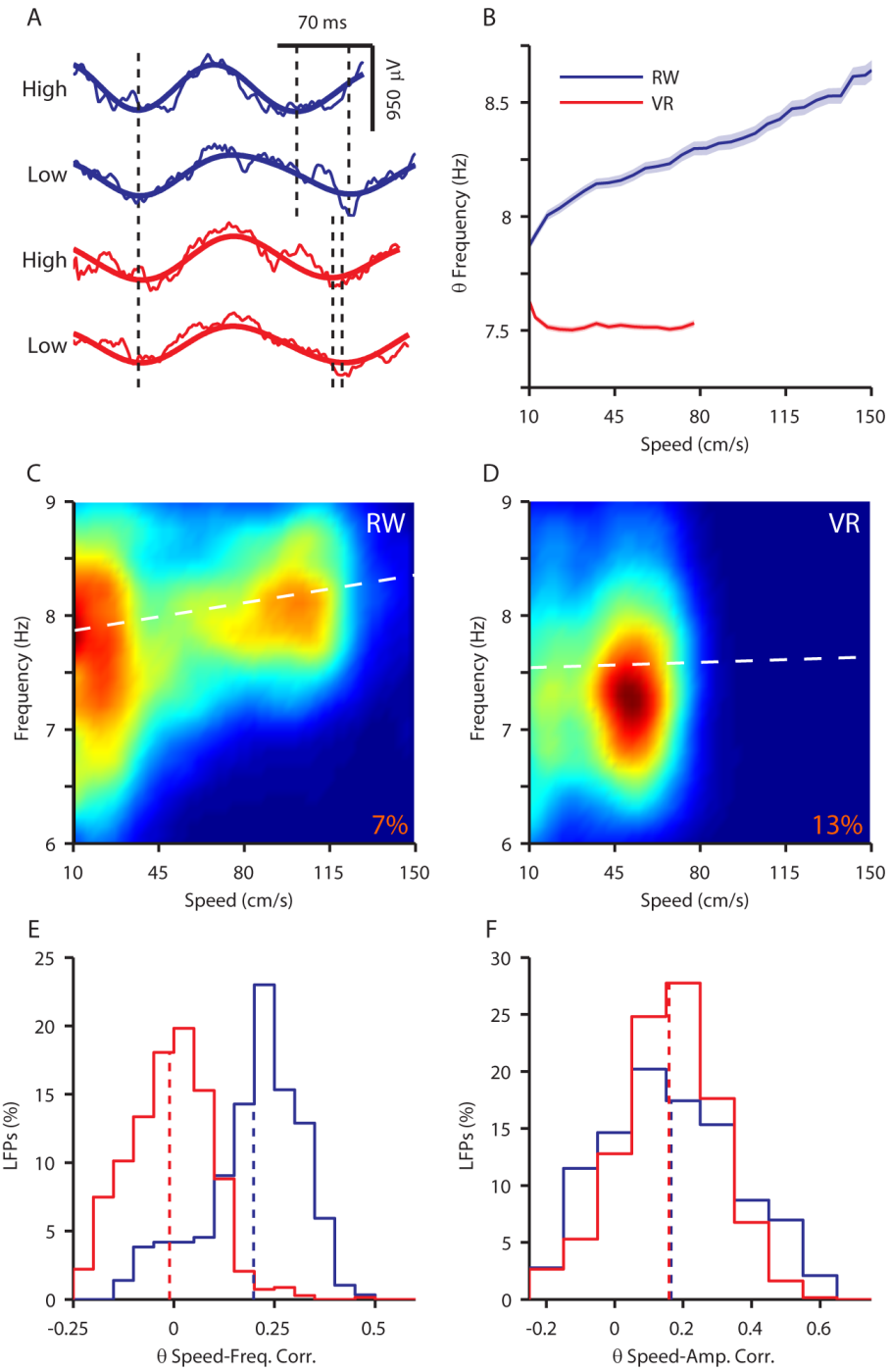


**Fig 3.30:** Absence of theta frequency speed dependence in VR. **A)** Sample theta cycles during high (>50cm/s) and low (<10cm/s) running speed in RW and VR from the same electrode as Fig 3A. Bold lines are filtered between 4 and 12 Hz, narrow lines are unfiltered traces (see Fig S15). **B)** Population average (mean ± s.e.m) speed dependence of theta frequency from 287 LFPs in RW and 681 LFPs in VR. **C)** Density map of individual theta cycle frequencies and corresponding speeds from a single LFP in RW (correlation=0.13, $p<10^{-10}$). **D)** As in C, for the same electrode in VR on the same day (correlation=0.01, p=0.48). **E)** The population of LFPs in RW shows significant correlation between theta frequency and speed (0.21 ± 0.01, $p < 10^{-10}$), while the population of LFPs in VR shows no significant correlation (-0.01 ± 0.01, p<0.01). **F)** Theta cycle amplitude is similarly (p=0.8) correlated with speed in both RW (0.16 ± 0.01) and VR (0.16 ± 0.01).

## 3.4 Discussion

These results reveal several important aspects of the sensory mechanisms governing the hippocampal rate and temporal codes. Comparable levels of spatial selectivity and firing rates of track active cells in VR and RW, as well as comparable strength of temporal code all show that a robust cognitive map can indeed be formed with only distal visual and self-motion cues providing spatial information. However these cues alone do not determine the location of place fields between VR and RW, as shown by the differences in ratemaps of the same cells.

The VR and RW environments had similar dimensions and nearly identical distal visual cues, and the rats' behavior was similar in the two conditions. Thus, these factors are unlikely to cause the observed differences in place cell activity between VR and RW. Several other factors could potentially contribute, in particular the absence of spatial information in vestibular and other sensory cues, or conflicts of other sensory cues with distal visual or self-motion cues in VR. One potential consequence of conflicting cues could be reference frame switching (between virtual and real space) occurring randomly along the track, resulting in loss of spatial selectivity in VR. The overwhelming presence of significant spatial information in cells recorded in VR argues against this possibility. Instead, these results suggest that additional sensory cues present in RW are necessary for the activation of a subpopulation of CA1 place cells, such that their removal reduces the activation of place cells without altering the firing rates of active cells. From the data in this study, spatially informative vestibular cues are not required for generating spatial selectivity in at least some place cells, in contrast to previous lesion based studies (Stackman et al., 2002) in which all hippocampal cells were unable to produce stable firing fields. In VR spatial information is provided by only distal visual and self-motion cues, which likely change more slowly than spatially informative proximal cues, such as odors along the track in RW. This could make place fields wider in VR, reducing their information content. Similar levels of directional tuning in VR and RW suggests that distal visual cues, which are the

only cues that differ along two movement directions on the track in VR, are sufficient to generate directional firing on a linear track.

The switch in coding observed in the bidirectional cell population is analogous to a previous report of different hippocampal cell response types (Pastalkova et al., 2008), which implies either distinct classes of principal cells or alternate responses from the same cells depending on the task. The latter seems to be more likely in our data since comparisons between VR and RW show that the same hippocampal cell can acquire a different form of representation given a different subset of inputs. We cannot rule out the possibility that higher order cognitive process may influence the place cell code; however it is likely that sensory inputs play a key role in our results. Bidirectional cells in RW exhibit position code (Battaglia et al., 2004; Resnik et al., 2012), which is enhanced by the addition of odors and textures (Battaglia et al., 2004). These points suggest proximal cues in RW are the most likely to generate the position code. Bidirectional cells in VR exhibit disto-code, and are likely governed by self-motion cues, which are the only cues that are similar along the two movement directions. Finally, we hypothesize that other sensory cues present in RW have a veto power over self-motion cues in determining the bidirectional code.

While disto-code has been reported on a single unit level in RW (Gothard et al., 1996a; Mizuseki et al., 2012), we do not see significant disto-code in the RW population. Further, the effect of self-motion cues on the hippocampal population code and the suggested competitive interaction between self-motion and other sensory cues are surprising. Such competitive effects between different sensory modalities may be driven by inhibitory mechanisms across multimodal inputs, as seen recently in the primary visual cortex (Iurilli et al., 2012), suggesting their broader applicability. We hypothesize that some other sensory cues reach CA1 via the lateral entorhinal cortex (LEC), because LEC neurons respond to local cues such as objects (Deshmukh and Knierim, 2011), while distal visual and self-motion cues reach CA1 via the medial entorhinal cortex (MEC) grid cells, which are influenced by these cues (Hafting et al.,

2005). Both LEC and MEC project directly and indirectly to CA1 and differentially modulate CA1 activity *in vivo* during sleep (Hahn et al., 2012), and engage local inhibition (Hahn et al., 2006). The competitive interactions governing the behavior of bidirectional cells in VR and RW may therefore be the result of inhibitory interactions between the LEC and MEC pathways.

Theta frequency was significantly reduced in VR, corroborating earlier results that vestibular inputs contribute to theta frequency (Russell et al., 2006), and its speed dependence was abolished. On the other hand, theta power had similar speed dependence in VR and RW suggesting that theta power is largely governed by distal visual and self-motion cues. Despite the large changes in theta frequency and its speed dependence, phase precession was intact in VR (Harvey et al., 2009), and its quality was identical in RW and VR, indicating that distal visual and self-motion cues are sufficient to generate a robust temporal code. Our results place restrictions on theories of phase precession that depend on the precise value of theta frequency or its speed dependence (O'Keefe and Recce, 1993; Burgess, 2008; Hasselmo et al., 2007; Blair et al., 2007). Instead they favor alternative mechanisms that are insensitive to the these phenomena (Mehta et al., 2000; Mehta et al., 2002; Hafting et al., 2008), that apply equally to networks with diverse connectivity patterns such as the entorhinal cortex and CA1, and hence do not require recurrent excitatory connections (Mehta et al., 2000; Mehta et al., 2002). These results thus provide insight about how distinct sensory cues cooperate and compete to influence theta rhythm and hippocampal spatiotemporal selectivity.

## 3.5 References

Aghajan, Z. M., Acharya, L., Moore, J. J., Cushman, J. D., Vuong, C., & Mehta, M. R. (2014). Impaired spatial selectivity and intact phase precession in two-dimensional virtual reality. *Nature Publishing Group*, *18*(1), 121–128. Nature Publishing Group.

Battaglia, F. P., Sutherland, G. R., & McNaughton, B. L. (2004). Local sensory cues and place cell directionality: additional evidence of prospective coding in the hippocampus. *The*

*Journal of neuroscience : the official journal of the Society for Neuroscience*, *24*(19), 4541–4550.

Berens, P. (2009). CircStat: A MATLAB Toolbox for Circular Statistics. *Journal of Statistical Software,* 31, 1–21.

Blair, H. T., Welday, A. C., & Zhang, K. (2007). Scale-invariant memory representations emerge from moiré interference between grid fields that produce theta oscillations: a computational model. *The Journal of neuroscience : the official journal of the Society for Neuroscience*, *27*(12), 3211–3229.

Burgess, N. (2008). Grid cells and theta as oscillatory interference: Theory and predictions. *Hippocampus*, *18*(12), 1157–1174.

Czurko, A., Hirase, H., Csicsvari, J., & Buzsaki, G. (1999). Sustained activation of hippocampal pyramidal cells by “space clamping” in a running wheel. *European Journal of Neuroscience*, *11*(June 1998), 344–352.

Deshmukh, S. S., & Knierim, J. J. (2011). Representation of non-spatial and spatial information in the lateral entorhinal cortex. *Frontiers in behavioral neuroscience*, *5*(October), 69.

Dombeck, D. A., Harvey, C. D., Tian, L., Looger, L. L., & Tank, D. W. (2010). Functional imaging of hippocampal place cells at cellular resolution during virtual navigation. *Nature neuroscience*, *13*(11), 1433–40.

Geisler, C., Robbe, D., Zugaro, M., Sirota, A., & Buzsáki, G. (2007). Hippocampal place cell assemblies are speed-controlled oscillators. *Proceedings of the National Academy of Sciences of the United States of America*, *104*(19), 8149–8154.

Gibson, S., Judy, J. W., & Markovic, D. (2008). Comparison of spike-sorting algorithms for future hardware implementation. *Conference proceedings : ... Annual International Conference of the IEEE Engineering in Medicine and Biology Society. IEEE Engineering in Medicine and Biology Society. Conference*, *2008*, 5015–5020.

Gothard, K. M., Skaggs, W. E., & McNaughton, B. L. (1996a). Dynamics of Mismatch Correction in the Hippocampal Ensemble Code for Space: Interaction between Path Integration and Environmental Cues. *J. Neurosci.*, *16*(24), 8027–8040.

Gothard, K. M., Skaggs, W. E., Moore, K. M., & McNaughton, B. L. (1996b). Binding of hippocampal CA1 neural activity to multiple reference frames in a landmark-based navigation task. *The Journal of neuroscience : the official journal of the Society for Neuroscience*, *16*(2), 823–835.

Hafting, T., Fyhn, M., Bonnevie, T., Moser, M.-B., & Moser, E. I. (2008). Hippocampus-independent phase precession in entorhinal grid cells. *Nature*, *453*(7489), 1248–1252.

Hafting, T., Fyhn, M., Molden, S., Moser, M.-B., & Moser, E. I. (2005). Microstructure of a spatial map in the entorhinal cortex. *Nature*, *436*(August), 801–806.

Hahn, T. T. G., McFarland, J. M., Berberich, S., Sakmann, B., & Mehta, M. R. (2012). Spontaneous persistent activity in entorhinal cortex modulates cortico-hippocampal interaction in vivo. *Nature neuroscience*, *15*(11), 1531–8. Nature Publishing Group.

Hahn, T. T. G., Sakmann, B., & Mehta, M. R. (2006). Phase-locking of hippocampal interneurons' membrane potential to neocortical up-down states. *Nature neuroscience*, *9*(11), 1359–1361.

Harvey, C. D., Collman, F., Dombeck, D. A., & Tank, D. W. (2009). Intracellular dynamics of hippocampal place cells during virtual navigation. *Nature*, *461*(7266), 941–6. Nature Publishing Group.

Hasselmo, M. E., Giocomo, L. M., & Zilli, E. A. (2007). An oscillatory interference model of grid cell firing. *Hippocampus*, *17*, 1252–71.

Hill, D. N., Mehta, S. B., & Kleinfeld, D. (2011). Quality metrics to accompany spike sorting of extracellular signals. *The Journal of neuroscience : the official journal of the Society for Neuroscience*, *31*(24), 8699–8705.

Itskov, P. M., Vinnik, E., Honey, C., Schnupp, J., & Diamond, M. E. (2012). Sound sensitivity of neurons in rat hippocampus during performance of a sound-guided task. *Journal of Neurophysiology*, *107*, 1822–1834.

Iurilli, G., Ghezzi, D., Olcese, U., Lassi, G., Nazzaro, C., Tonini, R., Tucci, V., et al. (2012). Sound-Driven Synaptic Inhibition in Primary Visual Cortex. *Neuron*, *73*(4), 814–828. Elsevier Inc.

Kraus, B., Robinson, R., White, J., Eichenbaum, H., & Hasselmo, M. (2013). Hippocampal "Time Cells": Time versus Path Integration. *Neuron*, *78*(6), 1090–1101. Elsevier Inc.

McNaughton, B. L., Barnes, C. A., & O'Keefe, J. (1984). The contributions of position, direction, and velocity to single unit activity in the hippocampus of freely-moving rats. *Experimental Brain Research*, *54*, 195.

Mehta, M. R., Lee, A. K., & Wilson, M. A. (2002). Role of experience and oscillations in transforming a rate code into a temporal code. *Nature*, *417*, 741–746.

Mehta, M. R., Quirk, M. C., & Wilson, M. A. (2000). Experience-dependent asymmetric shape of hippocampal receptive fields. *Neuron*, *25*, 707–715.

Mizuseki, K., Royer, S., Diba, K., & Buzsáki, G. (2012). Activity dynamics and behavioral correlates of CA3 and CA1 hippocampal pyramidal neurons. *Hippocampus*, *22*(8), 1659–1680.

Muller, R. U., & Kubie, J. L. (1987). The Effects of Changes in the Environment Hippocampal Cells on the Spatial Firing of. *Journal of Neuroscience*, *7*(July), 1951–1968.

Muller, R. U., Kubie, J. L., & Ranck, J. B. (1987). Spatial firing patterns of hippocampal complex-spike cells in a fixed environment. *The Journal of neuroscience : the official journal of the Society for Neuroscience*, *7*(July), 1935–1950.

Nguyen, D. P., Wilson, M. A., Brown, E. N., & Barbieri, R. (2009). Measuring instantaneous frequency of local field potential oscillations using the Kalman smoother. *Journal of Neuroscience Methods*, *184*, 365–374.

O'Keefe, J., & Dostrovsky, J. (1971). The hippocampus as a spatial map. Preliminary evidence from unit activity in the freely-moving rat. *Brain research*, *34*, 171–175.

O'Keefe, J., & Nadel, L. (1978). *The hippocampus as a cognitive map*. Clarendon Press, Oxford.

O'Keefe, J., & Recce, M. L. (1993). Phase relationship between hippocampal place units and the EEG theta rhythm. *Hippocampus*, *3*(3), 317–330.

Pastalkova, E., Itskov, V., Amarasingham, A., & Buzsáki, G. (2008). Internally generated cell assembly sequences in the rat hippocampus. *Science (New York, N.Y.)*, *321*(2008), 1322–1327.

Quirk, G. J., Muller, R. U., & Kubie, J. L. (1990). The Firing of Hippocampal Place Cells in the Dark Depends on the Rat's Recent Experience. *Journal of Neurophysiology*, *10*(June 1990), 2008–2017.

Resnik, E., McFarland, J. M., Sprengel, R., Sakmann, B., & Mehta, M. R. (2012). The effects of GluA1 deletion on the hippocampal population code for position. *The Journal of neuroscience : the official journal of the Society for Neuroscience*, *32*(26), 8952–68.

Russell, N. A., Horii, A., Smith, P. F., Darlington, C. L., & Bilkey, D. K. (2006). Lesions of the vestibular system disrupt hippocampal theta rhythm in the rat. *Journal of neurophysiology*, *96*, 4–14.

Save, E., Cressant, a, Thinus-Blanc, C., & Poucet, B. (1998). Spatial firing of hippocampal place cells in blind rats. *The Journal of neuroscience : the official journal of the Society for Neuroscience*, *18*(5), 1818–1826.

Save, E., Nerad, L., & Poucet, B. (2000). Contribution of multiple sensory information to place field stability in hippocampal place cells. *Hippocampus*, *10*(1), 64–76.

Schmitzer-Torbert, N., Jackson, J., Henze, D., Harris, K., & Redish, A. D. (2005). Quantitative measures of cluster quality for use in extracellular recordings. *Neuroscience*, *131*, 1–11.

Skaggs, W. E., & McNaughton, B. L. (1998). Spatial firing properties of hippocampal CA1 populations in an environment containing two visually identical regions. *The Journal of neuroscience : the official journal of the Society for Neuroscience*, *18*(20), 8455–66.

Spiers, H. J., Hayman, R. M. A., Jovalekic, A., Marozzi, E., & Jeffery, K. J. (2013). Place Field Repetition and Purely Local Remapping in a Multicompartment Environment. *Cerebral cortex (New York, N.Y. : 1991)*, 1–16.

Stackman, R. W., Clark, A. S., & Taube, J. S. (2002). Hippocampal spatial representations require vestibular input. *Hippocampus*, *12*(3), 291–303.

Thompson, L. T., & Best, P. J. (1989). Place cells and silent cells in the hippocampus of freely-behaving rats. *The Journal of neuroscience : the official journal of the Society for Neuroscience*, *9*(July), 2382–2390.

Tsodyks, M. V, Skaggs, W. E., Sejnowski, T. J., & McNaughton, B. L. (1996). Population dynamics and theta rhythm phase precession of hippocampal place cell firing: a spiking neuron model. *Hippocampus*, *6*(3), 271–280.

Wood, E. R., Dudchenko, P. a, & Eichenbaum, H. (1999). The global record of memory in hippocampal neuronal activity. *Nature*, *397*(February), 613–616.

Young, B. J., Fox, G. D., & Eichenbaum, H. (1994). Correlates of hippocampal complex-spike cell activity in rats performing a nonspatial radial maze task. *The Journal of neuroscience : the official journal of the Society for Neuroscience*, *14*(November), 6553–6563.

Zar, J. H. (1999). *Biostatistical Analysis*. 4th edition. Prentice Hill.

# Chapter 4

# Grid and Head Direction Cells on Virtual Open Fields

## 4.1 Introduction

The second project of this thesis was aimed to determine the relative contributions of sensory cues on grid and head direction cell firing.

As addressed in Chapter 3, spatial selectivity in place cells is most likely determined by many sensory cues in the environment. Indeed, a large body of literature shows that changing a wide variety of sensory cues can influence place cell firing (Muller and Kubie, 1987; Save et al., 2000; Terrazas et al., 2005; Hetherington and Shapiro, 1997; Knierim, 2002; Battaglia et al., 2004). On linear tracks in VR, we found that while distal visual, proprioceptive, and optic flow cues are sufficient for some spatial selectivity, local cues play a role in activating more place cells, increasing the information content of place fields, and allowing bidirectional place cells to code for absolute position rather than relative distance (Ravassard et al., 2013; also see Chapter 3). Subsequently, other members of the lab found that place cell selectivity is lost in 2D VR environments, leading to the additional conclusion that stable combinations of sensory cues are a necessary component as well (Aghajan et al., 2014). These results further suggest that while proprioceptive cues are informative in linear tracks, they are less so in open fields.

Grid cells in the medial entorhinal cortex (MEC) (Hafting et al., 2005), which provide one of the major spatial inputs to place cells (Zhang et al., 2013), may be controlled by a different subset of cues. Grid cells have multiple firing fields that are located on the vertices of a

triangular lattice. Since grid cells fire in many locations, it is unlikely that they are responding to particular constellations of external sensory input. Rather, they have been hypothesized to rely mostly on self-motion cues, with distal visual cues and environmental boundaries serving to anchor and orient (Hafting et al., 2005; Derdikman et al., 2009; Barry et al., 2007; Stensola et al., 2012). Unlike place cells, grid cells are active in every environment, and spatial relationships between firing fields remain stable within and between cells (Fyhn et al., 2007; Yoon et al., 2013), corroborating the hypothesis that they are controlled mostly by sensory cues that are similar across all environments, i.e. self-motion cues. Indeed, most of the models of spatial periodicity in grid cells rely on speed and heading direction of the animal (Burgess et al., 2007; Hasselmo et al., 2007; Blair et al., 2007; McNaughton et al., 2006; Fuhs and Touretzky, 2006; Burak and Fiete, 2009). There are three main self-motion cues that give redundant information and might play different roles in grid cell selectivity and periodicity. We used our VR to explore their separate contributions. The self-motion cues of proprioception and optic flow are both largely intact in the VR. In contrast, due to body fixation in the VR, the vestibular cues for linear acceleration are mostly absent and those for rotational acceleration are intermittently decorrelated with the rat's trajectory through the virtual environment. Thus, we used body-fixed VR to determine whether self-motion proprioceptive and optic flow cues, combined with stable distal visual cues for anchoring, were sufficient for spatial selectivity in grid cells.

Head direction (HD) cells provide another major spatial input to place cells (Zhang et al., 2013), and possibly also grid cells (Winter et al, 2015). These cells, found in the MEC and many other upstream areas, fire when the rat's head is oriented in a particular direction (Taube et al., 1990a; Sargolini et al., 2006). HD cells seem to be controlled by a combination of angular vestibular and visual inputs. These cells are strongly controlled by visual landmarks, such that they will reorient to maintain their preferred directions with respect to these stimuli (Taube et al., 1990b). However, lesions of the vestibular system destroy head direction tuning, even if directionally informative visual cues are available (Stackman and Taube, 1997). In a body-fixed

VR, heading angle in the virtual reference frame is only defined by visual cues, and in the RW reference frame by angular vestibular cues. When the rat turns in the virtual environment, he can orient himself partially in the direction of the turn, but is eventually stopped by the harness and has to complete the turn by rotating the spherical treadmill underneath him. At this point, visual information is consistent with turning, but vestibular information is consistent with not turning. Because of this, vestibular cues do not provide reliable angular information within the VR refrence frame. Thus, we recorded from HD cells in VR to determine the relative influence of visual and vestibular inputs on HD cells.

Three rats were trained to forage for randomly-placed rewards on 2 meter diameter circular platforms in both RW and VR. The dimensions and visual stimuli were similar in both environments. Cells in MEC and surrounding cortices were recorded using tetrodes, and monitored for spatially selective activity.

## 4.2 Methods

### 4.2.1 Subjects

Three adult male Long-Evans rats (approximately 3.5 months old at the start of training) were individually housed on a 12 hour light/dark cycle. Animals were food restricted (15-20 g of food per day) to maintain body weight. Animals were allowed to access a restricted amount of water (25-35 ml of water per day) after the behavioral session to maintain motivation. All experimental procedures were approved by the UCLA Chancellor's Animal Research Committee and were conducted in accordance with USA federal guidelines.

### 4.2.2 Virtual reality apparatus

The VR system contained a 61cm diameter Styrofoam sphere that floated freely on an acoustically quiet air cushion (see Chapters 2 and 3, Fig 3.1A). The ball rotation was measured

by two orthogonally placed laser sensors, merged by a microcontroller, and used by custom software to change the surrounding visual scene. There was one-to-one mapping between the rat's movements and the corresponding changes in the virtual environment. The standard deviation of the ball tracking for one revolution was 1.3% of a revolution. A micro projector projected visual stimuli on a custom made convex mirror, which reflected the stimuli onto a 300°, 68cm diameter, 75cm tall cylindrical screen made of white fabric. Our VR system allowed presentation of an undistorted visual scene in all directions including within 1cm of the rat. A hinged harness held the rat on the sphere. A stainless steel tube mounted in front of the rat dispensed liquid rewards (10% sucrose water, 150µl per reward) controlled by a software driven solenoid valve. The VR software was built in C++ using the Ogre 3D graphics engine and OpenAL. VR data, including the animal's (virtual) speed, position and heading, were recorded by the software at a sampling rate of 60Hz.

### 4.2.3 Task and environment

The virtual environment consisted of a 2m diameter white circular platform floating 50cm above the floor and centered in a 3x3x3m room. Regularly spaced 2cm diameter black circles spaced 4cm apart on the platform provided optic flow. A 30x30cm white grid on the black floor provided parallax-based depth perception. Distinct distal visual cues covered all 4 walls and provided the only spatially informative stimuli in the VR (Fig 4.2a). In RW, rats ran on a 2m diameter black platform that was placed 50cm above the floor. The track was surrounded by four 3x3m curtains that extended from floor to ceiling. The same stimuli on the walls in the virtual room were printed on the curtains, thus, the distal visual cues were similar in RW and VR.

### 4.2.4 Behavioral training

All experiments were conducted in identical acoustically- and EMF-shielded rooms. After pretraining (for a detailed description, see Chapter 2), animals were trained to run for hidden rewards on a platform with the same dimensions as those described above, but with different visual stimuli. This was done to control for the amount of experience on the final version of the task. Due to the relatively short training period needed, rats were trained in the same RW environment as the experimental environment. Total training time in RW and VR was approximately one week and four weeks, respectively, and training sessions for the two environments were interleaved.

In the RW, rats were encouraged to run by manually throwing small pieces of Froot Loops cereal onto the platform. In VR, sugar water reward was delivered when the rat entered the reward zone. Reward zones were hidden, so the rats learned to explore the environment continuously until the reward zone was found. The 18 predefined, evenly distributed reward zones were activated one at a time in a random permutation. The reward zones were 30cm in diameter, and the rat could enter them from any direction, introducing natural jitter in the effective reward delivery locations.

### 4.2.5 Surgery

Rats showing sufficient performance in the VR task were implanted with 25-30g custom-built hyperdrives containing up to 22 independently adjustable tetrodes (comprised of four 13μm nichrome wires). Two tetrodes were positioned over the right dorsal CA1, the rest over the right MEC. MEC coordinates were determined by a combination of previous measures and assessment of transverse sinus location during surgery (for a detailed description, see Chapter 2). The MEC cannula was positioned as far lateral as possible without having to drill into the bone ridge and as far posterior as possible without puncturing the transverse sinus. For the rats

used in this study, the MEC coordinates ranged from 9.5-10mm posterior and 4-4.5mm lateral to bregma. The CA1 coordinates ranged from 4.8-5.8mm posterior and 1.8-2.9mm lateral to bregma. Surgery was performed under isoflurane anesthesia and heart rate, breathing rate, and body temperature were continuously monitored. Analgesia was achieved by using Lidocaine (0.5mg/kg, sc) and Buprenorphine (0.03mg/kg, ip). The 1.3mm diameter hippocampal and 2.5mm diameter MEC craniotomies were drilled using custom software and a CNC device with a precision of 25μm in all 3 dimensions. Dura mater was removed and the hyperdrive was lowered until the cannulae were as close to the surface of the brain as possible. The implant was anchored to the skull with 7-8 skull screws and dental cement. The occipital skull screw was used as ground for recording. Rats were administered 40mg sulfamethoxazole and 8mg trimethoprim in drinking water and ~10mg/kg carprofen (Rimadyl bacon-flavored pellets) one day prior to surgery and for at least 10 days during recovery.

### 4.2.6 Electrophysiology

The tetrodes were lowered gradually after surgery into the hippocampus and MEC and allowed to stabilize. Positioning of the electrodes in CA1 was confirmed through the presence of sharpwave ripples during recordings. Positioning of the electrodes in MEC and subicular areas was confirmed through the presence of theta waves and spatially selective cells (Fig 4.1).

Signals from each tetrode were acquired by one of three 32-channel headstages, digitized at 40kHz, bandpass-filtered between 0.1Hz and 9kHz, and recorded continuously. Typical recording days included a RW session, a VR session, and a second RW session. Thirty-minute baseline sessions were recorded either at the very beginning or the very end. During baseline sessions, rats were allowed to rest in a box outside the task apparatus. By the time the first spatially selective cell was detected (~2 months after surgery), rats were fully habituated to run the VR and RW tasks with their implant. From this point on, rats ran the VR task in the final environment as described above.

Cells were monitored daily for spatially selective activity. In each day's recording, tetrodes with at least one spatially or directionally selective cell were marked for further analysis. In this Chapter, only the units recorded on these tetrodes are included. Thus, proportions of HD and grid cells are not reflective of the whole population because they were specially selected prior to analysis. A total of 261 putative cells from the first RW session, 218 in the VR session, and 221 in the second RW session were analyzed. Of these, 228, 195, and 160, respectively, had a mean firing rate above 0.2Hz and were considered active.

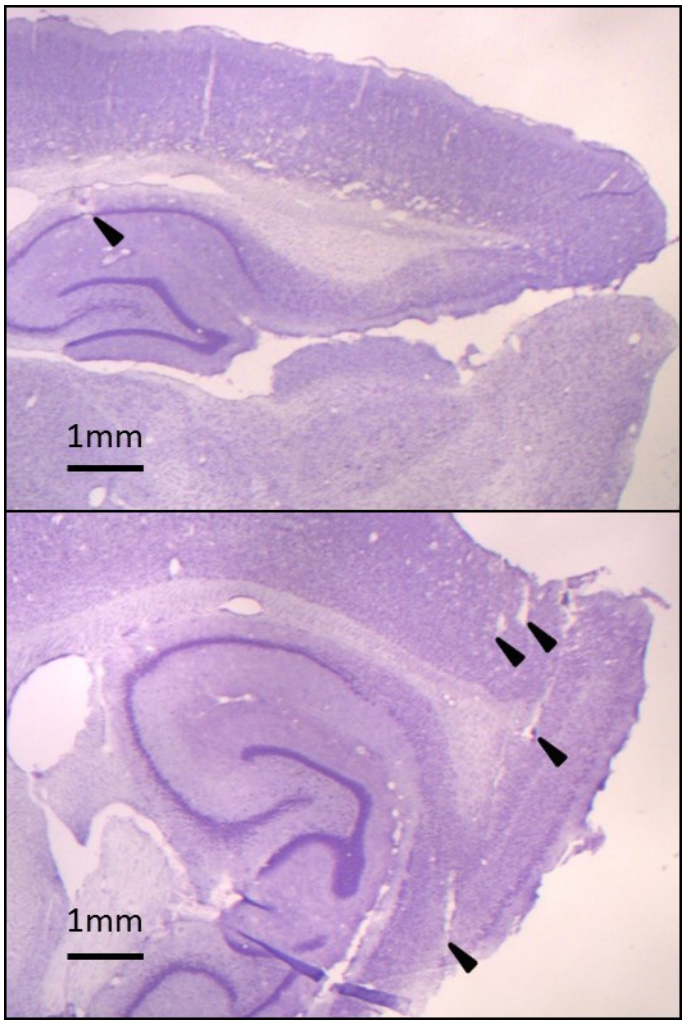


**Fig 4.1:** Histology showing tetrode tracks in the hippocampus and MEC. We implanted tetrodes to record cells in the right hippocampus and MEC. Histology micrograph of a sagittal section shows a tetrode track ending in CA1 (top) and several in MEC and surrounding cortices (bottom). Arrowheads mark the tetrode tip locations. Scale bar: 1mm.

### 4.2.7 Spike sorting

Spikes were detected offline using a nonlinear energy operator threshold (Gibson et al., 2008), after application of a noncausal 4$^{th}$ order Butterworth band pass filter (600-6000Hz). After detection, 1ms spike waveforms were extracted, upsampled fourfold using cubic splines, aligned to their peaks and downsampled back to 40 data points. Spike sorting was performed manually using custom clustering software (PyClust, Bernard Willers).

The same cells were identified between sessions run on the same day by comparing the peak projections and identifying units with similar relative amplitudes and waveforms. If cell identities were unclear due to electrode drift the data were discarded from the same cell analysis. No attempt was made to match cells across days of recording.

### 4.2.8 Statistics

All analyses were done in MATLAB using custom codes. To assess the significance between linear variables and distributions being different from zero, two-sided nonparametric Wilcoxon rank-sum test and Wilxocon singed-rank test were utilized respectively. All numbers are reported as mean±s.e.m unless noted otherwise.

### 4.2.9 Construction of spatial and angular rate maps and measures of selectivity

These methods were similar to those described previously (Aghajan et al., 2014; Acharya et al., 2015). Briefly, spatial firing rates were computed by an element wise division of spike count and occupancy time histograms with 5cmx5cm bins smoothed with a 7.5cm two-dimensional Gaussian kernel. Behavior data and spikes that occurred during periods of immobility or low running speeds (<5cm/s) were excluded from further analysis and bins with low occupancy were discarded. Angular rate maps were calculated in a similar manner using 80

angular bins. Information content, sparsity and mean vector length were computed using methods described earlier (Ravassard et al., 2013; Acharya et al., 2015).

### 4.2.10 Quantification of grid score

We calculated the grid score as described in Sargolini et al., 2006. To obtain the grid score, we first computed the autocorrelation of the spatial rate maps. We then extracted a circular ring from the autocorrelogram, centering around but excluding the central peak. We then rotated this ring by different angles ($\theta$) in steps of 30 degrees and calculated the Pearson correlation coefficient between the original and rotated rings ($r_\theta$). Grid score was then calculated as:

$$GS = \min(r_\theta)_{\theta=60°,120°} - \max(r_\theta)_{\theta=30°,90°,150°}$$

### 4.2.11 Control analysis for significance levels

To obtain the significance levels for different measures of selectivity, we performed a shuffling procedure identical to those described earlier (Aghajan et al., 2014). We circularly shifted the spikes with respect to the behavior data by different amounts (10–100s). All selectivity measures were computed from the resulting rate maps and for each neuron, all measures were expressed in the units of z-score or standard deviation around the mean value of the shuffled data. A z-score value of 2.0, corresponds to a significance level of 0.05.

## 4.3 Results

### 4.3.1 Behavior

During recordings, rats ran consistently for 20-30 minutes to obtain reward in both RW and VR. Linear and angular speeds in VR were lower perhaps due to increased effort required to turn the spherical treadmill (Fig 4.2).

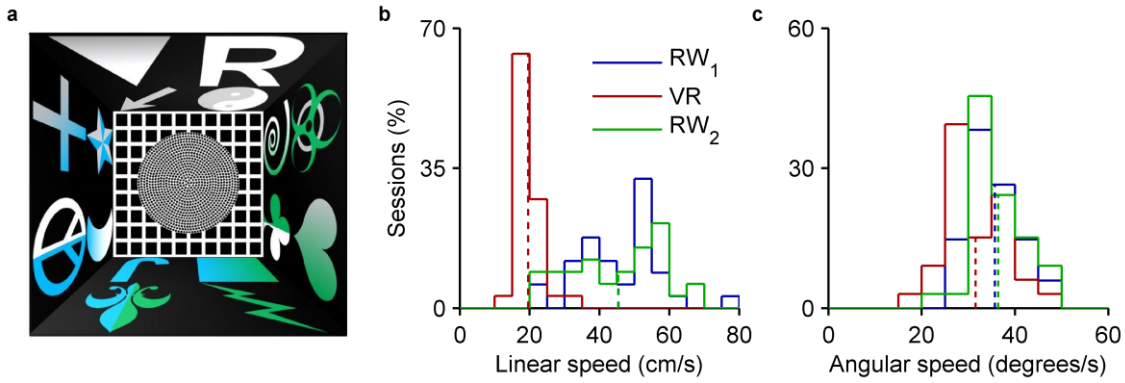


**Fig 4.2:** Schematic of the world and behavior: **a)** Top-view schematic of the experimental room. **b)** For 33 sessions in $RW_1$, the median running speed (45.45 ± 1.93 cm/s) was comparable to that in $RW_2$ (45.40 ± 2.25, p=0.84) and much greater compared to VR (19.55 ± 0.53, $p<10^{-11}$). **c)** In $RW_1$, after taking into account the actual head movements of the rat, the median angular speed (35.71 ± 0.96 degrees/s) was comparable to that in $RW_2$ (36.40 ± 0.02, p=0.40) and slightly greater compared to VR (31.54 ± 1.15, $p<10^{-2}$).

### 4.3.2 Grid cells in VR

#### *4.3.2.1 Cells with grid like activity were found in RW, but not VR*

Grid scores were measured for all active cells in the first RW session, the VR session, and the second RW session. Clear grid cells were found in RW (Fig 4.3), but not VR. Across the population of cells, grid scores were higher in the RW sessions (Fig 4.4). While we found cells with significant grid like activity in RW as expected, this incidence was likely below chance level in VR (Fig 4.4).

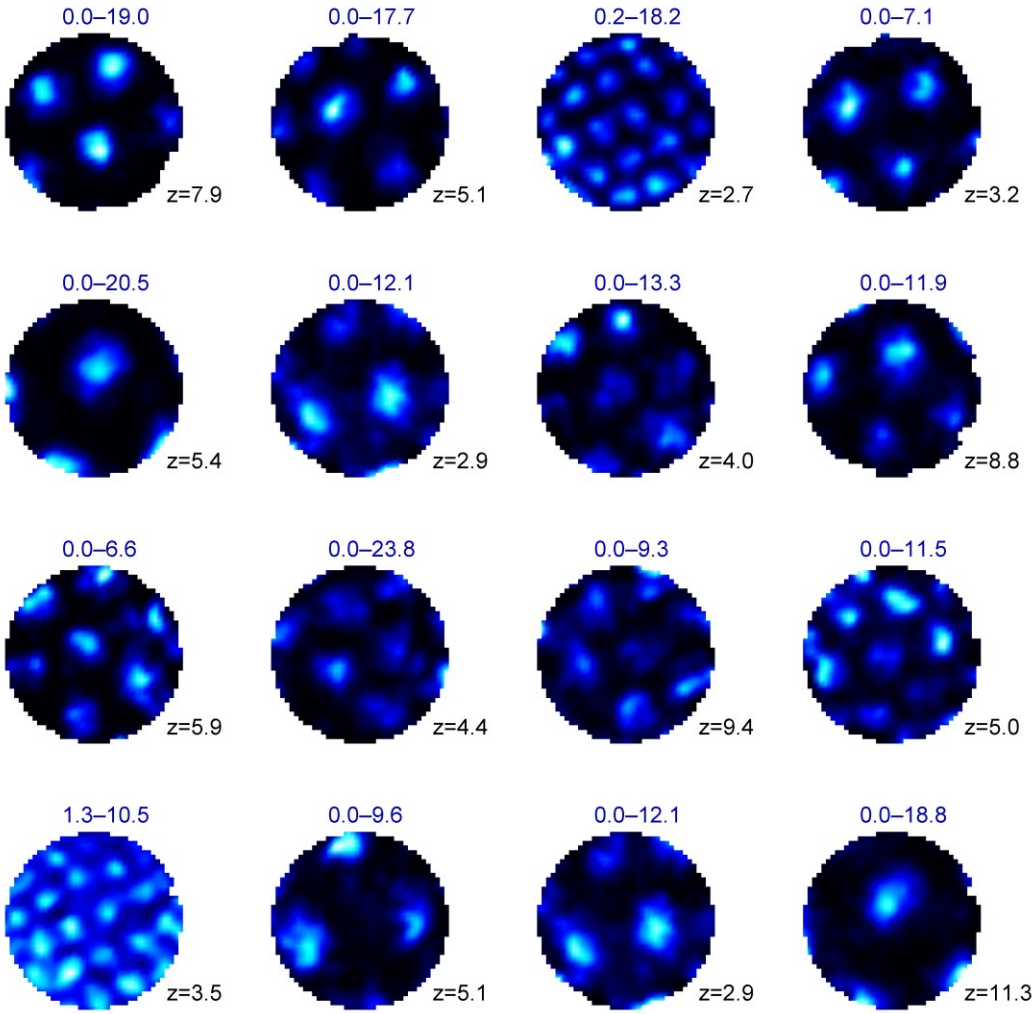


**Fig 4.3:** Example grid cells in $RW_1$: Spatial firing ratemaps (lighter colors correspond to higher firing rates). The numbers at the top indicate firing rate range in Hz. The number at the bottom right corner corresponds to z-scored grid score.

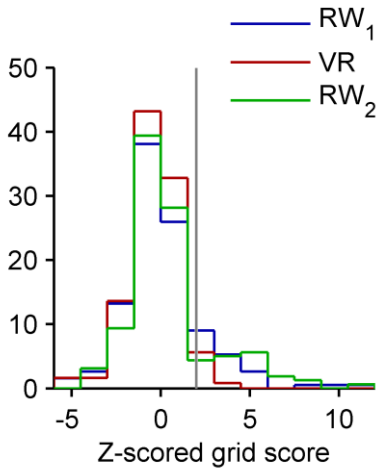


**Fig 4.4:** Grid scores of population of analyzed cells. For 228 (of 261 total) active cells in $RW_1$, the z-scored grid score in $RW_1$ (0.12 ± 0.15) was comparable to that in 195 (out of 218) active cells in $RW_2$ (0.34 ± 0.19, p=0.44) and also not statistically different to that in 160 (out of 221) active cells in VR (-0.35 ± 0.12, p=0.3). The vertical grey line, at a z-scored grid score of 2, represents the cutoff for cells with significant grid like firing. 28 cells showed a significant grid score in $RW_1$, 6 in VR, and 27 in $RW_2$.

#### *4.3.2.2 Grid cells lose their spatial selectivity and periodicity in the VR*

To further investigate the firing properties of putative grid cells in VR, we indentified the same cells across the sessions. Some grid cells reduced their firing rates dramatically in the VR (Fig 4.5a). Most, however, remained active in the VR, but did not fire in a spatially selective manner (Fig 4.5b). Similarly, all of the conjunctive gridxHD cells lost their grid like activity; however, a few retained their HD tuning (Fig 4.5c). Overwhelmingly, even cells identified as grid cells in RW could not maintain a grid pattern within the virtual reference frame.

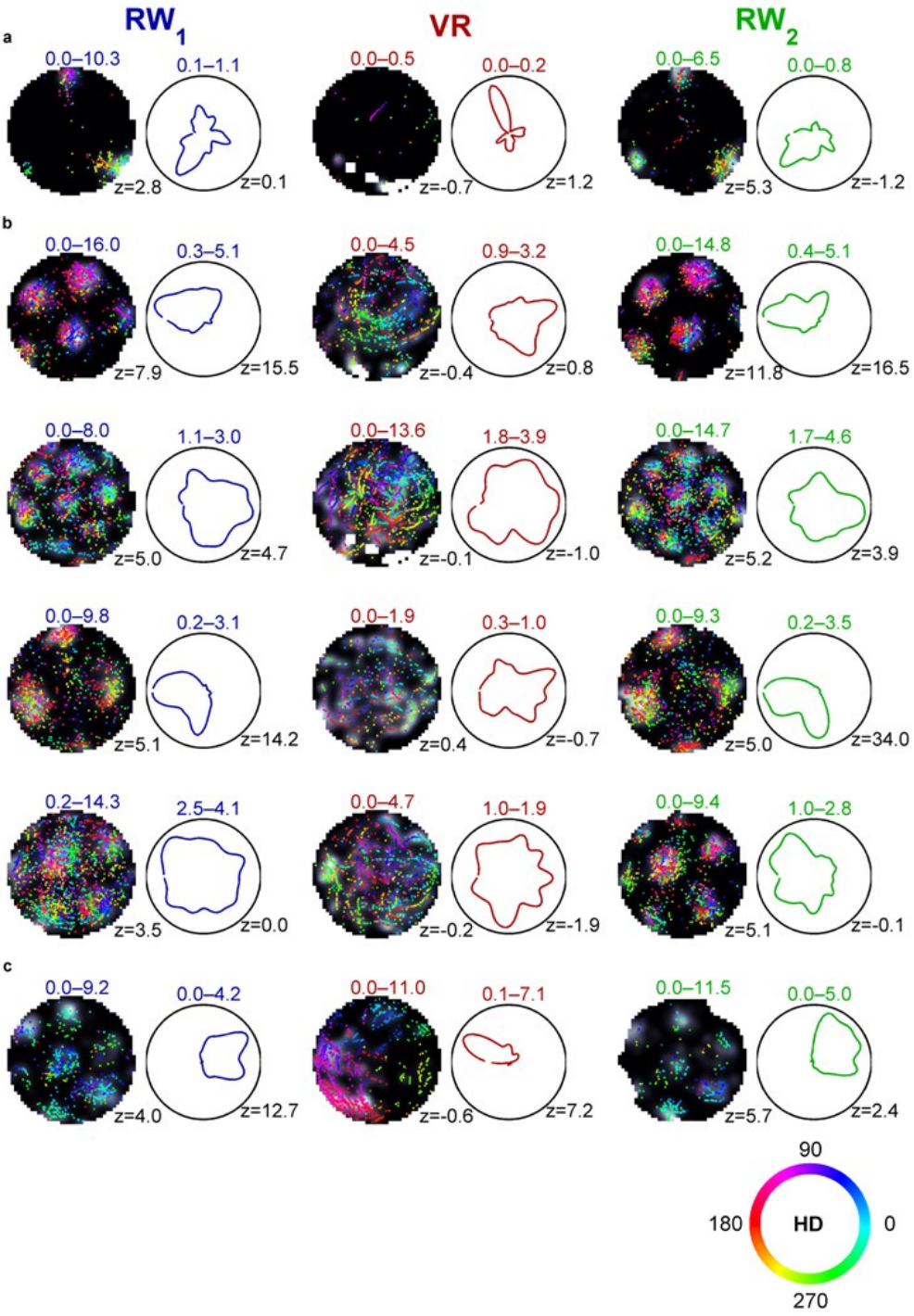


**Fig 4.5:** Example grid cells active in $RW_1$, VR, and $RW_2$: Left) Spatial firing rate of a neuron (grey scale range indicated by numbers; lighter shades correspond to higher values) overlaid with the position of the rat when spikes occurred (colored dots). Each color represents a distinct head-direction as shown in the color wheel. Number a the bottom right represents the z-scored grid score. Right) Angular firing rate of the same neuron. Numbers indicate firing range. Number at the bottom right corner of the polar plot is the z-scored sparsity of the angular ratemap. **A)** A sample grid cell that shuts down in VR. **B)** Four example grid cells that lose their grid activity in VR. **C)** An example conjunctive gridxHD cell that loses the grid but keeps its HD tuning in VR.

Over the population of matched grid cells, mean firing rates were slightly decreased in VR, but identical in the two RW sessions (Fig 4.6a-c). Grid scores dropped dramatically between the first RW session and the VR session (Fig 4.6d and f). However, many matched grid cells did not recover their high grid scores in the second RW session, showing only a loose correlation between grid scores in the two RW sessions (Fig 4.6e and f). This requires further investigation since grid cells have been previously reported to be stable between sessions. It is unclear from these data whether this is an artifact or if the preceeding session in the VR affects the cells' firing in the second RW session. Spatial sparsity, however, was similar between the two RW sessions and showed a significant decrease in the VR (Fig 4.6g-i).

The complete abolishment of grid like activity in VR suggests that distal visual, proprioceptive, and optic flow cues are insufficient for spatial selectivity in grid cells within the VR reference frame. These findings are in apparent contrast with those found in a slightly different type of VR apparatus (Aronov and Tank, 2014). In this apparatus, the rat can rotate freely on the ball, so angular vestibular cues remain correlated with the animal's path in the virtual environment. In these conditions, grid cells maintain their spatial selectivity and periodicity within the virtual reference frame. Taken together with our results, this suggests that angular vestibular cues may an important factor in grid cell mapping. Alternatively, the lack of grid-like activity in our data could be due to the lack of coherence between the virtual reference frame and the uncontrolled distal cues in the surrounding room. Since grid cells have multiple equally spaced firing fields, it is unlikely that such cues have a direct influence. However, they may exert an indirect effect through the abolishment of spatial selectivity in place cells (Aghajan et al., 2014) if such information is necessary for grid-like activity (Bonnevie et al, 2013).

The lack of periodicity within the virtual reference frame under these conditions provides a unique opportunity to probe the network dynamics of grid cells. With this dataset, evidence of periodicity with respect to a different reference frame would give insight to the mechanisms that give rise to grid cells. This requires futher analysis.

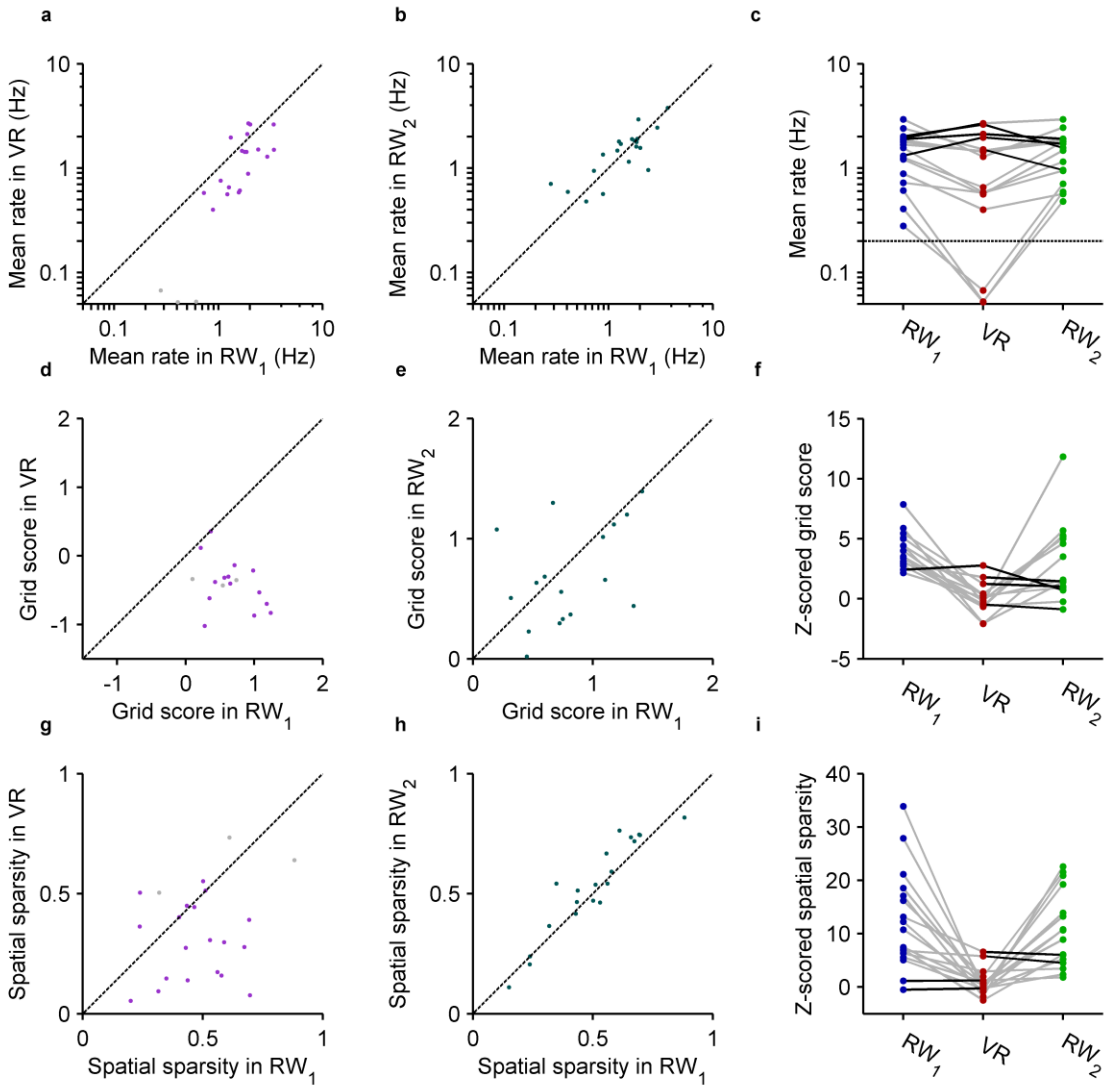


**Fig 4.6:** Grid scores of the same cells in $RW_1$ and VR and $RW_2$ **a)** Out of 22 grid cells identified in the first RW session, 19 were active (mean rate > 0.2 Hz) in both RW and VR (purple dots). For the grid cells active in both worlds, the mean firing rate was significantly (p=0.018, Wilcoxon signed-rank test) greater in RW compared to VR which could be partially due to lower running speeds in the latter. **b)** Out of 20 grid cells identified in the first and second RW sessions, 20 were active (mean rate > 0.2 Hz) in both $RW_1$ and $RW_2$ (green/blue dots). For the grid cells active in both real world sessions, the mean firing rate was identical (p=0.65, Wilcoxon signed-rank test). **c)** For 17 grid cells identified in all three cases, the majority of cells had lower mean firing rates in VR compared to the RW sessions which could be explained by lower running speed. The horizontal line at 0.2 Hz represents the cutoff of being considered active. **d)** For the grid cells active in both worlds, the grid score was significantly ($p<10^{-3}$, Wilcoxon signed-rank test) greater in RW compared to VR. **e)** For the grid cells active in both RW sessions, the grid score was identical (p=0.077, Wilcoxon signed-rank test). **f)** For 17 grid cells identified in all three cases, the majority of cells had lower grid scores in VR compared to the RW sessions **g)** For the grid cells active in both worlds, the sparsity of the spatial ratemaps was significantly ($p<10^{-2}$, Wilcoxon signed-rank test) greater in RW compared to VR. **h)** For the grid cells active in both RW sessions, the sparsity of the spatial ratemaps was identical (p=0.038, Wilcoxon signed-rank test). ). **i)** For 17 grid cells identified in all three cases, the majority of cells had lower spatial sparsity in VR compared to the RW sessions

### 4.3.3 Head direction cells in VR

#### *4.3.3.1 A smaller proportion of cells with HD tuning were found in the VR than in RW*

Mean vector lengths (MVLs) were measured for all active cells in the first RW session, the VR session, and the second RW session. A high proportion of clear HD cells was found in RW (Fig 4.7). In VR, some cells were found to have HD tuning in the virtual reference frame; examples are shown in Fig 4.8. Across the population of cells, MVLs and angular sparsity measures were much higher in the RW sessions (Fig 4.9). In RW, many cells showed significant HD tuning; and while that number dropped in VR, it was above chance level for the population sampled.

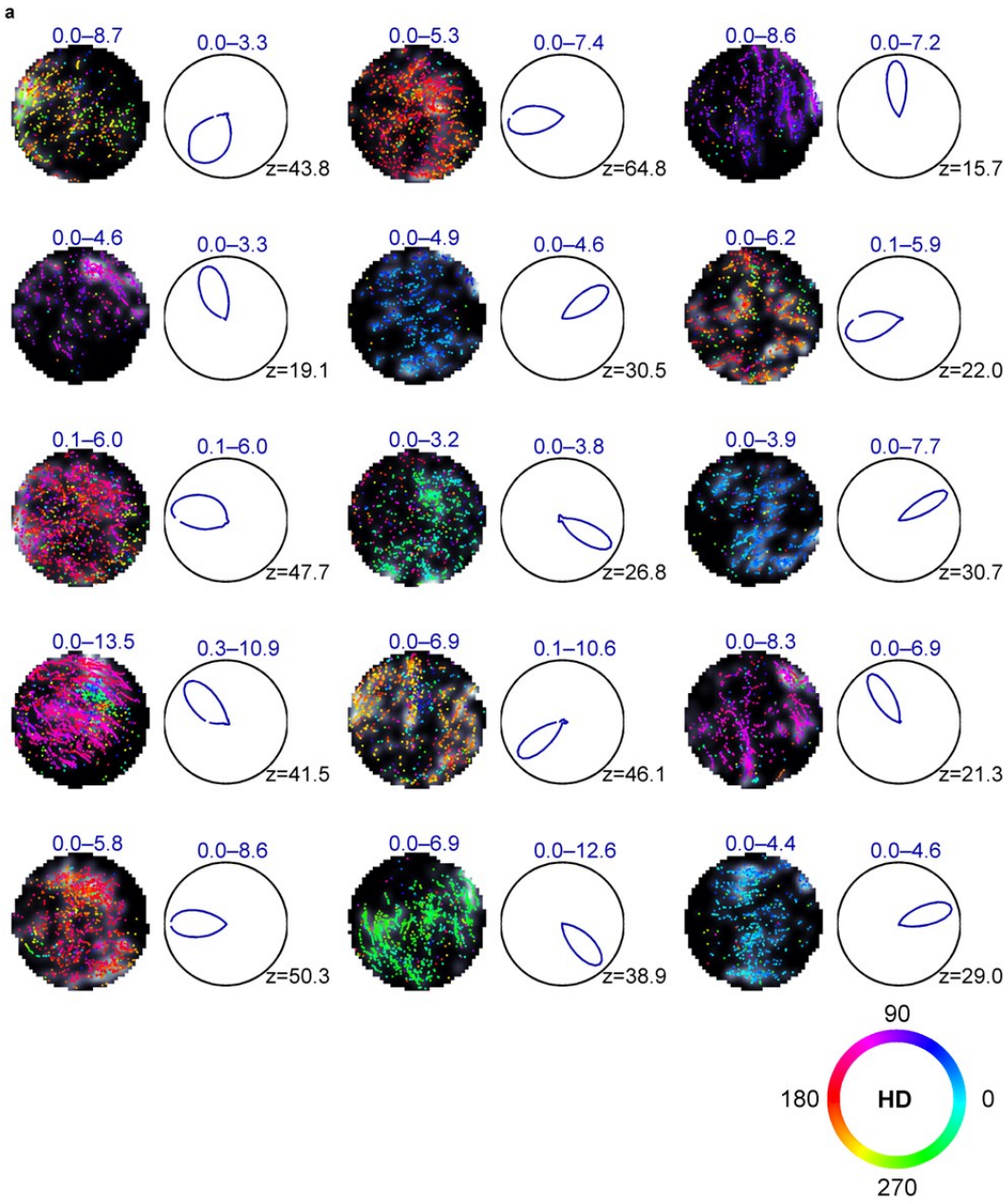


**Fig. 4.7:** Example HD cells in $RW_1$: Left) Spatial firing rate of a neuron (grey scale range indicated by numbers; lighter shades correspond to higher values) overlaid with the position of the rat when spikes occurred (colored dots). Each color represents a distinct head-direction as shown in the color wheel. Right) Angular firing rate of the same neuron. Numbers indicate firing range. Number at the bottom right corner of the polar plot is the z-scored sparsity of the angular ratemap.

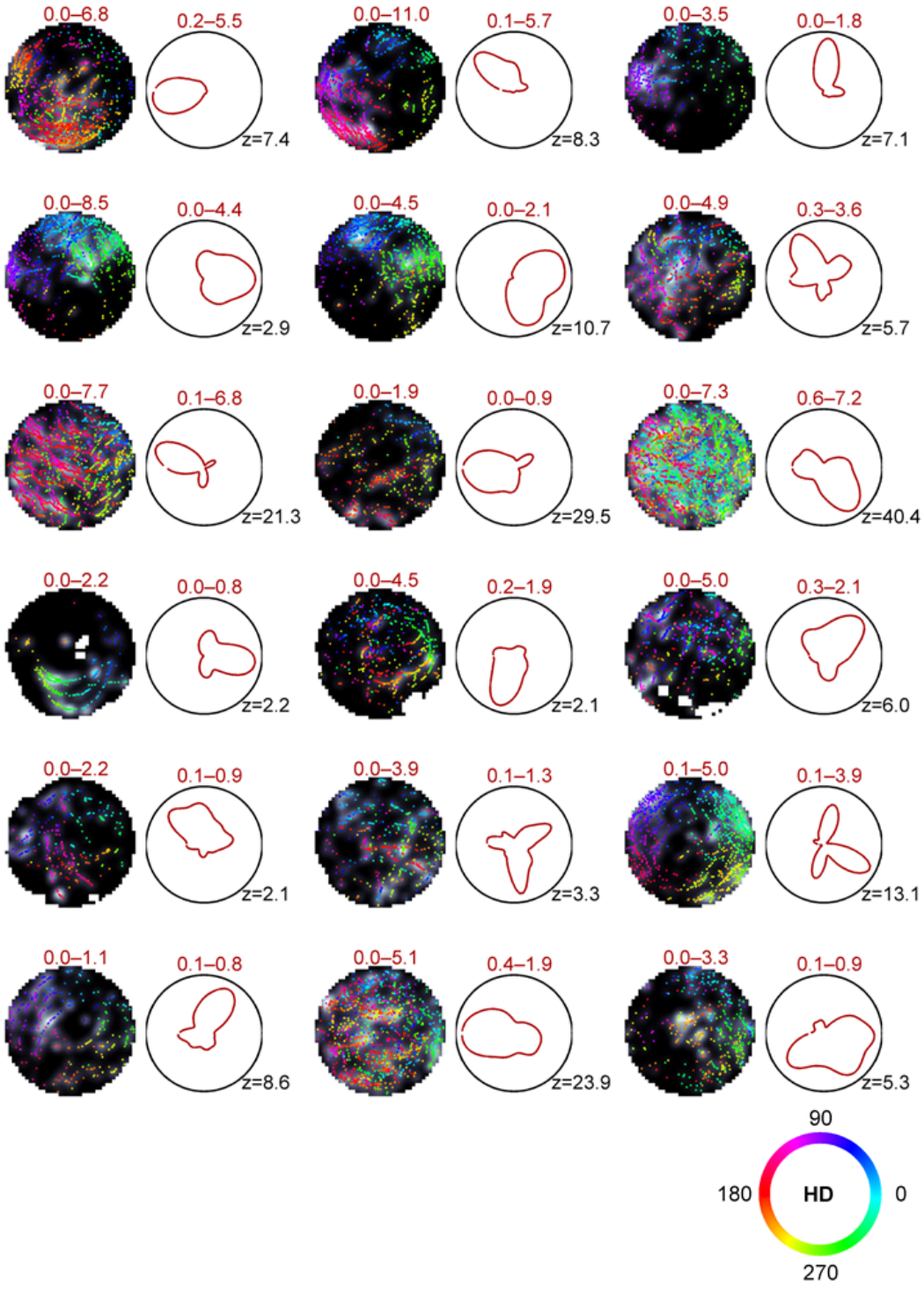


**Fig. 4.8:** Example HD cells in VR: Left) Spatial firing rate of a neuron (grey scale range indicated by numbers; lighter shades correspond to higher values) overlaid with the position of the rat when spikes occurred (colored dots). Each color represents a distinct head-direction as shown in the color wheel. Right) Angular firing rate of the same neuron. Numbers indicate firing range. Number at the bottom right corner of the polar plot is the z-scored sparsity of the angular ratemap.

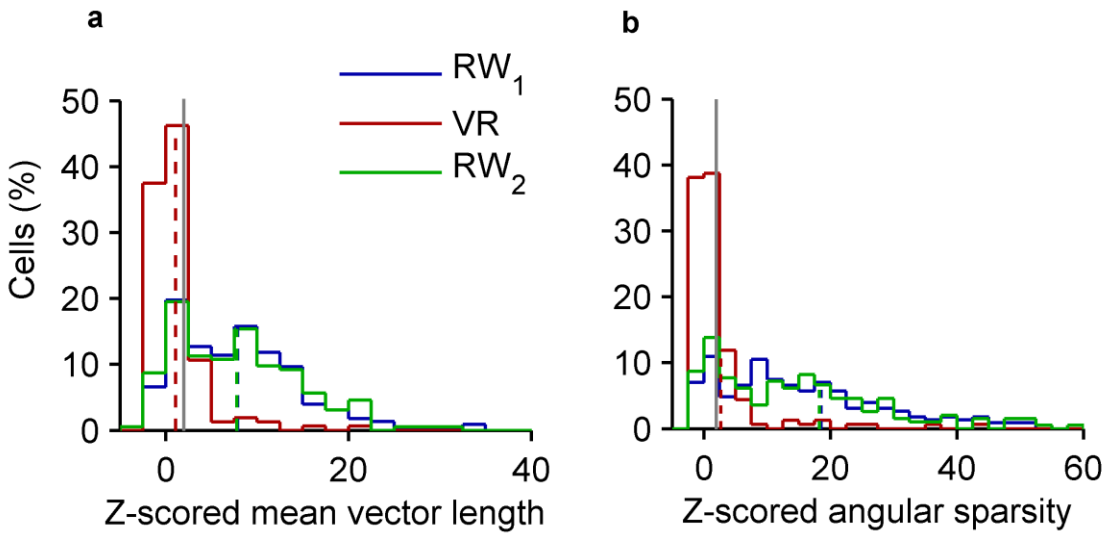


**Fig. 4.9:** HD firing of population of analyzed cells. **a)** For 228 (of 261 total) active cells in $RW_1$, the Z-scored MVL (7.90 ± 0.45) was comparable to that in 195 (out of 218) active cells in $RW_2$ (7.81 ± 0.49, p=0.82) and much greater compared to that in 160 (out of 221) active cells in VR (1.10 ± 0.24, $p<10^{-30}$). The vertical grey line, at a z-scored MVL of 2, represents the cutoff for cells with significant head direction tuning. 175 cells showed a significant MVL in $RW_1$, 34 in VR, and 142 in $RW_2$. **b)** Z-scored angular sparsity in $RW_1$ (18.52 ± 1.37) was comparable to that in $RW_2$ (18.25 ± 1.63, p=0.50) and much greater compared to that in VR (2.72 ± 0.67, $p<10^{-31}$). The vertical grey line, at a z-scored angular sparsity of 2, represents the cutoff for cells with significant head direction tuning. 193 cells showed a significant angular sparsity in $RW_1$, 44 in VR, and 154 in $RW_2$.

#### *4.3.3.2 Some HD cells had multiple preferred firing directions in RW*

Most HD cells in RW had one predominant peak. Upon visual inspection, however, we found some cells with multimodal responses (Fig 4.10). Some of these had firing responses reminiscent of the 3-fold symmetry found in grid cells, but the current data set cannot distinguish whether this phenomenon has any functional significance.

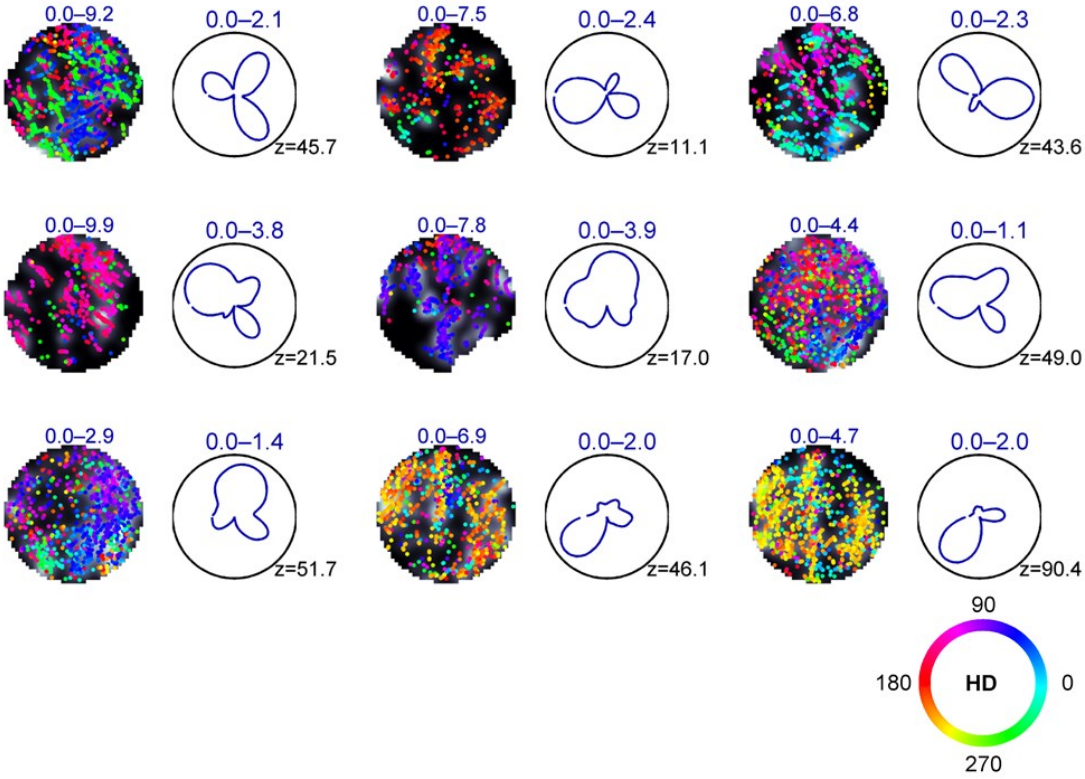


**Fig. 4.10:** Example HD cells in $RW_1$ with multipeaked angular rate maps: We found that the responses of some head direction cells were multimodal and the three detected peaks were oriented 120 degrees apart. The angular ratemaps were scaled and normalized to improve the visibility of all peaks. Left) Spatial firing rate of a neuron (grey scale range indicated by numbers; lighter shades correspond to higher values) overlaid with the position of the rat when spikes occurred (colored dots). Each color represents a distinct head-direction as shown in the color wheel. Right) Angular firing rate of the same neuron. Numbers indicate firing range. Number at the bottom right corner of the polar plot is the z-scored sparsity of the angular ratemap.

#### *4.3.3.3 Head direction cells lost their directional tuning within the virtual reference frame*

To further investigate the responses of HD cells in VR, we matched cells across sessions. Some HD cells reduced their firing rates dramatically in the VR (Fig 4.11a). Most, however, experienced only a mild reduction in firing rate, but lost their directional selectivity (Fig 4.11b). A small but significant portion retained their HD tuning in VR (Fig 4.11c).

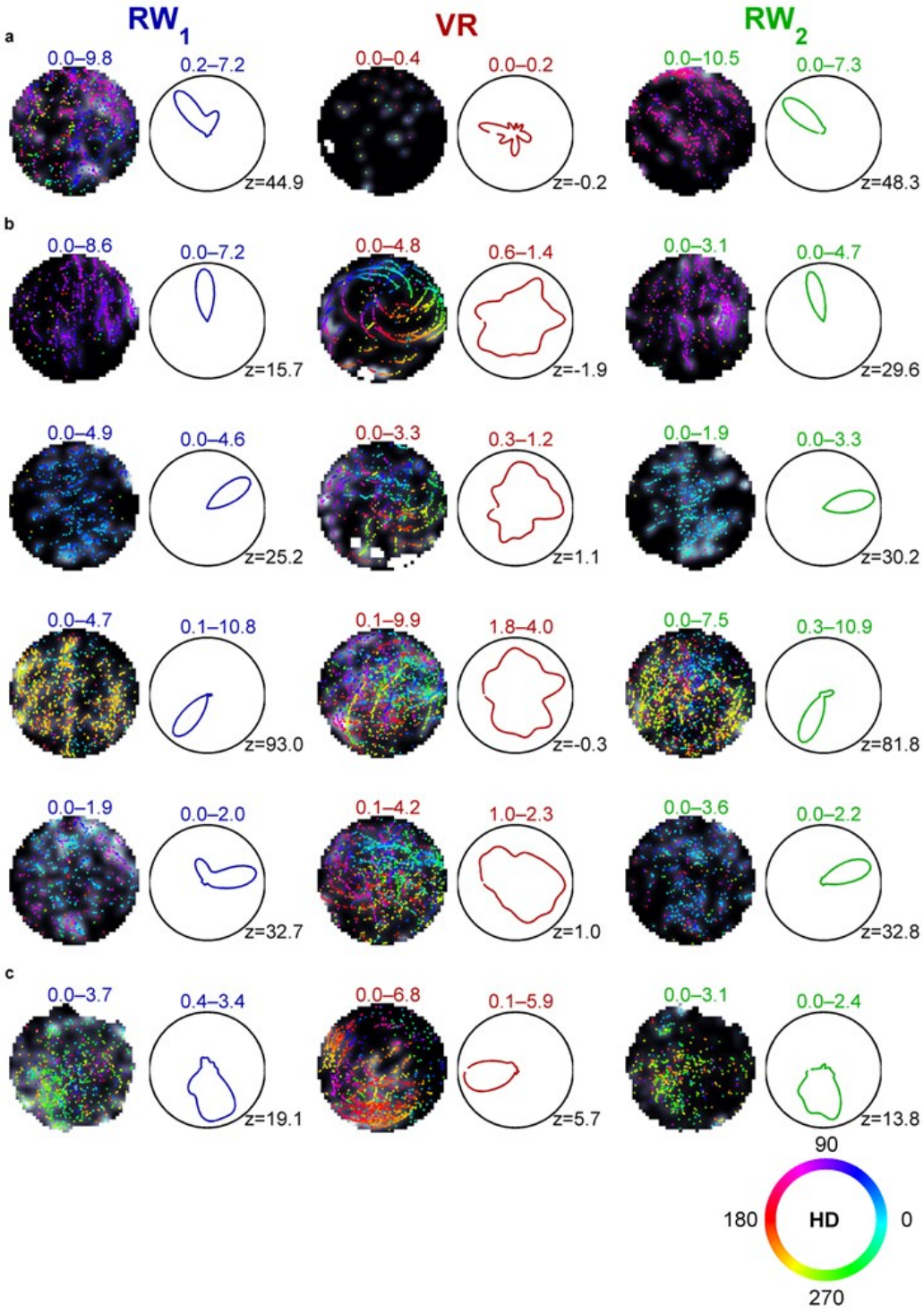


**Fig 4.**11 Example HD cells active in $RW_1$, VR, and $RW_2$: Left) Spatial firing rate of a neuron (grey scale range indicated by numbers; lighter shades correspond to higher values) overlaid with the position of the rat when spikes occurred (colored dots). Each color represents a distinct head-direction as shown in the color wheel. Right) Angular firing rate of the same neuron. Numbers indicate firing range. Number at the bottom right corner of the polar plot is the z-scored sparsity of the angular ratemap. **a)** A sample HD cell that shuts down in VR. **b)** Four example HD cells that lose their selectivity in VR. **c)** An example cell that keeps its HD tuning in VR. The numbers at the bottom right corner are the z-scored sparsity of the angular ratemaps.

Over the population of matched HD cells, mean firing rates were slightly decreased in VR, but the population showed mixed results, with some HD cells actually increasing their firing rates (Fig 4.12a and c). Same cell comparisons across the first and second RW sessions showed a high correlation of firing rates, indicative of the stability of recordings and cell responses (Fig 4.12b-c). Overall, MVLs and angular sparsity values dropped dramatically between the first RW session and the VR session, but returned to similar values in the second RW session (Fig 4.12d-i). Even though head directionality tends to decrease in VR compared to RW, some cells do retain significant levels of directional firing within the virtual reference frame. This is in contrast to grid cells, where the spatial signal seemed to be completely abolished.

These results show that for most HD cells, the visual cues alone are insufficient to elicit directional firing and uniquely determine the firing directions in these cells, similar to the conclusions from vestibular lesion studies (Stackman and Taube, 1997). Unlike these studies, however, we find that the visual cues alone are sufficient for a small subset of HD cells to retain their directional tuning. Taken together, these results suggest that for some HD cells, an intact vestibular system allows for directional tuning, even if the information from this system is unreliable within the virtual reference frame. Further analysis is required to determine whether there are any systematic differences between cells that retain their directional tuning in the VR and those that do not.

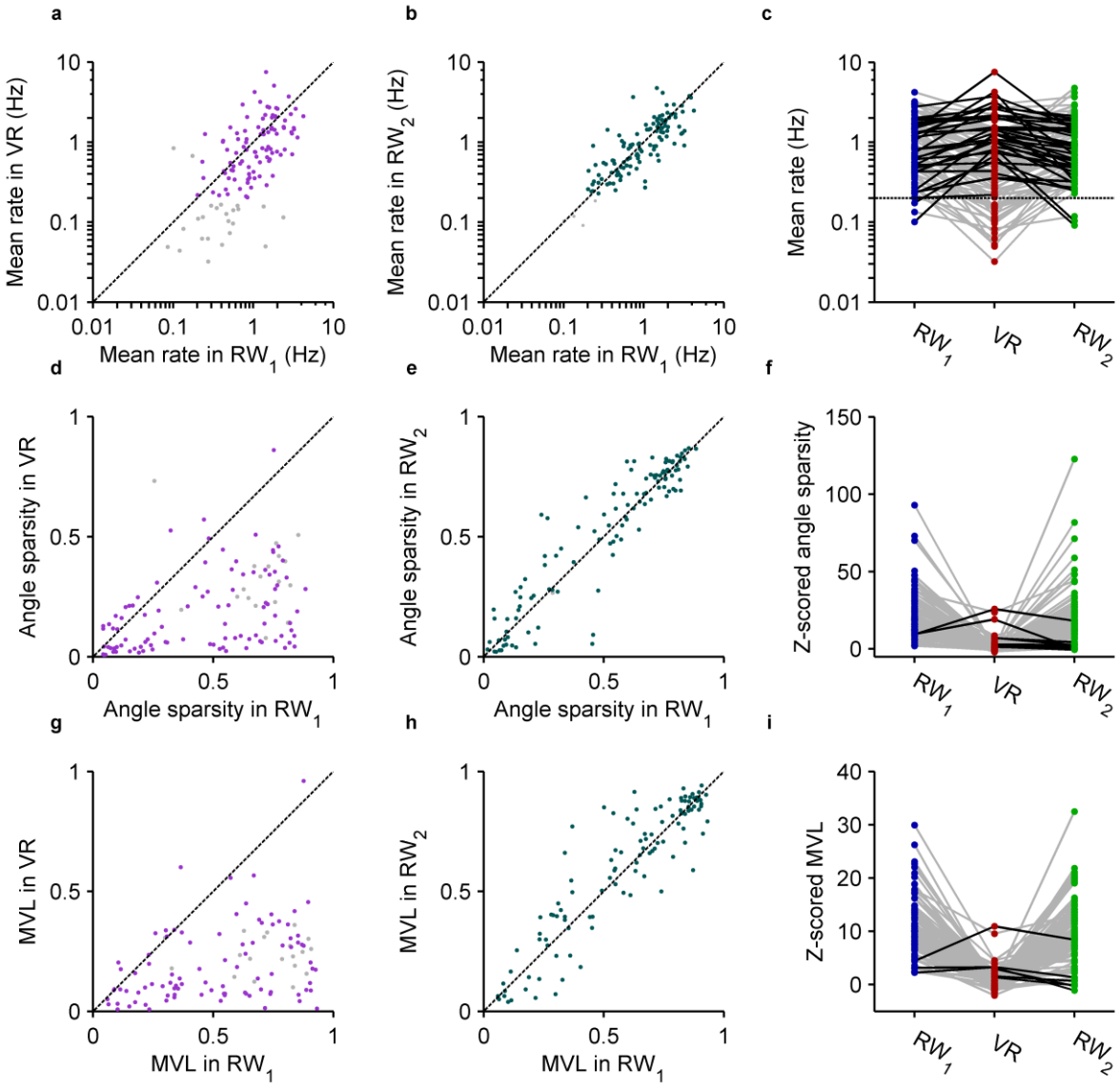


**Fig 4.12:** HD firing properties of the same cells in $RW_1$ and VR and $RW_2$: **a)** Out of 122 HD cells identified in the first RW session, 97 were active (mean rate > 0.2 Hz) in both RW and VR (purple dots). For the HD cells active in both worlds, the mean firing rate was significantly (p=0.027, Wilcoxon signed-rank test) greater in RW compared to VR. **b)** Out of 120 HD cells identified in the first and second RW session, 116 were active (mean rate > 0.2 Hz) in both $RW_1$ and $RW_2$ (green/blue dots). For the HD cells active in both real world sessions, the mean firing rate was identical (p = 0.41, Wilcoxon signed-rank test). **c)** For 104 cells identified in all three sessions, the majority of cells had lower mean firing rates in VR compared to the RW sessions. **d)** For the HD cells active in both worlds, the sparsity of angular ratemaps was significantly ($p<10^{-13}$, Wilcoxon signed-rank test) greater in RW compared to VR. **e)** For the HD cells active in both RW worlds, the sparsity of angular ratemaps was identical (p=0.10, Wilcoxon signed-rank test). **f)** For 104 cells identified in all three sessions, the majority of cells had lower angular sparsity in VR compared to the RW sessions. **g)** For the HD cells active in both worlds, the MVL of angular ratemaps was significantly (p = 5.7e-015, Wilcoxon signed-rank test) greater in RW compared to VR. **h)** For the HD cells active in both RW worlds, the MVL of angular ratemaps was identical (p = 2.2e-001, Wilcoxon signed-rank test) in RW sessions. **i)** For 104 cells identified in all three sessions, the majority of cells had lower MVLs in VR compared to the RW sessions.

#### *4.3.3.4 HD cells did not retain their directional tuning within the RW reference frame*

We then asked whether the HD cells were only incorporating the vestibular input and thus only maintaining tuning within the RW reference frame. Although the sampling of the angular space was small (30-90 degrees), it was clear that HD cells did not have a preferred firing direction within this range. In fact, the information content and sparsity obtained in the RW reference frame was even lower than that in the virtual reference frame (Fig 4.13).

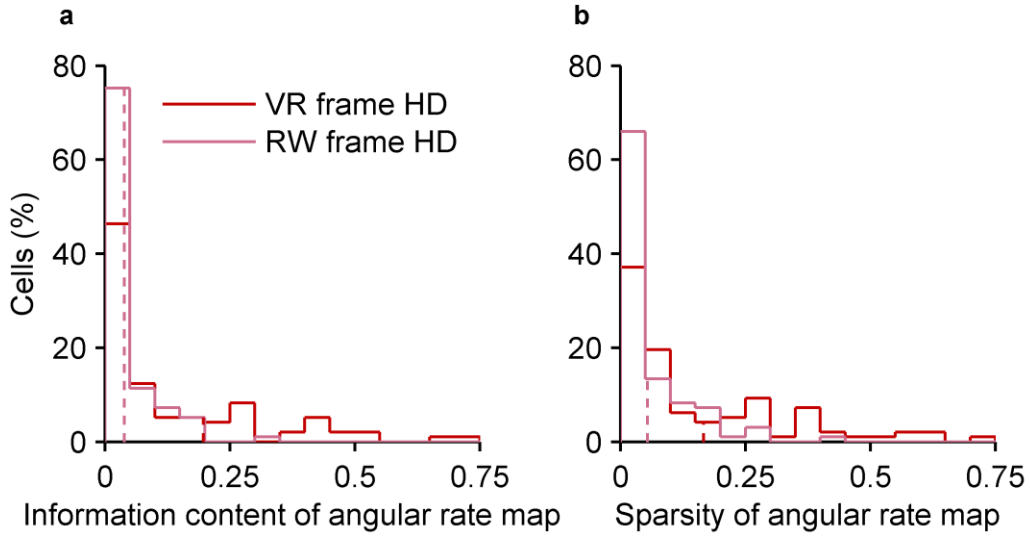


**Fig 4.13:** HD Cells are not selective to RW frame HD either. **a)** For 97 HD cells in VR (identified from the prior RW session), information content of the angular ratemap obtained from RW head-direction (0.04 ± 0.01) was even lower than that obtained from VR head-direction (0.20 ± 0.03, $p<10^{-7}$). **b)** For 97 HD cells in VR (identified from the prior RW session), sparsity of the angular ratemap obtained from RW head-direction (0.05 ± 0.01) was also lower than that obtained from VR head-direction (0.17 ± 0.02, $p<10^{-5}$).

This result, that most HD cells show no apparent tuning in either the RW or VR reference frames, could mean that the HD system breaks down under these conditions. Alternatively, this result could be due to an imperfect control of visual cues over HD preferred firing directions, due to conditions of unreliable vestibular cues. If this is the case, the HD representation might remain internally consistent, but continually shift with respect to the virtual reference frame, resulting in apparently low tuning when measured across the whole session.

Partial control of visual cues has been previously reported in HD cells. When a salient cue card is quickly rotated to a new position while the rat is in the environment, the HD representation rotates as well, but by a lesser amount (Goodridge and Taube, 1995). HD cells' preferred directions also rotate when a widefield visual stimulus is rotated continuously at approximately 4.5 degrees per second. Similar to the discrete condition, the HD representation rotates at a slower pace than the visual cues (Arleo et al., 2013), suggesting an imperfect control. The rate of the rotation of visual cues seems important, as slow rotations (0.2 degress per second) will impart complete control and the preferred firing directions of the HD cells will remain locked to the visual cues (Aronov and Tank, 2014).

In the present dataset, rats often turn the virtual scene with angular speeds well above those previously observed to create a lag in the HD representation. If this lag is occurring, HD selectivity would not be seen when looking at either reference frame because it might shift by an unpredictable amount every time the rat turns. When the rat makes random paths and thus makes turns of different directions, speeds, and turning radii throughout the session, it would be difficult to observe this shift. Thus, we looked for shifting preferred firing directions in sessions when the rat happened to display stereotyped behavior, i.e. when he ran in big circles of the same radius in the same direction throughout the session. There were a few sessions that met these criteria.

#### *4.3.3.5 There is some evidence that preferred firing direction of HD cells conintually drifts with respect to the virtual reference frame*

To observe any systematic shift in the HD cells' preferred firing directions with respect to the visual cues, we analyzed sessions where the rat ran in a stereotyped circular path throughout the VR session. In these conditions, the sensory experience was analogous to the one in the Arleo et al. study from 2013. There was a realtively constant rotation of the widefield visual cues, while vestibular cues gave inconsistent information about how much the rat was

rotating. As expected, we saw similar results in this condition. The preferred firing directions in HD cells drift in the same direction as the visual cues, but at a slower rate (Fig 4.14). This can be seen in the individual traces in the right panels in Fig 4.14. Each time the rat passes through a full rotation, the cells spike at progressively increasing heading angles. Further analysis is required to quantify this shift.

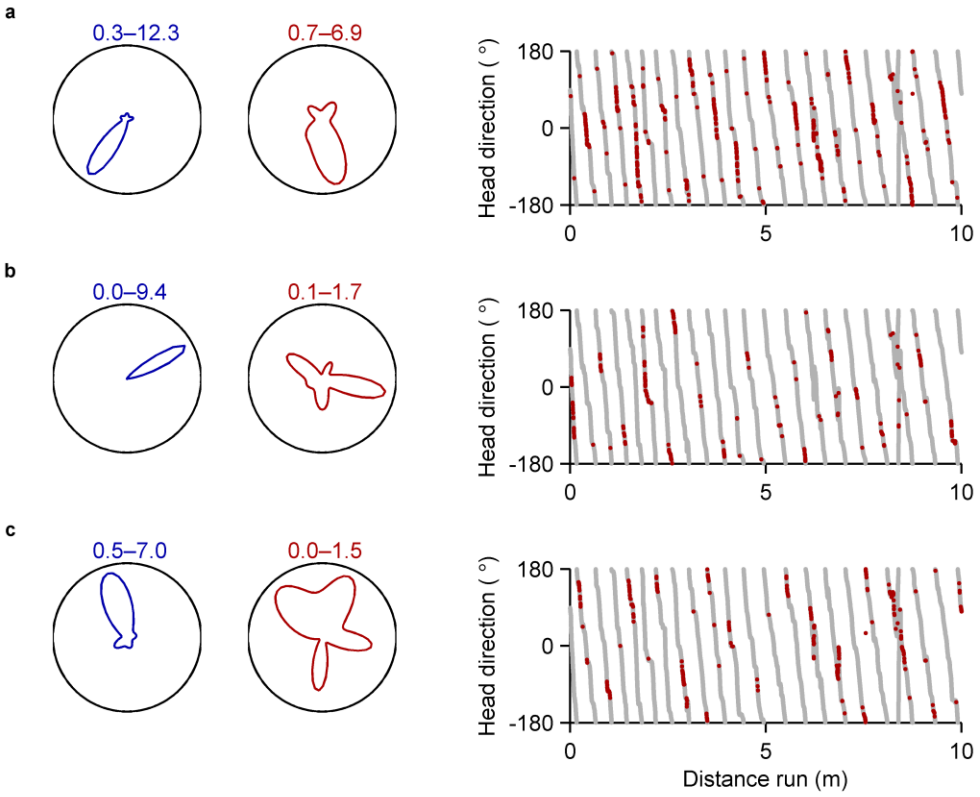


**Fig 4.14:** Example HD cells from a VR session with stereotyped circular behavior shows a drift in the HD cell representation. All cells were simultaneously recorded. Left panel shows the cell's directional activity in RW. Middle panel shows the same for VR. Right panel shows the heading direction of the rat over the distance run in grey. Superimposed red dots represent the firing of the cell. Note that in example a, even though there is apparent drifting in the preferred firing direction, there is more firing in one direction such that the cell has significant head direction selectivity.

## 4.4 Discussion

This preliminary study led to a few main findings. First, the spatially informative sensory cues in our VR apparatus were insufficient to support spatial selectivity or periodicity in grid cells. The fact that grid like firing is preserved in a different type of VR apparatus (Aronov and Tank, 2014) suggests angular vestibular cues or coherence between the RW and VR refrence frames may be a crucial factor.

Most HD cells, likewise, do not retain their directional tuning in a body-fixed VR, suggesting that visual cues alone are insufficient, even if the vestibular system is intact and can provide excitatory input. It appears that, for most HD cells, the angular information of vestibular input needs to be reliable within the VR reference frame in order to support directionally selective firing. We find some evidence that, under these conditions, the rotations in the visual scene only partially control the HD representation, perhaps causing a continual shift in the preferred firing direction. This phenomenon has also been observed in previous studies (Goodridge and Taube, 1995; Arleo et al., 2013). These results add to previous studies by confirming that even if the rat's voluntary movements are consistent with the visual information, the lack of vestibular information will continue to have a strong influence over HD cells.

The subset of HD cells that retain significant levels of directional selectivity within the VR reference frame warrants further investigation. Even though their directional selectivity is qualitatively worse than that found in RW, it is interesting that any is seen at all. Presumably, for these cells, visual input alone is sufficient for directional selectivity. This differential activity is particularly surprising because it is generally understood that all HD cells across many brain areas will respond coherently to changes in the environment. If substantiated with further data collection, this may be one of the few instances where a difference in HD cell responses has been found.

We have proposed that a change in spatially informative sensory cues causes the loss of spatial selectivity in HD and grid cells independently, but this need not be the only explanation. Instead, the loss of grid cell selectivity could be inherently linked to the lack of head direction tuning. In most theories and models of grid cells, information about heading direction is crucial for the selectivity and periodicity of grid cells (Burgess et al., 2007; Hasselmo et al., 2007; Blair et al., 2007; McNaughton et al., 2006; Fuhs and Touretzky, 2006; Burak and Fiete, 2009). Indeed, recent experimental evidence suggests that grid cells depend on input from HD cells to maintain grid-like firing (Winter et al, 2015). If this is true, the loss of grid cell selectivity and periodicity in VR might be due to lack of information from HD cells rather than the direct influence of sensory cues. It is quite possible that the HD and grid cells maintain a consistent spatial relationship, but this representation continually shifts with respect to both the RW and VR reference frames. The same could be true of place cells, as all of these cell types tend to respond coherently to changes in the environment (Hargreaves et al., 2007).

The apparent loss of HD cell tuning is particularly interesting considering recent data from the lab that is now in preparation. Even though place cells are not spatially selective within the VR reference frame, they do maintain their head directional modulation (Acharya et al., 2015). This is perplexing, since presumably the main source of head directional information is from HD cells, which mostly do not maintain their tuning within the VR reference frame. This suggests that the head direction information contained in HD and place cells possibly arise via independent pathways. While head direction information from HD cells seems to be governed by angular vestibular cues, widefield visual cues and optic flow, that information in place cells might be governed more by landmarks. In support of this hypothesis, it was found that in VR, place cell modulation by head direction increased when there was only one salient visual cue, and decreased when visual cues provided optic flow but no directional information (Acharya et al., 2015).

Taken together, the results presented here give insight into the sensory information necessary for a neural representation of space in the MEC, as well as possible interactions between spatially selective cell types.

## 4.5 Future Directions

This study only yielded enough data for a preliminary analysis at this time. A few major questions remain unanswered and warrant further data collection and analysis.

First, a large portion of the data was collected in only one animal, with a small number of cells recorded in two additional animals. Additional data collection is necessary to corroborate these results and to confirm the absence of subject specific effects.

Curiously, no border cells were detected in this dataset. These comprise a small proportion (10%) of the population in MEC (Solstad et al., 2008), so it is possible that none happened to be recorded. However, it will be important to explore this more and determine whether any experimental parameters influenced this seemingly low incidence of border cells.

In our VR, no spatial selectivity or periodicity is observed in grid cells when measured over the entire session. It is possible, however, that the grid structure is in fact intact, but shifts throughout the session, which might cause the observed drop in information content. This shifting could be due to the sensory experience of the VR itself, or due to a lack of absolute position information from place cells. Measuring the spatial correlations within and between simultaneously recorded grid cells will reveal whether any grid like activity remains intact in the VR reference frame.

Even if grid cells lose their spatial selectivity and periodicity within the VR reference frame, they could maintain periodicity with respect to another reference frame. It is possible that network properties could still be functioning, creating a natural periodicity. We briefly checked the periodicity of grid cells with respect to linear distance run; the results were mixed and there

was not enough data to make a strong conclusion. Another reference frame worth checking would be time. More complicated analyses could analyze grid activity over reconstructed paths based on different aspects of the sensory experience in VR. For example, a path could be reconstructed based on the linear distance run combined with the heading direction of the rat within the RW reference frame. It has been suggested that in order to maintain periodicity, the grid cell network requires excitatory input from the hippocampus, and not necessarily spatial information (Bonnevie et al., 2013). Since place cells remain active in the VR (albeit at moderately lower rates), but lose their spatial information content (Aghajan et al., 2014), evidence of periodicity in grid cells would be consistent with this hypothesis.

For HD cells, further investigation is needed for the subset that seems to retain head direction selelctivity in the VR. First, is there any systematic difference between HD cells that do or do not maintain selectivity in the VR? This apparent selectivity could be due to an anomaly in the recording session, or the rat's behavior. Alternatively, since these data come from both MEC and surrounding areas that also have HD cells, such as the postsubiculum, the different responses might be explained by differences in recording areas. If there is no systematic difference in the cells or the recording sessions, it will be important to quantify the level of visual and vestibular dominance in individual HD cells to determine whether there is a continuum of sensory control or two discrete classes.

Finally, it will be interesting to explore the correlations within and between simultaneously recorded cell types. For example, HD cells are hypothesized to arise from a ring attractor network (Redish et al., 1996; Zhang 1996), which means that cells with similar tuning should fire together at an above-chance rate, even if HD selectivity is absent. Looking for correlations between stimultaneoulsy recorded HD cells would give insight to the mechanisms of the putative ring attractor network. Similarly, if grid cells receive directional information from HD cells, there may be evidence of this in this dataset. Observing correlated activity between

HD and grid cells without the confound of spatially selective activity would be evidence that these connections exist and are involved in spatial processing.

## 4.6 References


Acharya, L., Aghajan, Z. M., Vuong, C., Moore, J. J., & Mehta, M. R. (2015). Visual cues determine hippocampal directional selectivity. bioRxiv doi: http://dx.doi.org/10.1101/017210.

Aghajan, Z. M., Acharya, L., Moore, J. J., Cushman, J. D., Vuong, C., & Mehta, M. R. (2014). Impaired spatial selectivity and intact phase precession in two-dimensional virtual reality. *Nature Publishing Group*, *18*(1), 121–128. Nature Publishing Group.

Arleo, A., Déjean, C., Allegraud, P., Khamassi, M., Zugaro, M. B., & Wiener, S. I. (2013). Optic flow stimuli update anterodorsal thalamus head direction neuronal activity in rats. *The Journal of neuroscience : the official journal of the Society for Neuroscience*, *33*(42), 16790–5.

Aronov, D., & Tank, D. W. (2014). Article Engagement of Neural Circuits Underlying 2D Spatial Navigation in a Rodent Virtual Reality System. *Neuron*, *84*(2), 442–456. Elsevier Inc.

Barry, C., Hayman, R., Burgess, N., & Jeffery, K. J. (2007). Experience-dependent rescaling of entorhinal grids. *Nature neuroscience*, *10*(6), 682–4.

Battaglia, F. P., Sutherland, G. R., & McNaughton, B. L. (2004). Local sensory cues and place cell directionality: additional evidence of prospective coding in the hippocampus. *The Journal of neuroscience : the official journal of the Society for Neuroscience*, *24*(19), 4541–4550.

Blair, H. T., Welday, A. C., & Zhang, K. (2007). Scale-invariant memory representations emerge from moiré interference between grid fields that produce theta oscillations: a computational model. *The Journal of neuroscience : the official journal of the Society for Neuroscience*, *27*(12), 3211–3229.

Bonnevie, T., Dunn, B., Fyhn, M., Hafting, T., Derdikman, D., Kubie, J. L., Roudi, Y., Moser, M. B., Moser, E. I. (2013). Grid cells require excitatory drive from the hippocampus. *Nature neuroscience*, *16*(3), 309–17.

Burak, Y., & Fiete, I. R. (2009). Accurate path integration in continuous attractor network models of grid cells. *PLoS Computational Biology*, *5*(2).

Burgess, N., Barry, C., & O'Keefe, J. (2007). An oscillatory interference model of grid cell firing. *Hippocampus*, *17*, 801–812.

Derdikman, D., Whitlock, J. R., Tsao, A., Fyhn, M., Hafting, T., Moser, M.-B., & Moser, E. I. (2009). Fragmentation of grid cell maps in a multicompartment environment. *Nature neuroscience*, *12*(10), 1325–32. Nature Publishing Group.

Fuhs, M. C., & Touretzky, D. S. (2006). A spin glass model of path integration in rat medial entorhinal cortex. *The Journal of neuroscience : the official journal of the Society for Neuroscience*, *26*(16), 4266–4276.

Fyhn, M., Hafting, T., Treves, A., Moser, M.-B., & Moser, E. I. (2007). Hippocampal remapping and grid realignment in entorhinal cortex. *Nature*, *446*(7132), 190–4.

Gibson, S., Judy, J. W., & Markovic, D. (2008). Comparison of spike-sorting algorithms for future hardware implementation. *Conference proceedings . Annual International Conference of the IEEE Engineering in Medicine and Biology Society. IEEE Engineering in Medicine and Biology Society. Conference*, *2008*, 5015–5020.

Goodridge, J. P., & Taube, J. S. (1995). Preferential use of the landmark navigational system by head direction cells in rats. *Behavioral neuroscience*, *109*(1), 49–61.

Hafting, T., Fyhn, M., Molden, S., Moser, M.-B., & Moser, E. I. (2005). Microstructure of a spatial map in the entorhinal cortex. *Nature*, *436*(August), 801–806.

Hargreaves, E. L., Yoganarasimha, D., & Knierim, J. J. (2007). Cohestiveness of spatial and directional representations recorded from neural ensembles in the anterior thalamus, parasubiculus, medial entorhinal cortex, and hippocampus. *Hippocampus*, *17*, 826–841.

Hasselmo, M. E., Giocomo, L. M., & Zilli, E. A. (2007). An oscillatory interference model of grid cell firing. *Hippocampus*, *17*, 1252–71.

Hetherington, P. A., & Shapiro, M. L. (1997). Hippocampal place fields are altered by the removal of single visual cues in a distance-dependent manner. *Behavioral neuroscience*, *111*(1), 20–34.

Knierim, J. J. (2002). Dynamic interactions between local surface cues, distal landmarks, and intrinsic circuitry in hippocampal place cells. *The Journal of neuroscience : the official journal of the Society for Neuroscience*, *22*(14), 6254–6264.

McNaughton, B. L., Battaglia, F. P., Jensen, O., Moser, E. I., & Moser, M.-B. (2006). Path integration and the neural basis of the “cognitive map”. *Nature reviews. Neuroscience*, *7*(August), 663–678.

Muller, R. U., & Kubie, J. L. (1987). The Effects of Changes in the Environment Hippocampal Cells on the Spatial Firing of. *Journal of Neuroscience*, *7*(July), 1951–1968.

Ravassard, P., Kees, A., Willers, B., Ho, D., Aharoni, D., Cushman, J., Aghajan, Z. M., Mehta, M. R. (2013). Multisensory control of hippocampal spatiotemporal selectivity. *Science (New York, N.Y.)*, *340*, 1342–6.

Redish, A., Elga, A., & Touretzky, D. (1996). A coupled attractor model of the rodent head direction system. *Network: Computation in Neural Systems*, *7*(4), 671–685.

Sargolini, F., Fyhn, M., Hafting, T., McNaughton, B. L., Witter, M. P., Moser, M.-B., & Moser, E. I. (2006). Conjunctive representation of position, direction, and velocity in entorhinal cortex. *Science*, *312*, 758–62.

Save, E., Nerad, L., & Poucet, B. (2000). Contribution of multiple sensory information to place field stability in hippocampal place cells. *Hippocampus*, *10*(1), 64–76.

Solstad, T., Solstad, T., Boccara, C. N., Boccara, C. N., Kropff, E., Kropff, E., Moser, M.-B., Moser, E. I. (2008). Representation of geometric borders in the entorhinal cortex. *Science*, *322*(December), 1865–1868.

Stackman, R. W., & Taube, J. S. (1997). Firing properties of head direction cells in the rat anterior thalamic nucleus: dependence on vestibular input. *The Journal of neuroscience : the official journal of the Society for Neuroscience*, *17*(11), 4349–4358.

Stensola, H., Stensola, T., Solstad, T., Frøland, K., Moser, M.-B., & Moser, E. I. (2012). The entorhinal grid map is discretized. *Nature*, *492*(7427), 72–8. Nature Publishing Group.

Taube, J. S., Muller, R. U., & Ranck, J. B. (1990a). Head-direction cells recorded from the postsubiculum in freely moving rats. I. Description and quantitative analysis. *The Journal of neuroscience : the official journal of the Society for Neuroscience*, *10*(February), 420–435.

Taube, J. S., Muller, R. U., & Ranck, J. B. (1990b). Head-direction cells recorded from the postsubiculum in freely moving rats. II. Effects of environmental manipulations. *The Journal of neuroscience : the official journal of the Society for Neuroscience*, *10*(February), 436–447.

Terrazas, A., Krause, M., Lipa, P., Gothard, K. M., Barnes, C. A., & McNaughton, B. L. (2005). Self-motion and the hippocampal spatial metric. *The Journal of neuroscience : the official journal of the Society for Neuroscience*, *25*(35), 8085–96.

Winter, S. S., Clark, B. J., & Taube, J. S. (2015). Disruption of the head direction cell network impairs the parahippocampal grid cell signal. *Science*, *347*(6224), 870–874.

Yoon, K., Buice, M. A., Barry, C., Hayman, R., Burgess, N., & Fiete, I. R. (2013). Specific evidence of low-dimensional continuous attractor dynamics in grid cells. *Nature neuroscience*, *16*(8), 1077–84. Nature Publishing Group.

Zhang, K. (1996). Representation of spatial orientation by the intrinsic dynamics of the head-direction cell ensemble: a theory. *The Journal of neuroscience : the official journal of the Society for Neuroscience*, *16*(6), 2112–2126.

Zhang, S.-J., Ye, J., Miao, C., Tsao, A., Cerniauskas, I., Ledergerber, D., Moser, M.-B., Moser, E. I. (2013). Optogenetic dissection of entorhinal-hippocampal functional connectivity. *Science (New York, N.Y.)*, *340*(6128), 1232627.